Dual regulatory role of Polycomblike-3 (PCL3/PHF19) in Prostate Cancer

Payal Jain

TESI DOCTORAL UPF / 2015

THESIS SUPERVISOR

Dr. Luciano Di Croce

GENE REGULATION, STEM CELLS AND CANCER PROGRAM

CENTRE DE REGULACIÓ GENÒMICA (CRG)

Acknowledgements

First and foremost, I will like to thank present and past members of laboratory and other members of the department who have provided immense support, encouragement, scientific discussions, technical help and motivation to drive the project. In particularly, I will like to thank Lilli who provided me with the initial guidance that was required to understand the technical competencies required for the project. I think there are no words that can describe the gratitude I feel for you Cecilia, an angel. Without you, I would not be the scientist I am today and I am deeply thankful to all the contributions you have made scientifically and emotionally for this project. Last but not the least, I will like to thank you Luciano for continuing to believe in me and encouraging me to think positively and constantly strive to find solutions to the problems.

Adam, you have been an immense emotional support through the most difficult part of this thesis. You have listened, cried and laughed with me through the ups and downs of the thesis. You have been my strength, my pillar and without you, I would not have the mental strength to keep fighting and believe in me to complete this thesis.

Mom and Dad, you have provided me with a strong foundation, an emotional backbone that helped to be patient, positive and kept me motivated.

Lastly, my friends: Meritxell, Lars, Anna, Cati Ana, Sophia, Lilli, Nadine, Andi, Alex…you have listened to my complaints, my frustrations, my struggle, my joy and you have been part of this beautiful journey in Barcelona. I thank you all for your constant support and encouragement and wish you all the best in your lives.

Abstract

Polycomblike proteins (PCLs) have been shown to regulate Polycomb Repressive Complex 2 (PRC2) by enhancing its catalytic activity and guiding PRC2 to its target genes in embryonic stem cells. However, little is known about the role of PCL proteins in cancer. Here, we describe the role of Polycomblike-3 (PCL3/PHF19) in prostate epithelial cells and prostate cancer. PHF19 maintains the prostate epithelial cells in undifferentiated state and has a multifaceted role in Prostate Cancer. PHF19 is required for cell growth and proliferation of prostate cancer cells but its downregulation confers a switch to an angiogenic and invasive state in prostate cancer. We further report distinct profiles of H3K27me3, deposited by PRC2, in PC3 and DU145 cells and report the presence of broad domains of H3K27me3 in PC3 cells. Lastly, we do not observe any global changes in H3K27me3 upon PHF19 depletion with only few local changes suggesting a PRC2 independent role of PHF19 in Prostate Cancer.

Resum

S'ha demostrat que les proteïnes Polycomblike (PCLs) regulen l'activitat del Complex Repressor de Polycomb 2 (PRC2) a les cèl·lules mare embrionàries a través de dos mecanismes; per una part, intensificant la seva activitat catalítica i per l'altra, conduint el PCR2 als seus gens diana.

No obstant això, poc se sap sobre la implicació de les proteïnes PCL en càncer. En el present estudi, describim el paper de PCL3 (PHF19) en cèl·lules epitelials de pròstata i en càncer de pròstata. PHF19 manté les cèl·lules epitelials de pròstata en estat indiferenciat i té un paper multifacètic en càncer de pròstata. PHF19 és necessari pel creixement i proliferació de les cèl·lules de càncer de pròstata però la seva sots-regulació els confereix capacitat angiogènica i invasiva. A més a més, presentem els perfils d'H3K27me3, modificació d'histona depositada per PRC2, en les cèl·lules PC3 i DU145, i reportem la presència d'amplis dominis d'H3K27me3 en les cèl·lules PC3. Per últim, no observem cap canvi global en els nivells d'H3K27me3 en cèl·lules sense PHF19, sinó que només veiem pocs canvis a nivell local, el que suggereix un paper de PHF19 independent de la funció de Polycomb en càncer de pròstata.

Preface

The work described in this thesis has been entirely conducted in the Gene Regulation, Stem cells and Cancer program at Centre for Genomic Regulation (CRG) under the supervision of Dr. Luciano Di Croce.

The results presented here illustrate a previously unreported role for the Poycomblike-3 (PCL3/PHF19) in normal prostate epithelium and prostate cancer in differentiation, proliferation and angiogenesis/invasion.

Table of contents

INTRODUCTION

1. Introduction

1.1 Prostate Cancer

According to the American Cancer society, prostate cancer (PCa) is the most common cancer among men in United States along with skin cancer. The estimates for 2014 stated that about 233,000 new cases of prostate cancer will be diagnosed and about 29,480 mean will die of prostate cancer. Thus, prostate cancer remains one of the leading causes of cancer related mortality in men. The prostate gland normally requires androgens for normal function of the prostate. The onset of prostate cancer is usually associated with interactions of these androgens with the Androgen Receptor (AR) that typically leads to elevated Prostate Specific antigen (PSA) levels in blood of the patients. This is now the most common diagnostic test to detect prostate cancer. A biopsy is usually performed to determine the histological grade that is usually assigned as Gleason score starting from more differentiated to poorly differentiated prostate cancer. Most of the localized and metastatic prostate cancer is treated with Androgen deprivation therapy (ADT) as at this stage the survival of prostate cancer cells depend on androgens; however, the vast majority of patients develop castration resistant disease within 2 to 3 years at which stage they stop responding to ADT (Harris *et al*., 2009). Most of the associated mortality comes from patients suffering from castration resistant disease. There are several mechanisms that lead to the development of castration resistance and these can depend on androgen receptor axis or become independent of androgen signaling. Therefore, it is important to understand the molecular mechanisms that may lead to development of castration resistant prostate cancer (CRPC). It should also be noted that some of the prostate cancers turn into neuroendocrine prostate cancer, poorly differentiated small cell carcinoma of the prostate. The neuroendocrine prostate cancer lacks AR, does not express PSA and is a highly aggressive disease (Tilki and Evans, 2014).

In order to understand the molecular basis of prostate cancer, it is important to understand the composition of the prostate epithelium as the cell type of origin can help in understanding of prostate cancer.

1.11 Prostate epithelium

The Prostate gland is located at the base of urinary bladder surrounding the urethra. The human prostate is composed of three distinct morphological zones: the peripheral zone, the transition zone and the central zone (Figure 1). Most of the prostate adenocarcinomas arise from the peripheral zone whereas benign prostatic hyperplasia (BPH) occurs in the transition zone. The mouse prostate differs from the human prostate and is more lobular in structure comprising of four distinct lobes (Abate-Shen and Shen, 2000). The dorsolateral lobe of mouse is considered to be most similar to human peripheral zone (Berquin *et al*., 2005). The prostate epithelium is composed of distinct cell types: undifferentiated but proliferative basal cells, intermediate or transit amplifying cells that are undifferentiated but primed for differentiation and secretory luminal cells that secrete PSA into the lumen. In addition to these three cell types, there is another kind called neuroendocrine cells that have been poorly characterized (Figure 2). The basal cells are believed to be composed of stem or progenitor cells of the prostate and can be distinguished by the presence of cytokeratins 5 and 14, CD44, and p63 among other markers. The neuroendocrine cells are considered to be androgen independent and typically express chromogranin A, serotonins and other neuropeptides. The differentiated secretory epithelial cells line the lumen of the prostate gland and express cytokeratins 8 and 18, and CD24 among other markers. Most importantly, these cells express AR and PSA. It is important to note that intermediate or transit amplifying cells express cytokeratins and markers of both basal and luminal cells simultaneously suggesting that these cells are stem-like or progenitor cells that are ready to differentiate but are still not committed (Peehl, 2005).

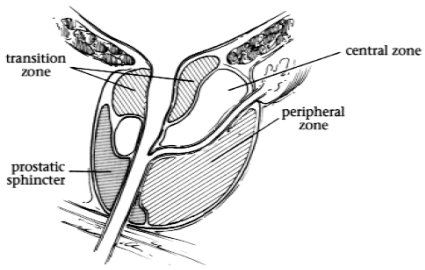

Figure 1: Schematic illustration of human prostate. (Adapted from Abate-Shen and Shen, 2000, Genes and Development)

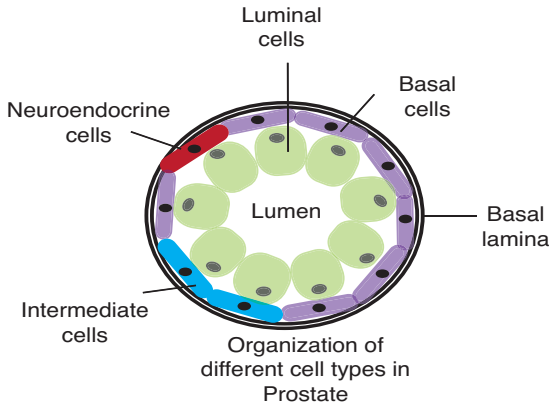

Figure 2: Organization of different cell types of prostate epithelium. Prostate epithelium is organized into basal cells, neuroendocrine cells, intermediate or transit amplifying cells and luminal cells expressing markers of each type.

1.12 Molecular pathways affected in Prostate Cancer

Prostatic intraepithelial neoplasia (PIN) is usually the primary lesion that gives rise to Prostate cancer and originates in the peripheral zone. The basement membrane is maintained in PIN and there is no invasion of stroma (Figure 3). PIN also does not secrete PSA and therefore biopsy is usually a favorable method to detect PIN. Early initiation of PIN is associated with loss of specific regions of chromosome 8p that occurs in 80% of prostate tumors. This loss is usually associated with *NKX3.1*, a tumor suppressor (Abate-Shen and Shen, 2000). NKX3.1 represses the expression of PSA and thus loss of this gene can lead to increased concentrations of PSA. This gene is also absent in 78% of prostate cancer metastasis. Progression can then occur through mutations is several other pathways which have been described below (Figure 3).

One of the major signaling pathways that are perturbed in prostate cancer includes the Phosphoinositide 3-Kinase (P13K) pathway. The Phosphatase and Tensin homologue (*PTEN*), that inhibits PI3K dependent signaling contains heterozygous and homozygous deletions in about 40% of primary prostate cancers and inactivating mutations in another 5-10%. *PTEN* is an important tumor suppressor and in Prostate cancer loss of *PTEN* is usually associated with advanced disease (Figure 3). Similarly, the catalytic subunit of PI3K, *PIK3CA* is amplified or contains activating point mutations in prostate cancer. Both these mutations lead to hyper activation of this pathway. Mutations can also occur in the mitogen-activated protein kinase pathway. Loss of *PTEN* is also related to low CDKN1B (p27) levels, which is another important tumor suppressor in prostate cancer (Graff *et al*., 2000). Somatic loss of sequences coding for p27 are reported in 23% of prostate cancers, 30% in regional lymph node metastasis and 47% in distant metastasis.

Although they are rare, overexpression of upstream regulation of MAPK such as Ras and Raf are commonly overexpressed in prostate cancer and usually associated with activation of AR. Deletion in the tumor suppressor p53 (*TP53*) occur in about 25-40% of prostate cancer and point mutations in 5-40% of cases (Figure 3). The retinoblastoma gene *RB1*, although not frequently deleted in clinically localized prostate cancer is inactivated in castration resistant prostate cancer in 45% of the cases (Figure 3). This gene has an important role in checking cell cycle progression as well as inhibiting progression to castration resistance. The transcription factor *MYC*, is associated with chromosome 8 that is commonly amplified in prostate cancer thereby leading to overexpression. BCL2 is commonly overexpressed in prostate cancer and prevents apoptosis and promotes survival of prostate cancer cells. The prostate stem cell antigen (PSCA) is overexpressed in 80% of prostate cancer specimens and is usually associated with androgen independence. Gene fusions between androgen regulated genes and ETS family of oncogenic transcription factors is very common is prostate cancer. The most common gene fusion reported in *TMPRSS2:ERG*. In general, expression of ETS family members is associated with development of PIN and in combination with AR overexpression or loss of *PTEN*; this can lead to invasive carcinoma. Among cytokines and growth factors, epidermal growth

factor receptor (EGFR) is usually implicated in growth and development of prostate cancer and with progression; this is replaced by transforming growth factor α (TGF- α) synthesis that contributes to loss of control of proliferation. TGF- α also can act with TGF-β and cause malignant transformation. TGF-β also acts with vascular endothelial growth factor (VEGF) to promote angiogenesis. Elevated levels of interleukin – 6 (IL6) are found in sera of patients with metastatic prostate cancer and believed to mediate its oncogenic effect via MAPK and STAT pathways. Among the STAT proteins, STAT5 is required for survival of prostate cancer cells and is usually associated with high histological grade of prostate cancer (Barbeiri *et* al., 2013; Mazaris and Tsiotras, 2013; Shen and Abate-Shen, 2010; Abate-Shen and Shen, 2000).

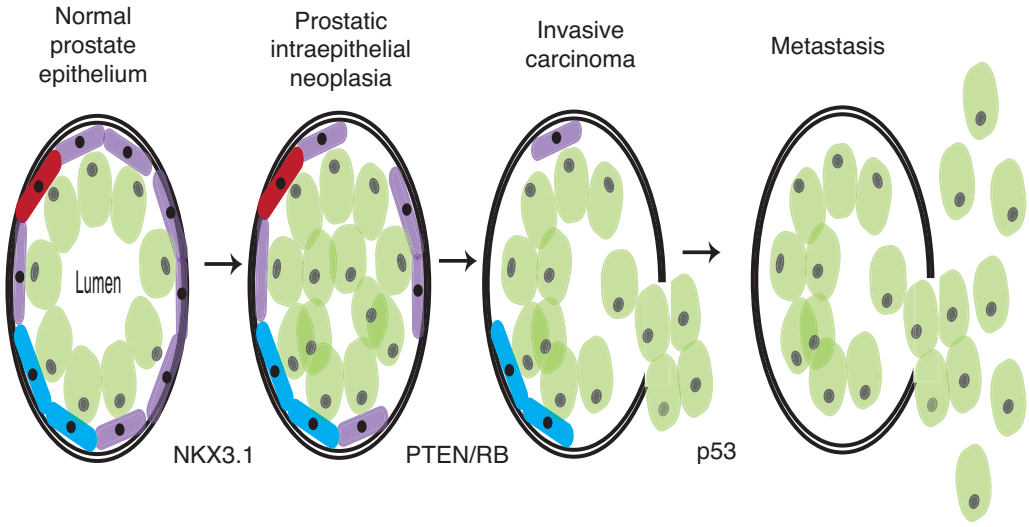

Figure 3: Loss of tumor suppressors during prostate cancer progression. (Adapted from Abate-Shen and Shen, 2000, Genes and Development)

1.13 Androgen receptor and development of castration resistance

Androgen and AR are main regulators of maintaining a ratio of proliferating to dying cells and in cancer the net ratio of proliferating cells is higher than dying cells. AR belongs to the steroid hormone group of nuclear receptors. The AR gene is located on X chromosome and codes for a 110-kDa protein. The AR consists of three major functional domains: the N-terminal domain, DNA binding domain and C-terminal ligand binding domain. AR is a ligand inducible transcription factor. Testosterone is the main circulating androgen and is converted to dihydrotestosterone (DHT) by the enzyme 5α-reductase. DHT is

a high affinity ligand for AR. AR when not with a ligand is bound by heat shock protein 90 (HSP90) chaperone complex in the cytoplasm and undergoes proteasome-mediated degradation. Upon ligand binding, AR is dissociated from HSP90, homodimerizes and translocates to the nucleus. In the nucleus, AR binds to androgen response elements (ARE) at both enhancers and promoters of its target genes (Figure 4). Two of the most well characterized AR target genes include PSA and transmembrane protease serine 2 (TMRSS2). AR can recruit coactivators at both enhancer and promoter of PSA. This coactivator complex includes p160 proteins, CBP, p300, pCAF and RNA polymerase that lead to histone acetylation at the promoter thus driving transcription (Shang *et al*., 2002). The phosphorylated RNA polymerase II tracks from PSA enhancer to the promoter through looped DNA and on members of mediator complex (Wang *et al*., 2005). AR binding depends on another transcription factor FOXA1 that plays a role in providing more accessible chromatin around AREs (Lupien *et al*., 2008). Most of the AR-regulated genes are involved in metabolic pathways that regulate protein and lipid synthesis. Androgens also regulate TORC1 activity and this is usually associated with increased translation of cyclins D that allow progression through cell cycle (Xu *et al*., 2006). AR negatively regulate p53 pathway and regulates apoptosis by repressing Caspase-2 (Rokhlin *et al*., 2005) and activating c-FLIP, an inhibitor of Fas/Fas-L mediated apoptosis (Gao *et al*., 2005). AR can negatively regulate transcription by interacting with other activators. AR inhibits c-Met expression by interacting with transcription factor Sp1 and prevents its recruitment on the Sp1 binding site on c-Met promoter (Verras *et al*., 2007). AR can also bind Smad3 and inhibit its binding to Smad-binding elements thereby affecting TGF- β transcriptional response (Chipuk *et al*., 2002).

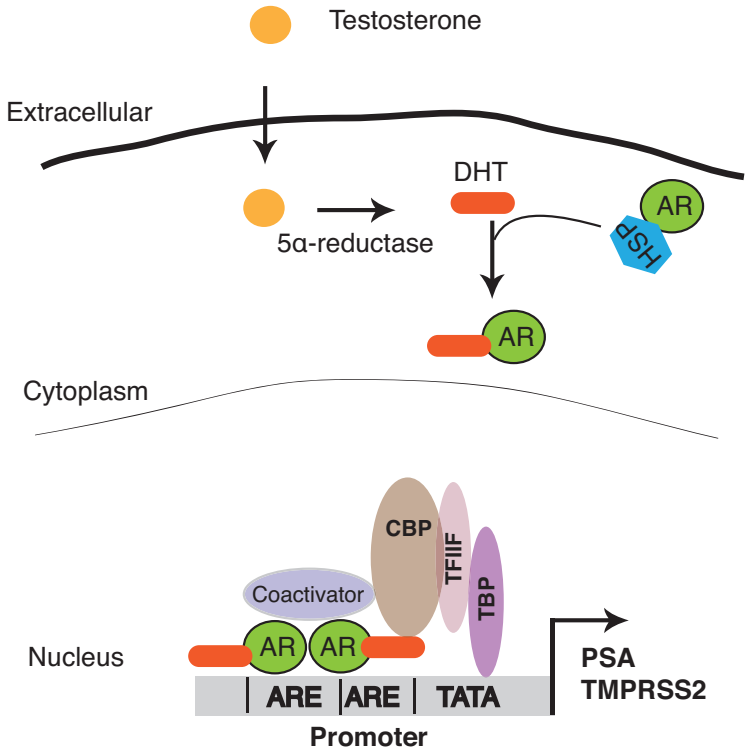

Figure 4: AR signaling in prostate cells. Circulating testosterone is transported to target tissues such as prostate where it is converted to dihydrotestosterone (DHT) by 5-α-reductase. DHT dissociates AR from heat shock proteins (HSP), translocates to the nucleus where AR dimerizes and binds to androgen response elements (ARE) of its target genes. AR recruits other members of transcription machinery (TFIIF, TBP) in addition to coactivators (CBP) to drive transcription. (Adapted from Tan *et al*., 2015, Acta Pharmacol Sin)

The expression of androgen receptor and its target gene PSA is still detected in CRPC (Gregory *et al*., 1998). However, there is a switch from paracrine androgen receptor signaling to autocrine signaling (Gao *et al*., 2001). There are several mechanisms responsible for sustained AR signaling in CRPC (Figure 5). The first one includes increased androgen sensitivity. This can take place through amplification of AR gene copy number (Xq11-q13), which is observed in 30% of recurrent tumors in patients after ADT. This can now facilitate tumor cell growth in low androgen conditions (Visakorpi *et al*., 1995). It is also reported that AR is exclusively nuclear and more stable in androgen independent prostate cancer cell lines compared to short life in androgen dependent cancer cells. This can also sustain the function under low levels of androgens (Gregory *et al*., 2001). The steroid transport proteins are encoded by *SLCO* gene family. Six members of this family are overexpressed in CRPC suggesting increased uptake of androgen into prostate cancer cells and thus influencing the response to ADT. Further, SNPs are found in some of these

members that are associated with increased mortality (Wright *et al*., 2011). The second mechanism is associated with mutations in AR receptor that makes it promiscuous. Gain of function mutations have been described in discrete parts of AR that usually results in broadening of ligand specificity and inappropriate receptor activation by estrogens, progestins, adrenal androgens, and other steroid hormones (Buchanan *et al*., 2001). Overexpression of co-activators that bind to AR such as TIF2 and SRC1 increases AR transactivation response under low levels of adrenal androgens or other steroids with affinity for AR (Gregory (a) *et al*., 2001). Ligand independent activation of AR can also occur in CRPC. This can take place by other growth factors such as IGF-1, KGF, and EGF (Culig *et al*., 1994). Using LAPC-4 xenografts and deriving androgen independent and dependent sublines, HER-2/neu receptor tyrosine kinase is found to be associated with progression to androgen independence. HER-2/neu activates the AR in the absence of a ligand and increases the AR response in low levels of androgen. The function of HER-2/neu in castration resistant requires the expression of AR (Craft *et al*., 1999). This is complemented by another study, which demonstrates AR transactivation by HER-2/neu in LNCaP and DU145 cells. This regulation takes place through MAP kinase pathway that phosphorylates AR. Further; the HER-2/neu kinase also increases the interaction between AR and its coactivators (Yeh *et al*., 1999). Src family kinase is required for androgen independent activation of AR that is mediated by neuropeptide, EGF and interleukin-8 (IL8). Src has been implicated to be important in several processes of prostate tumorigenesis in both androgen dependent and independent prostate cancer cells (Chang *et al*., 2008). The loss in copy number of *RB* gene occurs in CRPC, and this correlates with AR hyperactivation. Mechanistic insight is provided for this process through increased occupancy of AR on its target genes in the absence of RB. Secondly, increase in E2F1 that is concomitant with loss of RB, binds to the promoter of AR and activates it in CRPC (Sharma *et al*., 2010). It has been previously shown that that AR has a different transcriptional program in CRPC and most of the target genes are associated with mitotic cell cycle (Wang *et al*., 2009). The levels of E2F1 and AR correlate in cell cycle and this further supports a function of RB-E2F1-AR axis is regulation of cell cycle in CRPC as

opposed to metabolic function in androgen dependent cells (Sharma *et al*., 2010). In addition, novel isoforms or splice variants of AR have also been reported in CRPC that are usually ligand binding domain deficient (Sun *et al*., 2010; Guo *et al*., 2009). lncRNAs *PRNCR1* and *PCGEM1* are highly upregulated in prostate cancer. It is shown that *PRNCR1* interacts with acetylated AR and co-occupies AR binding sites at enhancers. This in turn leads to DOT1L methylation of AR that is required for its interaction with *PCGEM1*. These two lncRNAs can bind to truncated AR as well as bind to full length AR in both absence and presence of a ligand. Moreover, the lncRNAs presence at enhancers promotes enhancer-promoter looping of AR target genes (Yang *et al*., 2013). Lastly, new mechanisms of steroid synthesis can arise as a result of ADT. One such fatty acid, arachidonic acid induces steroidogenic acute regulatory protein (StAR), which when bound to hormone sensitive lipase (HSL) shuttles free cholesterol into the mitochondria for downstream conversion into androgens in steroid starved LNCaP cells (Locke *et al*., 2010). Lastly, a study elucidated different steps of steroid synthesis in prostate cancer cells and showed that most of enzymes involved in the process continue to be expressed in CRPC. Further, they see an upregulation of certain enzymes such as *CYP17A1* that is required for production of adrenal androgens from progestin and *HSD17B3*, that converts androstenedione to testosterone further confirming the maintenance of intratumoral androgens in response to ADT (Montgomery *et al*., 2008). Another study complementing the same results further shows that SRD5A1 and RDH5, enzymes responsible for progesterone metabolism to dihydrotestosterone are upregulated in response to castration resistance along with AKR1C1, AKR1C2 and AKR1C3 which convert androstenedione to testosterone (Locke *et al*., 2008). The *AR* gene itself contains an enhancer located within the second intron that it can bind to and activate itself in conditions of low signaling. Once, the AR signaling is restored, AR recruits lysine specific demethylase -1 (LSD1) at this enhancer element that demethylates H3K4me1 and H3K4me2 and cause transcriptional repression forming a negative feedback loop (Cai *et al*., 2011). However, LDS1 can also aid in androgen dependent transcription. LSD1 interacts with AR *in vivo* and *in vitro*. LSD1 is recruited to AR binding sites where it demethylates mono and di

methylation at histone H3 at lysine 9 (H3K9) in a ligand dependent manner and activates gene transcription (Metzger *et al*., 2005). A Jumonji C domain containing protein (JMJD2C) also interacts with AR and demethylates trimethlyation at H3K9 in androgen dependent activation. JMJD2C colocalizes with AR and LSD1 thus providing a mechanism for coordinated action of two demethylases to drive AR dependent gene regulation (Wissmann *et al*., 2007). Additionally, AR can associate with serine/threonine kinase, protein kinase C-related kinase 1 (PRK1) that phosphorylates H3 on threonine 11 and this augments the ability of LSD1 to demethylate H3K9me1, 2 (Metzger *et al*., 2008). AR and PRK1 also activate protein kinase C β1 (PKCβ1) that phosphorylates histone H3 on threonine 6 and this is required for switching the substrate specificity of LSD1 from H3K4 to H3K9 thus allowing androgen dependent transcription (Metzger *et al*., 2010).

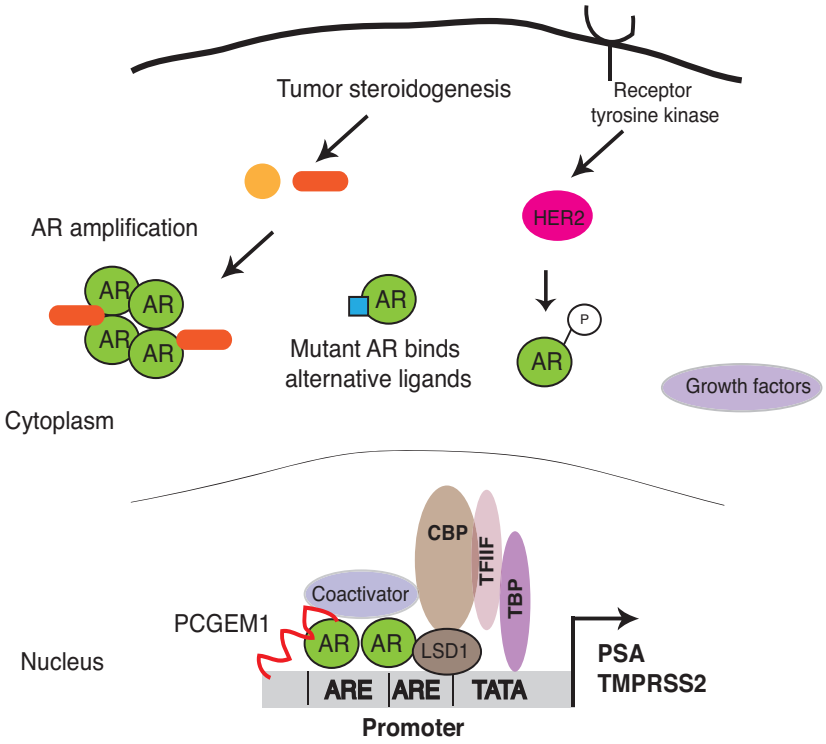

Figure 5: Mechanisms of castration resistant prostate cancer. AR amplification is usually coupled with novel tumor steroidogenesis. Mutant AR can bind promiscuously other ligands including estrogen and progesterone. Ligand independent mechanisms occur through phosphorylation of AR via HER2 kinase and growth factors. The long non-coding RNA *PCGEM1* and co-operation through LSD1 includes AR gene transcription via epigenetic mechanisms. (Adapted from Tan *et al*., 2015, Acta Pharmacol Sin)

1.14 Epigenetic modifications in Prostate Cancer

There are three epigenetic modifications that are commonly reported in Prostate cancer. This includes DNA methylation, changes in histone modifications and microRNAs (miRNA) (Figure 6).

DNA methylation

Prostate cancer is usually characterized by increasing levels of global hypomethylation in intergenic and intragenic regions with the stages of the disease and gene-specific DNA hypermethylation associated with cell cycle, DNA damage, apoptosis and tumor suppression. Global hypomethylation is associated with retrotransposon elements such as *LINE-1* and *Alu* repeats (Cho *et al*., 2007). DNA hypomethylation is also associated with aberrations on chromosome 8 (Schulz *et al*., 2002).

GSTP1, glutathione-S-transferase is hypermethylated in more than 90% prostate cancers. It plays an important role in detoxification and protects DNA from hydrophobic and electrophilic compounds. Hypermethylation of *GSTP1* can also predict disease recurrence. However, since a single gene is usually not 100% reliable method to distinguish cancer from normal tissue, several studies have focused on using a combination of methylated genes to predict disease. Methylation profile of four genes *GSTP1, RASS1FA, RARβ* and *APC* can distinguish between normal and prostate cancer with high sensitivity. Further, hypermethylation of *PTGS*2 and *CD44* are also associated with biochemical recurrence. *PTGS2* is also used as a diagnostic and prognostic marker (Chiam *et al*., 2014). Global loss of hydroxymethylation is also reported in prostate tumors (Yang *et al*., 2013; Haffner *et al*., 2011). In addition, cooperation of Polycomb group of proteins and DNA methylation is observed in prostate cancer, which is discussed in detail in the following chapter.

Histone modifications

Changes or patterns in histone modifications have been proposed to act as biomarker or predict disease recurrence. Global loss of H4K16ac and H4K20me3 has been associated with wide variety of cancers including prostate cancer (Fraga *et al*., 2005). H3K18ac, H3K4me2, H4K12ac,

H4R3me2 are shown to be associated with increasing grade of prostate cancer. H3K18ac and H4R3me2 are proposed to be associated with increased gene activity owing to high proliferation of dedifferentiated tumors (Seligson *et al*., 2005). Additionally, histone modifications H3K4me1, H3K9me2, H3K9me3, H3Ac and H4Ac are significantly reduced in prostate cancer compared to normal prostate tissues and H3K9me2 levels is the best indicator of distinguishing between prostate cancer and normal tissues whereas H3K4me1 is a reliable predictor of recurrence after radial prostatectomy (Ellinger *et al*., 2010). In addition, it is shown that H3K4me3 can predict the risk of biochemical recurrence for low-grade prostate cancer and H4K20me3 and H3K9ac can predict the same for high-grade prostate cancer after radial prostatectomy (Zhou *et al*., 2010). Lastly, a study found that H3K27me3 levels increases in metastatic prostate tumors compared to non-malignant prostate tissues (Ellinger *et al*., 2012). This is consistent with overexpression of histone methyltrasferase, EZH2 that deposits this mark in prostate cancer, the implications of which are discussed in the following chapter.

MicroRNAs (miRNAs)

MicroRNAs are small non-coding RNAs (19-25 nucleotides) that post-transcriptionally regulate gene expression. miRNA profiling from 40 prostatectomy specimens and comparison between early relapse and no relapse cancer patients compared to normal tissue of the same patient identified five miRNAs miR-23b, miR-100, miR-145, miR-221 and miR-222 to be significantly downregulated in malignant tissues. Expression of these miRNAs has a negative effect of growth of LNCaP cells suggesting a role in growth. Further, comparing the outcome of relapse, 16 miRNAs are differentially expressed between relapse and no relapse but statistical significance of this result is considered inconclusive by this study due to sample size (Tong *et al*., 2009). Circulating miRNAs have also been characterized in prostate cancer. Analysis of miRNAs in serum of patients with metastatic tumors and localized disease revealed two miRNAs, miR-375 and miR-141 to be specifically overexpressed and correlate with high Gleason score or lymph node positive status (Brase *et al*., 2011). Genome wide

profiling of prostate tumors with adjacent normal tissues identified 15 differentially expressed miRNAs in prostate cancer. These include miR-16, miR-31, miR-125b, miR-145, miR-149, miR-181b, miR-184, miR-205, miR-221 and miR-222 that are downregulated and classified as prognostic markers and miR-96, miR-182, miR-183, miR-141, miR-375 that are upregulated and indicative of early detection or prognosis. Further, miR-205 that is upregulated gives the most reliable score as a diagnostic marker (Schaefer *et al*., 2010). miR-34c is expressed at lower levels in patients with metastasis compared to patients with no metastasis. It can also distinguish between aggressive and non-aggressive prostate cancer. Expression of miR-34c in prostate cancer cells decreases cell growth, suppresses proliferation, promotes apoptosis and decreases cell migration and invasion. BCL-2 and E2F3 are targets of miR-34c in PC3 cells explaining the phenotype observed upon ectopic expression of miR-34c in these cell lines (Hagman *et al*., 2010). miR-29a and miR-1256 are methylated in prostate cancer samples compared to the normal counterparts. Further, TRIM68 and PGK-1 are targets of these miRNAs. Treatment of prostate cancer cells with demethylating agents inhibits the expression of TRIM68 and PGK-1, which in turn inhibits cell growth, and invasion of C4-2B and LNCaP cells (Li *et al*., 2012). miR-205 has been further characterized and in agreement with previous studies is methylated in prostate cancer cells. Further, expression of miRNA in LNCaP cells negatively affects cell viability. As miR-205 has been previously shown to target MED1 in human trophoblasts, and also can act as a coactivator of AR, expression of miR-205 in LNCaP cells decreases the total and phosphorylated forms of MED1. Further, high levels of methylated miR-205 are associated with shorter time to biochemical relapse (Hulf *et al*., 2013).

Lastly, there are several miRNAs that inhibit the expression of EZH2 and this is discussed in detail in the following chapter.

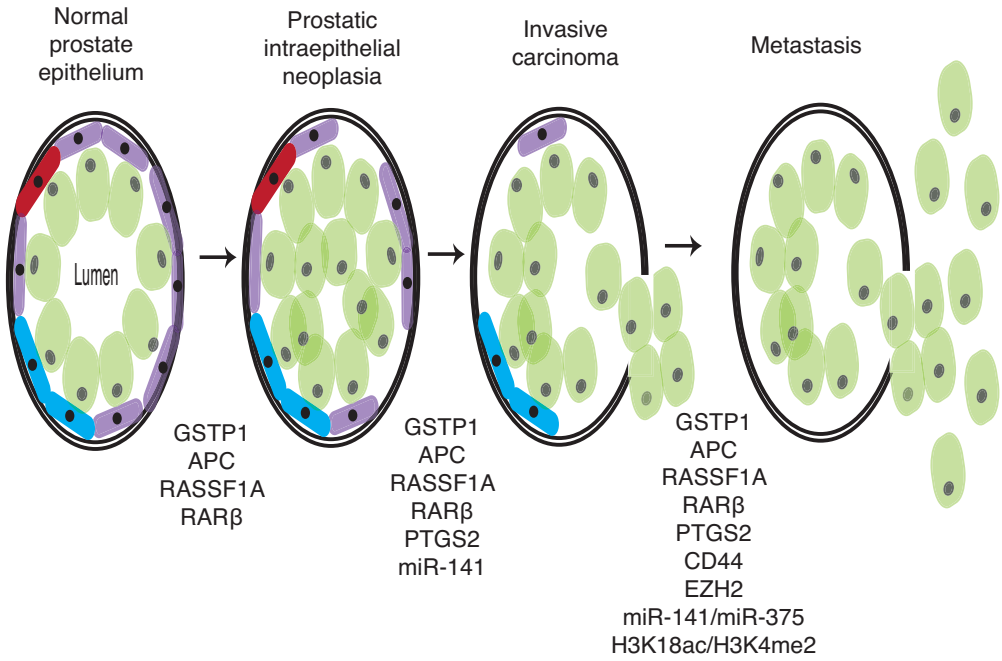

Figure 6: Examples of common epigenetic alterations including DNA methylation, over and under expression of miRNAs and histone modifications in prostate cancer progression. (Adapted from Chiam *et al*., 2014, Cancer Lett).

1.2 PRC2 and Prostate Cancer

The Polycomb group of proteins (PcG) exists in two multimeric complexes: Polycomb Repressive complex 1 (PRC1) and Polycomb Repressive complex 2 (PRC2). Each complex can exist in several variations as demonstrated below:

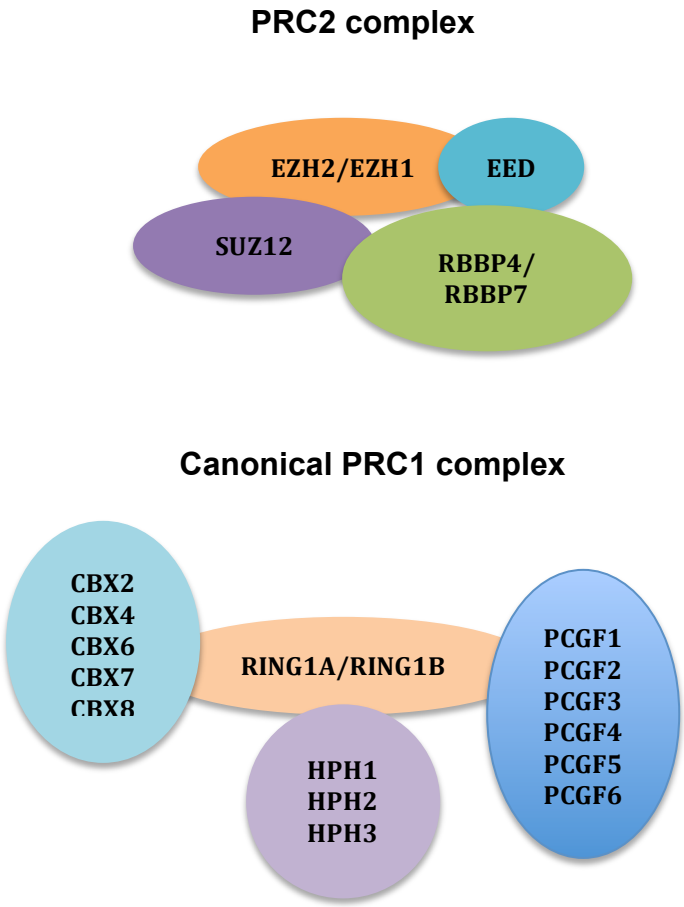

Figure 7: Composition of the main Polycomb complexes. (Adapted from Di Croce and Helin, 2013, Nat Struct Mol Biol).

The core components of PRC2 complex consists enhancer of zeste 2 (EZH2) or its close homolog EZH1, suppressor of zeste 12 (SUZ12) and embryonic ectoderm development (EED). EZH2 and EZH1 are histone methyltransferases that catalyze mono-, di- and trimethylation of H3K27. SUZ12 is required for the stability and catalytic activity of the complex. RBBP4/RBBP7 are histone chaperones that confer nucleosome-binding ability to PRC2 complex and are essential for catalytic activity of the complex *in* vivo. EED directly interacts with H3K27me3 and is required for propagation

of the mark. The PRC1 complex can contain multiple variations of core PRC1 complex that usually contains one of the CBX proteins, which recognize and bind to H3K27me3 through its chromobox-domain, on member of the PCGF family, of the RING1 family and of the HPH family as demonstrated above. RING1A and RING1B are E3 ubiquitin ligases and when present in the complex mono-ubiquitinate histone H2A at K119 (H2AK119ub1). In addition to the canonical PRC1 complex, a non-canonical PRC1 complex without the CBX protein has been characterized. In general, the mode of polycomb recruitment in thought to occur in two sequential steps: PRC2 is thought to be recruited first that leads to deposition of H3K27me3 on its target histones. CBX7 component of PRC1 complex directly binds to H3K27me3 and recruits the PRC1 complex, which in turn deposits H2AK119 ubiquitynation via uibiquitin ligase RING1A/RING1B (Di Croce and Helin, 2013) (Figure 8). An opposite mechanism has also been recently proposed which demonstrate that presence of a variant PRC1 complex and H2A ubiquitynation is sufficient to recruit PRC2 complex and impairment of H2A ubiquitynation can disrupt PRC2 binding (Blackledge *et al*., 2014; Cooper *et al*., 2014 and Kalb *et al*., 2014).

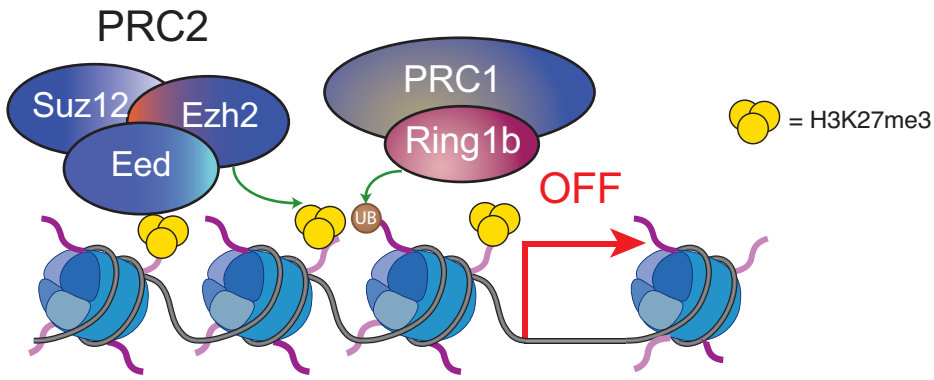

Figure 8: Mode of transcriptional silencing by Polycomb complexes. (Adapted from Di Croce and Helin, 2013, Nat Struct Mol Biol).

These two complexes are often deregulated in cancer, which in turn leads to aberrant histone modifications on target genes that can lead to cancer. Different mechanisms have been reported in different cancers and below I will

discuss the most relevant literature reported on the role of PRC2 in Prostate Cancer.

1.21 Overexpression of EZH2 in prostate cancer

EZH2 was initially discovered to be overexpressed in localized and metastatic prostate cancer compared to benign prostate cancer tissues using gene expression profiling across a set of clinical samples. The function of EZH2 was assessed in RWPE, an androgen responsive prostate cancer cell line as well in PC3 cell line and in both cases EZH2 inhibition leads to decrease in cell growth mediated by G2/M arrest in cell cycle (Varambally *et al*., 2002). The role of EZH2 in cell proliferation was explained by the binding of E2F family of transcription factors to the promoter of EZH2 and EED thereby leading to transactivation of mRNA levels of two proteins and activation of Cyclins required for cell proliferation (Bracken *et al*., 2003). Later, it was shown that EZH2 competes with HDAC as partner of pRb2/p300 complex on cyclin A promoter interfering with cell growth suppression of this complex and promoting cell cycle progression (Tonini *et al*., 2004). EZH2 can also transform normal prostate epithelial cells BPH1 both *in vitro* and *in vivo* at rates stronger than myristoylated Akt but weaker than Ras (V12) (Karanikolas *et al*., 2009).

Amplification of locus containing EZH2 is also commonly reported in hormone refractive prostate cancer thereby leading to amplification of the gene that could account for high expression commonly observed in metastatic prostate cancer. Among the widely studied prostate cancer cell lines, most of the cell lines are reported to contain 4 copies of the gene (Saramaki *et al*., 2006). There are additional mechanisms such as genomic loss of micro-RNA-101 that binds to 3´UTR of EZH2 gene that accounts for overexpression of EZH2 in Prostate cancer (Cao *et* al., 2010; Varambally *et al*., 2008).

Androgens and androgen receptor have been linked to expression of EZH2 and development of castration-resistant disease. In LNCaP cells treated with androgens, EZH2 expression is lower compared to its androgen depleted derivatives C4-2 and Rf. LNCaP xenografts obtained from castrated animals after 6 weeks show higher expression of EZH2. Thus, androgen seems to repress *EZH2*. This repression requires the presence of intact AR although

AR is not bound directly to *EZH2*. This repression is mediated via RB-dependent and p130/E2F4/5 dependent pathways. Thus, androgen depletion serves to increase EZH2 expression that can lead to development of castration resistant prostate cancer (Bohrer *et al*., 2010)

In addition to this, MYC has been shown to bind to E-box upstream of TSS of *EZH2* promoter thereby directly affecting its transcriptional outcome. MYC also inhibits two microRNAs, miR-26A and miR-26b that bind to 3´UTR of EZH2 and inhibit its expression in different prostate cancer cell lines as well in PIN lesions of MYC driven murine model of prostate cancer (Koh *et al*., 2011). Further, on mimicking oncogenic events that take place during prostate cancer, it has been shown that collaboration between activation of Kras and overexpression of AR leads to increase in tumorigenic reinitiation capability due to elevated expression of EZH2 (Cai *et al*., 2012). EZH2 and CBX2 are also upregulated in neuroendocrine prostate cancer (Clermont *et al*., 2015). Beside the mechanisms that explain the overexpression of this histone methyltransferase, there have been numerous publications explaining the mechanism by which EZH2 via repression or activation can promote Prostate cancer.

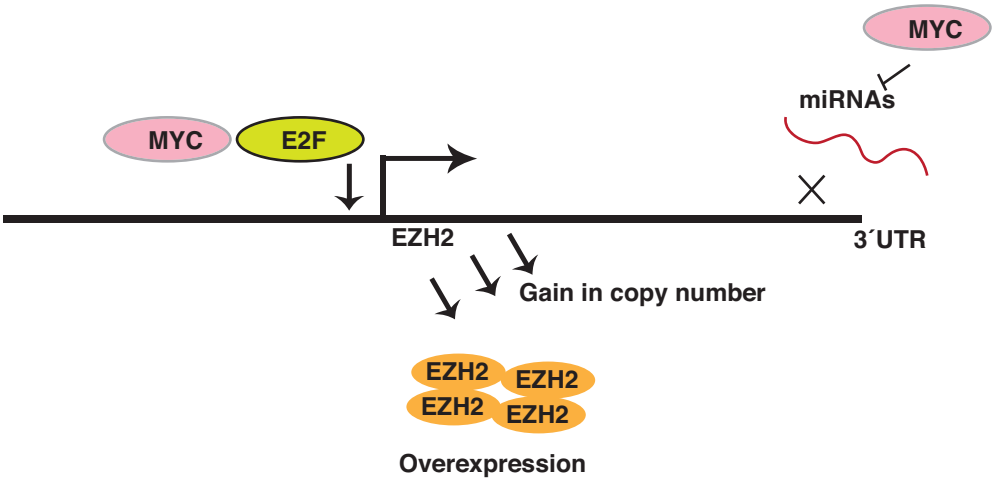

Figure 9: Mechanisms of EZH2 overexpression in prostate cancer involving gain in copy number, binding of transcription factors to the promoter of EZH2 and inhibition of miRNAs by MYC that binds to 3´UTR of EZH2.

1.22 EZH2 mediated transcriptional repression in Prostate Cancer

Most of the studies explain the role of EZH2 in oncogenesis via its role in transcriptional repression. One of the first genes to be identified was *DAB2IP* (DAB2 interacting protein), a Ras GTPase-activating protein that acts as tumor suppressor. EZH2 is required for silencing of *DAB2IP* by recruitment of HDAC1 and deposition of H3K27me3 at DAB2IP gene promoter in prostate cancer cells (Chen *et al*., 2005). In primary prostate epithelial cells (PrECs), *DAB2IP* loss leads to activation of Ras, ERK and AKT. Orthotopic injections of PrECs expressing oncogenic Ras or DAB2IP shRNAs develop prostate adenocarcinomas in a similar fashion. Interestingly, although the H-Ras^{V12} driven tumors are non-invasive, *DAB2IP* loss makes tumors invasive and metastatic. *DAB2IP* loss also activates NF-κB and its transcriptional targets in PrEC. Therefore, EZH2 mediated silencing of *DAB2IP* is an important event in EZH2 mediated metastasis by activation of Ras and NF-κB (Min *et al*., 2010).

ADRB2 (Adrenoreceptor, beta2) was initially identified as a direct target of EZH2 is different prostate cancer cell lines and shown to regulate cell invasion and transformation in an EZH2 dependent manner. The repression of the gene however has no effect on proliferation. This study connected EZH2 with β−adrenergic signaling in prostate cancer. It was also a first example of integrative genome analysis by incorporating expression data with genome occupancy data to identify direct targets of EZH2 in Prostate cancer (Yu *et al*., 2007).

EZH2 also represses E-cadherin promoter in breast and prostate cancers. E-cadherin is a Ca^{2+} dependent transmembrane receptor that is usually downregulated in metastasis. The recruitment of EZH2 and the PRC2 complex usually takes place at E-boxes present on E-cadherin promoter and HDACs are required for PRC2 recruitment as treatment with SAHA, HDAC inhibitor leads to reduced occupancy of PRC2 and H3K27me3 levels in DU145 prostate cancer cells (Cao *et al*., 2008).

Kruppel like factor – 2 (KLF2) has growth inhibitory, pro-apoptotic and anti-angiogenic roles in cancer. KLF2 is silenced by EZH2 in breast and prostate cancer. Upon induction of KLF2, EZH2 mediated silencing is affected leading to reduced growth of cancer cells. However, in EZH2 depleted cells,

knockdown of KLF2 can rescue the oncogenic phenotype suggesting a close correlation between KLF2 and EZH2 is oncogenesis (Taniguchi *et al*., 2012).

RKIP is a metastasis suppressor Raf1 kinase inhibitor protein whose expression levels correlate negatively with EZH2. In prostate cancer cells, RKIP promoter is bound by EZH2 and Suz12 at E-boxes and HDACs at the promoter. This leads to subsequent silencing and the promoter is associated with H3K27me3 and H3K9me3. Further, the recruitment of EZH2 to E-boxes is mediated by Snail, a transcription factor required for silencing of E-cadherin. Lastly, expression of miR-101 leads to depression of *RKIP* confirming the regulation of EZH2 by miR-101. This repression is necessary for tumor cell invasiveness (Ren *et al*, 2012).

Cbp (histone acetyltransferase) deletion in mouse against a *Pten* heterozygous background leads to development of early high grade (PIN)/low grade cancer. In DU145 cells, concomitant depletion of CBP and PTEN leads to a switch between H3K27ac to H3K27me3 at bulk histones as well as EZH2 repression of tumor suppressors DAB2IP and $p27^{KIP1}$. Thus, low levels of CBP and loss of PTEN can trigger epigenetic changes via EZH2 activation in Prostate cancer (Ding *et al*., 2014).

Along with tumor suppressors, EZH2 also silences tissue inhibitor of metalloproteinases (TIMPs) and activate matrix metalloproteinases (MMPs) for degradation of extracellular matrix required for tumor invasion. EZH2 silences TIMP3 in PC3 and DU145 cells leading to recruitment of HDACs, deposition of H3K27me3 and subsequent DNA methylation. In addition to TIMP3, TIMP2 is also targeted by EZH2. Further, this silencing leads to increase in enzymatic activity of MMP9 in prostate cancer cells (Shin and Kim *et al*., 2012)

IFNGR1 has been shown to be a direct target of EZH2 in DU145 and PC3 cells, which were postulated to be MYC driven cancer and not in LNCaP cells that is PI3-K driven. This process is shown to be MYC dependent as knockdown of *MYC* in these cells leads to reduced EZH2 enrichment at *IFNGR1* promoter in DU145 and PC3 cells. Using clinical samples dataset, the authors show that this phenomenon is present in a subset of aggressive prostate cancer tissues where expression of *MYC* is high. This is also confirmed by immunocytochemistry on tissue microarray containing prostate

cancer tissues where high MYC corresponds to high EZH2 but lower IFNGR1 expression. Using a combination of DZNep that reduces EZH2 and EED and IFN- Ɣ leads to therapeutic results *in vivo* as well as induce apoptosis in DU145 cells. This study also showed that inhibitors that target H3K27me3 are not effective in inducing *IFNGR1* expression and only lead to loss of H3K27me3. However, inhibitors specifically targeting the components of PRC2 lead to induction of *IFNGR1.* Thus, PRC2 and not H3K27me3 is important for de-repression of some of the EZH2 targets (Wee *et al*., 2014).

RUNX1, runt related transcription factor can act as a tumor suppressor and an oncogene in prostate cancer. In androgen dependent prostate cancer, RUNX1 interacts with AR and co-occupies its binding sites. It is required for recruitment of AR and therefore necessary for proliferation of androgen dependent cells. However, in androgen independent prostate cancer, EZH2 binds to the promoter of *RUNX1* and silences it and this silencing is required for the proliferation of androgen independent prostate cancer cells (Takayama *et al*., 2015).

Lastly, a 14-gene signature of PcG represses genes is proposed for prostate cancer using genome wide localization studies of SUZ12 and H3K27me3. The most repressed gene shares similarity with genes occupied by PcG in ES cells suggesting that stem cell like signature is maintained in cancer cells. Additionally, this gene signature predicts poor survival in patients and therefore can be of prognostic value (Yu(a) *et al*., 2007)

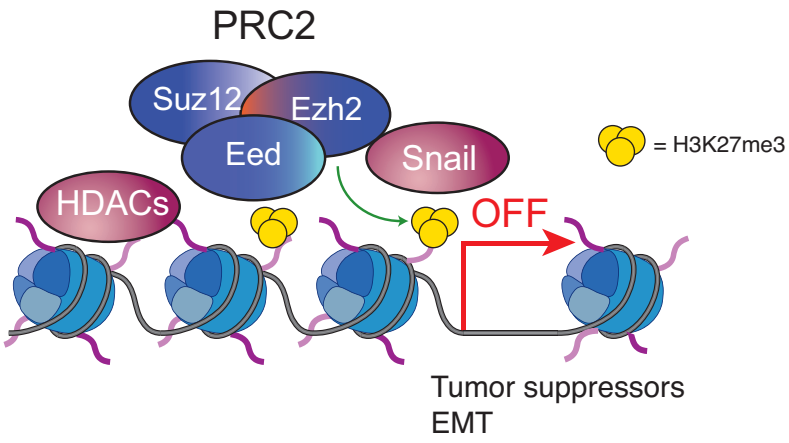

Figure 10: PRC2 mediated silencing of tumor suppressors and EMT drivers in prostate cancer. This epigenetic silencing usually involves recruitment of HDACs and transcription factors such as Snail for transcriptional repression by PRC2.

1.23 EZH2 and miRNAs/lncRNAs in Prostate Cancer

The regulation between miRNAs and Polycomb comes from previous observations that miRNAs can inhibit the expression of EZH2 and that their expression tend to correlate negatively with both PRC2 and PRC1 components in cancer. In order to find the miRNAs that can regulate Polycomb, EZH2 was knocked down in DU145 cells. 14 miRNAs were found to be upregulated, have higher expression in benign or normal cells compared to prostate cancer cells and bind 3´UTR of PRC1 components. Indeed, miR-181a, b can bind RING2, miR-203 to BMI1 and miR-200b,c to both. This also leads to global decrease in H2A ubiquitynation and depression of PRC1 targets p16 and p21 in DU145 cells. These miRNAs are directly bound and repressed by PRC2 as well as BMI1 suggesting a feedback loop. Expression of these miRNAs in prostate cancer cells leads to reduced growth, invasiveness and self-renewal (Cao *et al*., 2011).

A comprehensive analysis by RNA-seq across prostate cancer tissue samples and cell lines identified 121 lncRNAs whose expression can be stratified in benign, localized and metastatic prostate cancer. This study also identified a novel lncRNA *PCAT-1*, that in RWPE1 cells, when expressed leads to increase in proliferation. In LNCaP cells, where it has high expression, knockdown results in decrease in proliferation. However, in DU145 cells and VCaP cells, where it is silenced by PRC2, it does not have any effect on proliferation (Prensner *et al*., 2011).

The let-7 family of miRNAs acts by silencing several oncogenes and their expression correlates negatively with EZH2 in prostate cancer cells and clinical samples in aggressive prostate cancer. Indeed, let-7 miRNAs bind to 3´UTR of EZH2 and can silence its expression. Expression of let-7 leads to decrease in clonogenic and self-renewal capability of prostate cancer cells suggesting that this suppression is necessary for clonogenic expansion of cancer stem cells in prostate cancer (Kong *et al*., 2012).

Along with silencing gene promoters, EZH2 has also been demonstrated to silence micro-RNAs that regulate biological processes such as apoptosis. EZH2 silences miR-205 and miR-31 that normally promote apoptosis by targeting anti-apoptotic protein Bcl-w. This in turn provides resistance against

these apoptotic pathways that contribute to chemoresistance against drugs (Zang *et al*., 2014).

The repression of miRNAs mediated by EZH2 can also influence the post-transcriptional outcome of genes that these miRNAs can bind to. One such example is the MMSET-miRNA-EZH2 axis where it has been demonstrated that MMSET, H3K36me2 methylase that is involved in chromosomal translocation t(4;14) is regulated by EZH2. The expression of MMSET positively correlates with EZH2 in metastatic prostate cancer samples. Knockdown of EZH2 in prostate cancer cell lines leads to reduced MMSET and H3K36me2 levels although knockdown of MMSET does not affect EZH2 or H3K27me3. Overexpression of EZH2 in normal prostate cells does not induce expression of MMSET suggesting that this regulation takes place at post-transcriptional level. Among a set of miRNAs that are repressed by EZH2, miR-26A, miR-31 and miR-203 are shown to bind to 3´UTR of MMSET. Therefore, repression of these miRNAs is essential for activation of MMSET. In the knockdown of EZH2, which causes reduction in MMSET, several genes loose H3K36me2. MMSET is required for cell proliferation, invasion and metastasis mediated via EZH2 (Asangani *et al*., 2013). Thus, this axis can serve to activate and repress genes that are essential for malignant processes in prostate cancer.

1.24 EZH2 co-operation with other proteins

Immunohistochemistry across a range of normal prostate and human tissues as well in early lesions and invasive cancer clinical samples shows that H3K27me3 levels are reduced in basal cells of the prostate compared to luminal cells. This correlates with other tissues and in general there is a direct association with H3K27me3 levels to degree of differentiation. Interestingly, EZH2 expression does not always correlate with H3K27me3 levels or staining and the levels are reduced in invasive carcinomas and PINs. Overexpression of MYC has been explained as one mechanism as knockdown of MYC in prostate cancer cells leads to increased levels of H3K27me3. This suggests a cooperation between MYC and H3K27me3 levels that is independent of EZH2 expression (Pellakuru *et al*., 2012)

ERG can directly bind the promoter of EZH2 in Prostate cancer cells and activate its expression. Knockdown of ERG decreases the expression of EZH2 while its overexpression increases the expression of EZH2. ERG also binds to several EZH2 target genes. Thus, it is required for EZH2 activation but supports repression on EZH2 target genes (Yu(a) *et al*., 2010).

EZH2 has been shown to cooperate with AR in transcriptional repression. In LNCaP cells stimulated with 1nM R1881, consistent with upregulation of AR induced genes, there are several genes that become downregulated. These downregulated genes tend to lack the classical ARE motif and AR is usually found at the promoters of these genes as opposed to distal enhancers. Further, these genes are associated with EZH2 and H3K27me3. AR binding to these genes is required for EZH2 recruitment and H3K27me3 deposition. These genes are usually associated with developmental regulators that are required to maintain undifferentiated state of ESCs. This could mean that these genes could aid in dedifferentiation of prostate cancer. Indeed, in androgen independent derivate of LNCaP cells, LNCaP-abl, these genes are found to be even more downregulated and contain higher levels of H3K27me3 independent of AR and androgen activation. This could also explain the eventual development of castration resistant disease in prostate cancer (Zhao *et al*., 2012). In cancers harboring *TMPRSS2:ERG* fusion, androgen stimulation shows a different binding kinetic for AR and ERG. AR is recruited to its binding sites 2 hours upon stimulation but is eventually displaced after 18 hours. On the other hand, ERG is expressed in the basal state and its expression is increased upon androgen stimulation. This results in ERG being initially bound at its binding site that tends to be distal or proximal promoters that are bound by AR at distal enhancers. ERG binding increases upon AR binding and continues to be present at 18 hours suggesting that ERG is required for silencing of AR mediated transcription. Indeed, a cooperation of ERG with EZH2 and HDACs is observed genome wide although EZH2 binding is seen at distal enhancers as opposed to promoters. This presents collaboration between EZH2, HDACs and ERG in AR transcriptional network. Most of these genes are associated with cellular migration and EMT and an example of this is Vinculin, VCL, which is required for optimal function of E-cadherin but needs to be silenced for EMT. Therefore, a rationale of this

network could be to silence AR stimulated genes that play a role in differentiation and maintenance of epithelial phenotype to promote mesenchymal transition that is required for progression of the disease (Chng *et al*., 2012).

Another example includes NOV; nephroblastoma overexpressed that plays essential roles in cell differentiation and its role in cancer is context specific. In prostate cancer, upon androgen receptor activation, AR is recruited to the enhancer region of NOV where it forms a loop with the promoter to mediate recruitment of EZH2 that leads to inhibition of *NOV*. This inhibition is necessary for AR-dependent prostate cancer cell growth and proliferation (Wu *et al*., 2014)

Scaffold attachment factor B1 (SAFB1) has been shown to regulate AR activity and shown to interact with serine/threonine kinase MST1 along with EZH2 and SUZ12. MST1 can phosphorylate SAFB1, which in turn is required for the presence of MST1 at AR binding regions. SAFB1 in complex with MST1 and PRC2 binds to AREs and silences the promoter of AR regulated genes such as *PSA*. Therefore, it can to inhibit the growth of LNCaP cells as well as PC3 cells, in the latter case, the growth defect not being attributed to AR (Mukhopadhhyay *et al*., 2014).

Additionally, it has been recently shown that heat chaperone protein 90 HSP90 can modulate the expression of EZH2 and its transcriptional repression via activation of ERK pathway. HSP90 has been previously shown to drive EMT in prostate cancer cell models and this is molecularly linked to EZH2 mediated repression of E-cadherin. Use of both ERK inhibitors and HSP90 inhibitors show that this results in decreased EZH2 and reduced H3K27me3 (Nolan *et al*, 2015).

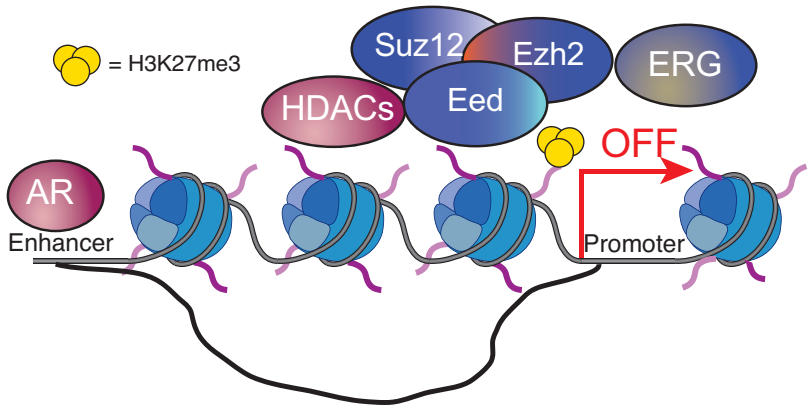

Figure 11: A model of promoter-enhancer looping mediated by AR bound at enhancer and ERG, HDACs and PRC2 at the promoter to drive AR mediated transcriptional repression.

1.25 DNA methylation and PRC2 in Prostate cancer

There are several publications suggesting that DNA methylation and EZH2 mediated silencing can occur independently or synergistically.

One of the very first genes where a cooperation of PRC2 and DNA methylation was reported is PSP94, a tumor suppressor and a protein abundantly secreted in the seminal fluid by prostate gland. There is an inverse correlation in expression with EZH2 in PC3 and DU145 cells. In PC3 cells, *MSMB*, gene-encoding PSP94 is bound by EZH2 and H3K27me3. There are two CpG islands present on the gene and treatment with 5´azacytidine leads to depression of *MSMB*. Bisulfite sequencing showed that indeed the CpG islands are methylated in PC3 cells (Beke *et al*., 2007)

ChIP coupled with CpG promoter microarrays initially revealed that H3K27me3 and DNA methylation are independent processes. Genes that are associated with DNA methylation are usually enriched for H3K4 hypomethylation and H3K9 hypermethylation with no enrichment for H3K27me3. On the other hand, genes associated with EZH2 and H3K27me3 are usually devoid of DNA methylation and lack these signatures. Further, knockdown of EZH2 does not affect DNA methylation state of silenced genes. Use of inhibitors that target either methylation or HDACs show that deprepression occurs only in the context of single epigenetic modification and does not affect silencing of the other. This study also identified new targets of H3K27me3 such as *GAS2* and *PIK3C4* that act as tumor suppressors and

silencing is required to prevent apoptosis and promote growth of cancer (Kondo *et al*., 2008).

SLIT2, neuronal repellent has been shown to inhibit migration of different cell types toward chemotactic factors. The promoter of *SLIT2* is hypermethylated in many cancers. In prostate cancer, *SLIT2* is a target of EZH2. Further, it is found to be hypermethylated suggesting a cooperation of PRC2 and methylation for effective silencing. Treatment with methylation inhibitor 5-aza and PRC2 inhibitor DZNep leads to derepression suggesting that both the factors are required for silencing (Yu *et al*., 2010)

RARβ is a tumor suppressor that is commonly silenced in many tumors. The absence of expression of RARβ in prostate cancer cell lines is mediated by DNA methylation and presence of PRC2 on its promoter (Moison *et al*., 2014; Moison *et al*., 2013). The mechanism can very between cell lines. DU145 cells show both DNA methylation and PRC2, LNCaP cells have only DNA methylation associated with RARβ promoter (Moison *et al*; 2013) whereas in PC3 cells, the silencing is mediated solely by PRC2 (Kondo *et al*., 2008)

In a recent study, MYC and EZH2 were shown to positively regulate each other expression, and cooperate with each other to silence MST1 promoter. MST1 is a kinase that has been reported previously to negatively influence tumor growth and proliferation. This promoter contains both DNA methylation and H3K27me3 and removal of either MYC or EZH2 leads to decreased DNA methylation and H3K27me3 occupancy. This suppression is shown to be necessary for androgen independence and resistance to EZH2 or MYC inhibitor induced growth retardation in LNCaP cells (Kuser-Abali *et al*, 2014).

Co-operation of DNMT and EZH2 is also reported for ID4 promoter that is commonly silenced by DNA methylation is prostate cancer. ID4 plays a role in prostate morphogenesis and loss of ID4 leads to development of PIN. In cancer cells, loss of ID4 increases invasion. Analysis of ID4 in prostate cancer cell lines where it is silenced shows that EZH2 and H3K27me3 are perhaps early events that are followed by recruitment of DNMT1 and DNA methylation. EZH2, H3K27me3 and DNMT1 co-occupy the same region in promoter of ID4. Treatment of DU145 cells with 5-azacitidine, leads to displacement of EZH2 and H3K27me3 clearly showing that the processes are related (Chinaranagari *et al*., 2014).

BAZ2A (TIP5), an epigenetic regulator that has been shown to regulate transcription of rRNA genes in non-malignant cells acquires a different role in metastatic prostate cancer cells. In PC3 cells, TIP5 executes an rRNA independent function where it physically interacts with EZH2 and aids in hypermethylation of Polycomb associated regions in specific aggressive subtype of Prostate cancer. The presence of TIP5 is required for EZH2 mediated H3K27me3 at these promoters and loss of either TIP5 or EZH2 leads to reduced occupancy of the other as well as loss of H3K27me3. They have also been postulated to act via similar pathways as they share many differentially expressed genes upon knockdown. In addition, the ability of TIP5 to interact with DNA methyltransferases could further explain the function by which DNA methylation could act as a mediator of Polycomb recruitment at these promoters or vice versa (Gu *et al*., 2015).

It has also been shown recently that expression of TET1 and 5-hydroxymethylation are reduced in prostate cancer compared to normal tissues. This paper describes a dual role of TET1 suggesting that TET1 only target genes are downregulated in prostate cancer consistent with loss of H3K4me3 and hypermethylation of their promoters whereas TET1 and PRC2 common bivalent targets contain hypomethylation and loss of H3K27me3 at their promoters in prostate cancer leading to their upregulation (Feng *et al*, 2015).

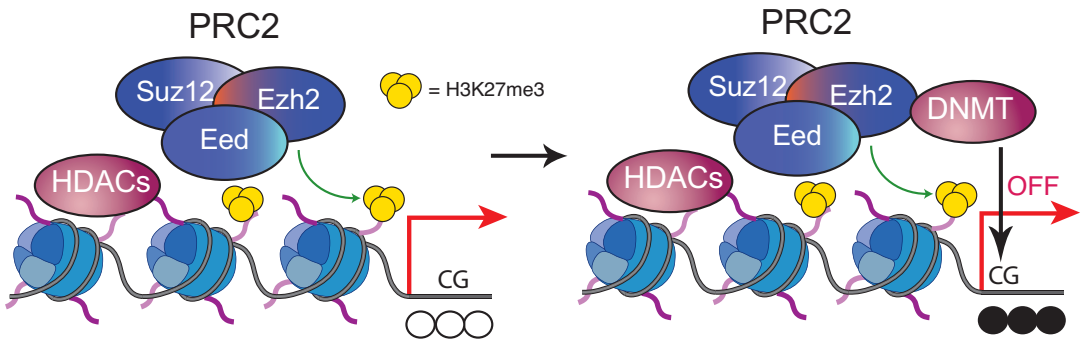

Figure 12: Co-operation of PRC2 and DNA methylation for gene silencing in prostate cancer.

1.26 Non-canonical functions of EZH2 in Cancer

EZH2 has been reported to methylate non-histone substrates independently of the PRC2 complex. The earlier observation came from the fact that often

cells exhibiting high levels of AKT are associated with low levels of H3K27me3. EZH2 was identified as substrate of AKT kinase and phosphorylation of EZH2 by AKT was shown to reduce its affinity to H3K27me3. This phosphorylation did not affect the ability of EZH2 to associate with other components of PRC2 complex but specifically its affinity to histone H3. Therefore, it was proposed that this phosphorylation could enable EZH2 to methylate non-histone targets (Cha *et al*., 2005). It was also shown that EZH2 could methylate cell specific transcription factors such as GATA4 via direct interaction in cardiomyocytes and attenuate its transcription activity by impairing its interaction with p300 (He *et al*., 2012). Specifically, in the context of prostate cancer, in androgen independent derivative of LNCaP cells called LNCaP-abl cells, EZH2 has been found to be associated with active genes and transcriptional activation. This activation is dependent on interaction with and methylation of Androgen Receptor. The levels of AR are not affected upon knockdown of EZH2 and therefore the recruitment of AR to these target genes is dependent on its methylation status. The methylation of AR is mediated by phosphorylation of EZH2 by AKT switching its role from a transcriptional repressor to an activator (Xu *et al*., 2012).

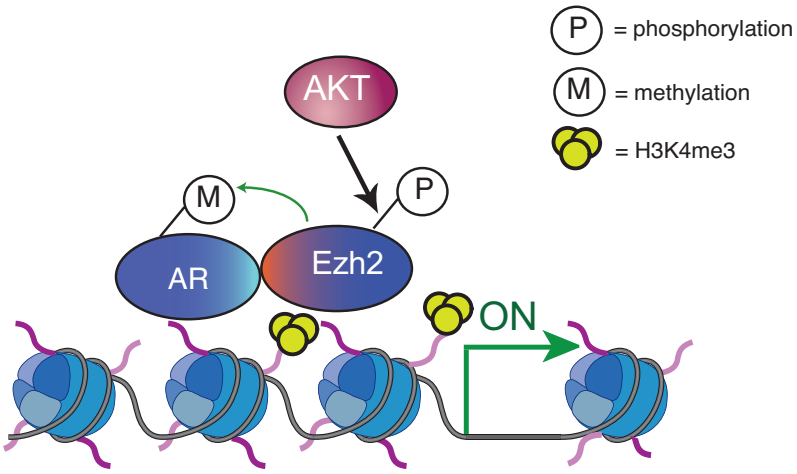

Figure 13: Polycomb independent role of EZH2 in prostate cancer. The phosho-AKT kinase phosphorylates EZH2, which in turn methylates AR. The methylated AR and phosphor-EZH2 are associated with active genes and H3K4me3 and are required for transcriptional activation. (Adapted from Xu *et al*., 2012, Science).

In a different example, EZH2 is shown to directly interact and methylate STAT3 in stem like glioblastoma cells. Further, it was shown that PI3K/AKT

mediated phosphorylation of EZH2 is required for STAT3 methylation. STAT3 methylation in turn is associated with increased transcriptional activity of its downstream target genes (Kim *et al*., 2013). These examples illustrate that in addition to repressing function of EZH2 by methylation of H3K27, it can also methylate non-histone substrates, which in turn can repress or activate transcription contributing to lineage specification, self-renewal and malignancy in cancer respectively.

1.3 Recruitment of PRC2 complex

Extensive research has been carried out to understand the recruitment of Polycomb complexes to its target genes in mammals. Different factors have been implicated in the recruitment of both PRC1 and PRC2 complex. In this chapter, relevant publications highlighting different mechanisms of PRC2 recruitment are discussed.

1.31 DNA sequence

In the context of DNA sequence, PRC2 complex has been shown to bind preferentially to CpG islands or GC rich sequences that tend to lack features of activating transcription factors in embryonic stem (ES) cells (Ku *et al*., 2008; Mendenhall *et al*., 2010). These CpG rich islands tend to be unmethylated and PRC1 complex prefers to bind CpG rich islands that are twice as longer than those bound by PRC2 and in proximity to other bivalent CpG islands (Ku *et al*., 2008). These findings have been further validated by comparison of same genes in mouse and human ES cells that lack or contain H3K27me3 confirming that the presence of dense CG-rich sequences are sufficient to recruit PRC2 (Lynch *et al*., 2012). In addition, it has been shown that presence of DNA methylation on CpG islands inhibits PRC2 binding (Riising *et al*., 2014) and de novo recruitment of PRC2 can occur in wild type ES cells lacking DNA methyltransferases (Lynch *et al*., 2008). Elegant genome editing techniques have strengthened these findings where insertion and deletion of sequences demonstrate that PRC2 binding occurs on CpG rich regions of promoters that lack any signatures of transcriptional activity (Jermann *et al*., 2014). Thus, presence of CpG rich sequences of a certain density, lack of methylation and lack of any sequence that may confer

transcriptional activation is sufficient to recruit PRC2 and gain H3K27me3. This also illustrates that PRC2 does not initiate transcriptional repression but rather maintain it (Riising *et al*., 2014).

1.32 Transcription factors

SNAIL1, a transcriptional repressor that has been shown to bind E-boxes in CDH1 promoter, in ES cells, during differentiation, depend on PRC2 for repression of Cdh1. Murine embryos, ES cells and cancer cells lacking Suz12 show that Snail1 cannot repress Cdh1 promoter leading to derepression. H3K27me3, Suz12 and Snail1 occupancy is reduced in ES cells lacking Suz12 at Cdh1 promoter. This phenomenon is not only restricted at this promoter as in other cancer cell lines this can be demonstrated on *PTEN* promoter thus suggesting an important cooperation of PRC2 and Snail1 in EMT process. In addition, the E-boxes are required for efficient transcriptional repression thus suggesting that both Snail1 and PRC2 depend on each other for transcriptional repression at specific promoters. Snail1 also interacts with members of the PRC2 complex (Herranz *et al*., 2008). Rest, a transcriptional repressor of neuronal genes in ES cells and during neuronal differentiation, coimmunoprecipitates with Cbx2 and Cbx7 in ES cells. In addition, it is demonstrated that REST is required for PRC1 occupancy at distal RE elements whereas there are no changes at proximal RE elements (Ren and Kerppola, 2011). Another study using NT2-D1 cells as a model of neuronal differentiation, upon retinoic acid stimulation, supports displacement of PRC1 at REST binding sites. Interestingly, the recruitment of PRC1 to Rest binding sites in ES cells does not depend on CpG islands or H3K27me3. Furthermore, the authors demonstrate that in Rest knockout ES cells, there is increased binding of PRC2 and H3K27me3 at CpG rich regions. Therefore, on one hand, Rest can mediate recruitment of PRC1 and on the other hand may inhibit PRC2 binding in a context dependent manner (Dietrich *et al*., 2012). Contradictingly, Epi-MARA, a computational tool to predict TFs binding sites associated with transcription factors identified REST as a potential transcription factor associated with H3K27me3. Using an *in vitro* neuronal differentiation protocol to differentiate ES cells into neuronal precursors and terminal neurons, it is shown that CpG-high promoters containing REST

binding loose H3K27me3 and SUZ12 occupancy in neuronal precursor cells from REST knockout ES cells. Targeted insertion of 1.2-2.2 kb sequences containing either REST binding sites or SNAIL binding sites is sufficient for H3K27me3 deposition (Arnold *et al.*, 2013). Lastly, it has been shown that REST can repress genes independently of Polycomb by recruitment of HDACs and lack of EED in its list of interactors in ES cells. The RE1 element was sufficient to recruit REST complex and only 3% of REST occupied sites contained H3K27me3 (McGann *et al*., 2014). Therefore, it is clear that REST has an important role in repression of neuronal specific genes in ES cells and during neuronal differentiation, however, there is not one clear mechanism explaining the mode of repression.

1.33 Long non-coding RNAs

Perhaps, the most widely studied RNA mediated recruitment of Polycomb complex is via *cis*-acting RNA, *Xist* (X inactive specific transcript) during the process of X-chromosome inactivation (XCI). The presence of components of Polycomb on inactive X chromosome (Xi) such as Eed and Enx1 is reported in XX trophoblast stem cells (TS) (Mak *et al*, 2002). This is further explored by an extensive analysis in TS, inner cell mass of embryo, and ES cells where it is shown that Eed-Ezh2 complex is recruited to Xi upon Xist induction, but this recruitment is transient and is not required during maintenance of XCI. Using a transgene expressing Xist in HeLa cells of female origin, where no XCI is present, the authors demonstrate that EED-EZH2 can be recruited upon XIST induction that leads to silencing of X chromosome. However, in ES cells containing mutant Xist transgene that cannot silence anymore, upon mutant Xist induction, there is still transient recruitment of Eed-Ezh2 which shows that Eed-Ezh2 is not required for silencing of XCI but is rather a consequence of Xist RNA coating on Xi or is only required in the initial inactivation phase (Plath *et al.*, 2003). However, during early differentiation, when the mark is established, it confers a chromosomal memory that maintains H3K27me3 later in differentiation independent of Xist (Kohlmaier *et al*., 2004). Using an inducible *Xist* expression system in ES cells, H2AK119ub1 is also deposited during early stages of Xist expression and differentiation. This mark can also be established in the absence of repeat A sequences of Xist required for

silencing. Thus, this can provide an additional layer of chromosome memory mediated by PRC1. This is evident in ES cells lacking Eed where although PRC1 components Mph1 or Mph2 cannot be recruited anymore, Ring1b can still be recruited in response to *Xist* expression suggesting a PRC2 independent role of PRC1 in XCI, as well as providing a rationale for lack of defective XCI in Eed -/- ES cells (Schoeftner *et al*., 2006). Therefore, from the above two studies, it is clear that both PRC2 and PRC1 are recruited to Xi upon Xist expression although they are not dependent on *Xist* silencing and that these events are important during early stages of ES cell differentiation and thus may place a role in establishing a chromosome memory. Mechanistic insight are further provided in a model, where in pre-XCI state, Repeat A RNA (RepA) from Xist 5´end are shown to be associated with PRC2. In this state, *Tsix*, transcriptional repressor of *Xist* competes with RepA for binding to PRC2. On the Xi, *Tsix* is supressed and RepA RNA recruits PRC2 to Xist promoter. This recruitment in turn methylates Xist, which is activated, and the full length Xist can now interact with PRC2 that leads to silencing across the Xi. Further, this silencing in maintained by interaction of Xi with PRC2 during the S-phase in the perinucleolar space (Zhao *et al*., 2008). The interaction between RepA and PRC2 has been further refined by solution structure of Xist A region which contains two long stem loop structures each containing 4 repeats. It is shown that in ES nuclear extracts, isolated 4-repeat structures from A region are required to recruit most of the components of PRC2 for X chromosome inactivation whereas entire A region is required for interaction with Suz12 (Maenner *et al*., 2010). CHART-seq, a technique that allows you to map genome wide binding profiles of lncRNA was used to study the binding of Xist in a timely manner. The Xist accumulation at the Xi is shown to be linear with PRC2 and H3K27me3 deposition. This did not occur on active X chromosome or other chromosome suggesting that this specific recruitment of PRC2 on Xi is Xist dependent (Simon *et al*., 2013).

Super resolution microscopy has been used to detect the spatial localization of Xist RNA and PRC2. Using an inducible Xist transgene system, the authors aimed to determine the sites of H3K27me3 deposition upon Xist induction. However, the authors found a very poor overlap and spatial separation

between binding sites for Xist and regions that acquire H3K27me3. One must observe that many regions that acquire H3K27me3 are found on gene bodies as opposed to gene promoters and associated with active genes instead of inactive genes. Nevertheless, this challenges if the interaction between Xist RNA and PRC2 occurs at all (Cerase *et al*., 2014). A previous study also challenged the requirement of PRC2 and H3K27me3 for the formation of Barr body in the nucleus by silent X chromosome. This study showed that PRC2 is dispensable for formation of this Barr body and that another complex that deposits H3K9me3 is required for compact Xi structure formation (Nozawa *et al*., 2013).

Using the rationale that macroH2A is enriched on regions of inactive X chromosome (Xi) along with Xist and PRC2, FLAG-macroH2A purification identified ATRX, a chromatin remodeler that plays a role in XCI. ATRX is found to be enriched on Xi by immunofluorescence and in MEFs stably knocked down for ATRX, the occupancy of Ezh2 and H3K27me3 levels are reduced on Xi. Using both male and female ESC, the authors show that in female ESC, ATRX depleted cells cannot inactivate Xi because of inability to upregulate Xist RNA and mediate Polycomb recruitment. Using UV crosslinking followed by immunoprecipitation, ATRX is shown to bind Xist RNA *in vivo* and this direct interaction is important for interaction between EZH2 and Xist RNA. ATRX binds to Repeat A of Xist RNA with high affinity and EZH2-ATRX-Xist may form a ternary complex. ATRX in general is required for correct targeting of PRC2 as loss of ATRX leads to no PRC2 recruitment on X chromosome and misplaced displacement on other chromosomes (Sarma *et al*., 2014). Thus, ATRX may provide a RNA mediated recruitment of PRC2 in a context specific manner.

To understand the general binding kinetics of PRC2 with RNA, it was shown that PRC2 binds to RepA RNA with higher affinity although its can bind RNAs in a promiscuous manner (Davidovich *et al.,* 2015). Recently, SHARP has been identified as a novel protein that binds to Xist RNA. This protein interacts with SMRT repressor that recruits HDAC3 that deacetylates histones and is required for recruitment of PRC2 complex to X-chromosome. This also excludes RNA polymerase II across the X chromosome (McHugh *et al*., 2015).

There are several other lncRNA that have been identified in the due course that interact with PRC2. *Kcnq1ot1*, lncRNA is expressed in the nucleus and interacts with Ezh2 and G9a to establish H3K27me3 and H3K9me3 at distant and nearby imprinted genes in placenta. This is not evident in the liver where it is expressed at the same level suggesting that different factors may exist in embryonic lineage (Pandey *et al*., 2008). *HOTAIR*, is shown to interact with PRC2 complex through its 5´region and LSD1/CoREST/REST complex with 3´region. This dual binding can aid in demethylation of H3K4me2 from PRC2 bound regions allowing PRC2 to then deposit H3K27me3. The interaction is found in HeLa cells and in primary foreskin fibroblasts it has been shown that HOTAIR dependent recruitment of PRC2 and LSD1 complex is required for effective silencing of *HOXD* locus. This has been extended genome wide and although this phenomenon may not occur on all the genes, several genes are found to depend on HOTAIR for the presence of H3K27me3 and LSD1 on their promoters (Tsai *et al*., 2010). Mechanistic insight into the binding properties of PRC2 with HOTAIR are provided by a study that showed that EZH2-EED heterodimer interacts specifically with 89-mer sequence of HOTAIR RNA, a sequence that is highly structured. This structure differs from the RepA of Xist RNA previously described thus showing that PRC2 can bind to different lncRNAs in different ways (Wu *et al*., 2013).

In addition, another lncRNA, *ANRIL*, transcribed in reverse direction to *INK4A-ARF-INK4B* gene cluster, is proposed to recruit PRC2 and H3K27me3 deposition at this locus. Deletion of *ANRIL* in WI38 fibroblasts results in specific upregulation of *p15(INK4B)* and loss of SUZ12 and H3K27me3 at the *p15(INK4B)* locus. It is also demonstrated that *ANRIL* and SUZ12 interact *in vivo*. Consequently, this results in reduced cell proliferation and senescence (Kotake *et al*., 2011).

RIP (RNA immunoprecipitation)-seq has been developed to identify RNAs interacting with PRC2. It was shown that more than 9000 RNAs are present in ES cells that can interact with PRC2. This study also identified Gtl2 RNA required to recruit PRC2 to imprinted region of Dlk1 (Zhao *et al*., 2010). Custom designed microarray has been used to identify new lncRNA in a model of hESCs differentiated to neuronal precursor cells (NPCs) and mature neurons with more than 90% efficiency. lncRNA_ES1 and lncRNA_ES2 were

identified to have NANOG and OCT4 binding sites close to their TSS suggesting a role in pluripotency. RIP experiments showed that these lncRNA interact with SOX2 and SUZ12 and depletion of either leads to loss of pluripotency. The authors also identified lncRNAs important for neurogenesis and found them to interact with SUZ12 and REST complex. Loss of neuronal specific lncRNAs switches the cell differentiation state from neurogenic to gliogenic (Ng *et al*., 2012). This strengthens the hypothesis that lncRNA can interact with multiple complexes thus acting as scaffold on the target gene for effective complex recruitment and action.

Braveheart (Bvht), was identified in mouse necessary for cardiovascular lineage commitment. It interacts with Suz12 and control a network of core transcription factors involved in cardiac differentiation (Klattenhoff *et al*., 2013). Along the same time, *Fendrr* was discovered, required for lateral mesoderm differentiation in the mouse. *Fendrr* interacts with PRC2 complex and recruits it to silence lateral plate mesoderm (LDM) genes *Fox1, Pitx2 and Irx3*. These genes loose Ezh2/Suz12 and H3K27me3 in the absence of *Fendrr*. On the other hand, on genes such as *Gata6* and *Nkx2-5*, there is no change in H3K27me3 levels but increased levels of H3K4me3 suggesting that Fendrr interaction with PcG inhibits the Trithorax complex. Thus, it seems to be required for fine-tuning of transcription of LDM genes regulating heart and body wall formation and cardiac mesoderm differentiation (Grote *et al*., 2013).

Lastly, *ANRASSF1*, lncRNA, transcribed from the reverse strand of *RASSF1A* gene, interacts with DNA to form DNA/RNA hybrid and specifically recruits PRC2 to the *RASSF1A* promoter and not other isoforms or nearby genes leading to silencing of this tumor suppressor in cancer cells (Beckedorff *et al*., 2013)

1.34 Accessory proteins

JARID2, AEBP2, and PCLs interact with fraction of PRC2 complex in different cellular contexts. It has been proposed that these complexes can provide targeting specificity to the complex. In the following paragraph, a detailed overview of each protein has been described.

JARID2

Two studies in the same year independently demonstrated and identified a novel binding partner of PRC2 called JARID2. Mass spectrometry using two different approaches identified Jarid2 to interact with PRC2 complex. Jarid2 is not a core subunit of PRC2 complex and only a fraction of PRC2 complex contains Jarid2 (Peng *et al.,* 2009; Shen *et* al., 2009). Peng *et al.*, 2009 showed Jarid2 directly interacts with Suz12 via a conserved amino acid motif whereas Shen *et al.,* 2009 showed that this occurs via Ezh2 and its SET domain. ChIP-seq studies showed that almost all PRC2 targets are Jarid2 targets and bind to CCG-rich repeat motif. Jarid2 and PRC2 depend on each other for binding to their target genes as depletion of one leads to displacement of the other. Although Jarid2 is required for PRC2 recruitment, it inhibits the HMT activity of the complex instead of activating it. This is supported by the fact that depression of genes associated with Jarid2 knockdown is not dependent on H3K27me3 (Peng *et al.*, 2009; Shen *et al*., 2009). Jarid2 may play a role in fine tuning H3K27me3 levels as Jarid2 knockout ES cells show increased level of Oct4, delay in differentiation and compromised lineage commitment (Shen *et al.,* 2009). In the following year, two other studies study demonstrated the same results showing in addition that Jarid2 is required for H3K27me3 at the promoters bound by PRC2 and Jarid2 (Li *et al*., 2010; Pasini *et al.*, 2010). Jarid2 knockdown leads to global reduction in the levels of H3K27me3 and H3K27me2 and does not affect PRC2 enzymatic activity (Pasini *et al.,* 2010). Further, Jarid2 stimulates PRC2 mediated mono and dimethylation of H3K27 *in vitro* as opposed to inhibiting it (Li *et al*., 2010). Both the studies used embryoid bodies to study differentiation and supported the results published earlier observing increase in pluripotency markers and delay in expression of genes associated with differentiation. Further, Jarid2 has also been shown to be necessary for recruitment of PRC1 complex and poised RNA polymerase II at bivalent genes and loss of Jarid2 results in reduced levels of H3K4me2/me3 and H3K27me3 (Landeira *et al*., 2010). The function of Jarid2 has also been extended to adult tissues where it is shown that Jarid2 loss leads to increase in differentiation and decrease in proliferation in epidermal progenitors of the skin. This is consistent with reduced occupancy of Polycomb components and reduced H3K27me3 on

genes associated with epidermal differentiation (Mejetta *et al.*, 2011). In *Drosophila*, Jarid2 is part of the PRC2 complex but inhibits H3K27me3. Upon overexpression of *Jarid2*, Su(z)12 and H3K27me3 are displaced from chromatin. The occupancy of Jarid2 on *Hox* genes is very low and therefore given as a rationale for non-identification of this factor in Polycomb mutant screens in *Drosophila* (Herz *et al.*, 2012). A nucleosome-binding domain using PRC2-Jarid2 HMT assays has been identified for Jardi2 between residues 350-450. Further, Jarid2 has been shown to stimulate in addition, the PRC2-Ezh1 complex (Son *et al*., 2013).

A new role has emerged for Jarid2, where it binds HOTAIR, long non-coding RNA (lncRNA) *in* vitro via an internal fragment spanning residues 332-358. The interaction of Jarid2 with RNA is confirmed *in vivo* and it has been shown that Ezh2 and Jarid2 bind to 53 common lncRNAs. The authors focussed on Meg3, lncRNA that plays a role in ESCs pluripotency and found that Meg3-Jarid2 interaction is required for PRC2 and H3K27me3 deposition at regions dependent on Meg3. Many of the differentially bound regions in *Meg3*+ and *Meg3*- ESCs are associated with embryonic development. In a mutant lacking the RNA binding region of Jardi2, PRC2 is not recruited to *HOX* locus in foreskin fibroblasts suggesting a link between *HOTAIR* lncRNA and JARID2 (Kaneko *et al*., 2014). Using polymorphic female ESCs differentiated towards Epi stem cell sate as a model of X chromosome inactivation (XCI), it has been shown that Jardi2 through its N-terminal region implicated before in binding to RNA mediates interaction with Xist RNA that is required for XCI. Jarid2, Xist and Ezh2 localize chromosome wide as opposed to localized region on X chromosome. The conserved repeats F and B repeats of Xist are required for Jarid2 and PRC2 recruitment to X chromsome. A functional PRC2 or H3K27me3 are not required for Jarid2 recruitment by Xist RNA although in Jardi2 depleted female ESCs, there is a general delay in differentiation affecting XCI and PRC2 recruitment to X chromosome (da Rocha *et al.*, 2014). A mechanism was later proposed where *cis*-regulatory RNA was shown to mediate recruitment of PRC2 to its targets but inhibiting PRC2 enzymatic activity. Jarid2 weakens this interaction between RNA and PRC2 thereby allowing PRC2 to load onto the chromatin and preventing this inhibition (Cifuentes-Rojas *et al.*, 2014).

Lastly and recently, it has been shown through lysine methyltransferase assays that JARID2 is methylated by EZH2 at lysine 116. By using specific antibodies against di and tri-methylated JARID2, the authors show that this mark is lost in Eed -/- ES cells. The occupancy of methylated Jarid2 completely co-localizes with total Jarid2. The methylated Jarid2 binds with higher affinity to Eed aromatic cage than H3K27me3 due to increased contacts and thus may help in allosteric activation of PRC2 activity. The methylated Jarid2 is also required for H3K27me3 on an artificial promoter although it does not affect PRC2 occupancy. This study although provides interesting biochemical links that could explain the role of Jarid2 with PRC2, however, lacks mechanistic links as to how this can modulate changes or recruitment of PRC2. The authors do not observe any role of methylated Jarid2 in ES cell pluripotency and provide weak evidence that it may have a role in differentiation. Lastly, they demonstrate that in Jardi2 knockout and the K116A mutant, there is a loss of H3K37me3 from promoters and gain of peaks in other regions that are not associated with genes (Sanulli *et al*., 2015).

AEBP2

AEBP2, a transcriptional repressor and zinc finger protein initially identified to be able to bind to promoter region of adipose P2 gene *in vitro* (He *et al*., 1999), interacts with all the members of the PRC2 complex and enhances the catalytic activity of the complex (Cao and Zang, 2004). Mammalian AEBP2 consists of two isoforms with a specific expression pattern in embryo and adult tissues. The protein binds to a DNA-binding motif, CTT(N)15-23cagGGC. This loci map closely to known PRC2 loci and co-occupancy experiments show that AEBP2 and SUZ12 bind to the same loci. The DNA binding ability of AEBP2 is postulated to be a mechanism through which PRC2 may be recruited to its target genes (Kim *et al.*, 2009). However, it was later shown that although AEBP2 does increase the activity of the PRC2 complex is histone methyltrasnferase assays; the binding to either nucleosomes or DNA ccannot not be detected (Son *et al.*, 2013). Lastly, the cryoEM structure of PRC2-AEBP2 has been constituted and it is proposed

that AEBP2 could act as an allosteric factor to stabilize the complex through DNA binding (Ciferri *et al*., 2012)

The last family of accessory proteins that have been implicated in recruitment of PRC2 include Polycomblike group of proteins (PCLs). These are discussed in detail in the next chapter.

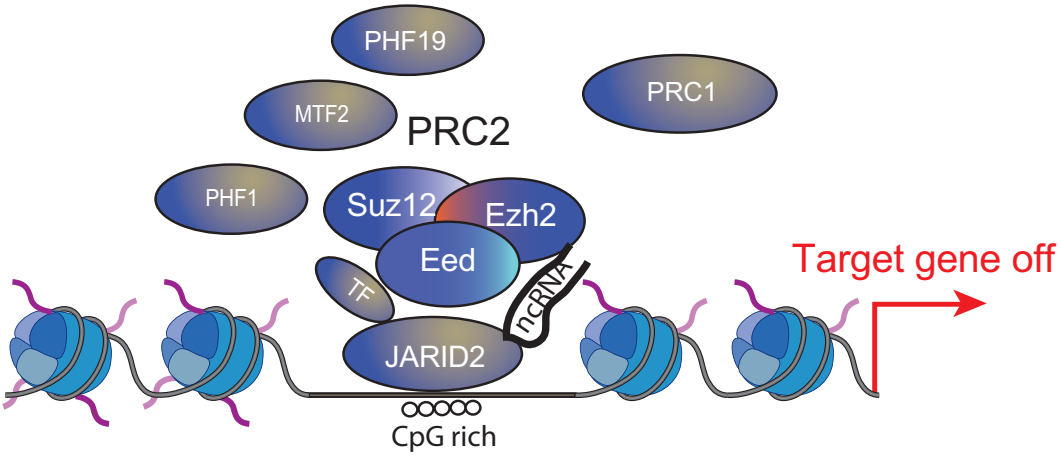

Figure 14: Mode of PRC2 recruitment widely described in ES cells. DNA sequence, transcription factors, non-coding RNAs, and accessory proteins have been implicated in recruitment and target specificity of PRC2 complex in context specific manner. (Adapted from Christophersen and Helin, 2010, J Exp Med)

1.4 Polycomblike proteins (PCLs)

The polycomblike gene (*Pcl*) was first discovered in *Drosophila melanogaster* presenting the same mutant phenotype to those of PcG genes (Duncan, 1982). It was then molecularly characterized to bind to polytene chromosomes at the same loci as Polycomb proteins and repress homeotic (Hox) genes (Lonie *et al*, 1994). This then led to discovery of human polycomblike protein PHF1 and mouse Mtf2 found to have sequence similarity to *Pcl* consistent with the evidence that functional homologues exist in mammals for PcG members. Drosophila PCL contains two PHD fingers that share 55% sequence similarity with PHF1 and Mtf2 (Coulson *et al*, 1998). Pcl2 was also discovered in *Xenopus* and *Chicken*, where it was shown to regulate anterior to posterior patterning of the neural tissue (Kitaguchi *et al*, 2001) and left-right symmetry by repressing Shh expression (Wang *et* al, 2004) respectively. The same group (Wang *et al*, 2004) also characterized the role of mouse Pcl2.

Pcl2 was expressed at different stages of embryonic development and predominantly expressed in skin, thymus and testis in adult mouse. Gene trap studies were employed to generate a mutant mouse for Pcl2 which showed defects in posterior transformation of axial skeleton consistent with phenotype shown by PcG mutants but showed normal development of left-right axis (Wang(a) *et al*, 2007). Finally, the third novel human homologue of the *Drosophila* PCL protein, hPCL3 was discovered. The gene was found to be located on chromosome 9q33.3 and code for two transcripts *hPCL3L* and *hPCL3S*, both of which were found to be upregulated in a wide variety of cancers (Wang (b) *et al*, 2004).

Figure 15: The three PCL paralogues in humans – PHF1, MTF2 and PHF19.

In vitro binding assays were used to show the direct interaction of E (Z) with PCL mediated by plant homeodomain (PHD) fingers domain of PCL. A similar association between PHF1 and EZH2 was also reported by the same study (O´Connell *et al*, 2001). This raised the possibility that PCL is maybe a subunit of a subset of ESC.E(Z) complexes. This complex was further characterised and it was shown that PCL binds to ESC.E(Z) in a 1-MDa complex that is different from the prominent 600-kDa complex. PCL was shown to be present in complex with ESC.E(Z) and histone deacetylase RPD3. Almost complete colocalization was observed for E(Z) and PCL and some colocalization was observed with RPD3 on polytene chromosomes strengthening the evidence that PCL functions with PcG (Tie *et al*, 2003). Functional insight into the epigenetic role was provided by biochemical purification of the Pcl-PRC2 complex in Drosophila that confirmed that Pcl exists in a stable complex with PRC2 and only a fraction of PRC2 complex is associated with Pcl. The Pcl protein was shown to play a role in increasing H3K27me3 on PRC2 target genes thus maintaining the PRC2 complex on these genes as the *Pcl* mutants show reduced H3K27me3 and depression of

PRC2 target genes. However, the binding of Su(z)12 and H3K27me3 is not completely lost in *Pcl* mutant suggesting that PRC2 can still be targeted to PREs independently of Pcl (Nekrasov *et al*, 2007). This provided a very important role of Pcl protein in PcG mediated repression. Specific roles of the three mammalian paralogues of Polycomblike protein later emerged in functional context.

1.41 PHF1

Two publications published at the same time characterized the role of PHF1 in relation to Polycomb and H3K27me3. PHF1 was found to elute with a subset of EZH2-EED complex in HeLa cells. Histone methyltransferase assays were used to show that this complex has increased relative activity towards oligonucleosome substrates as well as increased kinetics of methylation reaction. In GC1Spg (immortalized mouse male germ cell line), where Phf1 was initially discovered, was used to study the role of this complex *in vivo*. In general, there is upregulation of Hox genes cluster in the knockdown cells. Particularly, on HoxA10 promoter, there is an increased loss of H3K27me2 and to a lesser extent H3K27me3 and Suz12 occupancy. Pcl1 knockdown also resulted in decrease in global levels of H3K27me2 and H3K27me3 (Cao *et al*, 2008). At the same time, Sarma *et al*, 2008 validated the same findings in HeLa cells, confirming that PHF1 is found in a small fraction of PRC2 complex. They extended the binding to PHF1 to other promoters that are bound by EZH2 such as Myt1 and Wnt1 in HeLa cells. Targeting to an artificial promoter showed that presence of PHF1 increases H3K27me3 at the expense of H3K27me2. Contradictory to what was published earlier, loss of PHF1 resulted in increased levels of H3K27me2 at several HOX genes and decreased levels of H3K27me3 at these promoters resulting in deprepression. These results were consistent with loss of EZH2 at the same genes. Although this study observed the same global loss of H3K27me3, they did not observe a global decrease in H3K27me2 levels. A new role emerged of PHF1 emerged in context of DNA damage. It was shown that PHF1 is recruited at an early time point to DNA double stranded breaks upon irradiation through its Tudor domain and central region. This recruitment occurs via interaction with Ku70/Ku80, proteins involved in non-homologous end joining (NHEJ).

Proteomics analysis revealed that in addition to PRC2 complex, PHF1 also interacts with proteins involved in DNA damage such as Rad50, SMC1, DHX9 and P53 thus making it an important component of this machinery (Hong *et al*., 2008). This was further explored when p53 was shown to interact with PHF1 via its C-regulatory domain. Further, PHF1 promotes p53 stability by increasing its half-life. In the context of DNA damage, PHF1 controls p53 stability and activity as knockdown of PHF1 prevents posttranslational modifications of p53 that are required for its stability. In addition, PHF1 also controls transcription of some p53 target genes. Lastly, PHF1 prevents MDM2-mediated ubiquitynation and degradation of p53 and leads to reduced cell proliferation and induced apoptosis in response to DNA damage (Yang *et al*., 2013). Another novel function of PHF1 emerged in its ability to bind H3K36me3 via its TUDOR domain. This is discussed more in detail with PCL3/PHF19.

1.42 PCL2/MTF2

In ESCs, Mtf2/Pcl2 was demonstrated both to maintain a check on the pluripotency network (Walker *et al*, 2010) and target PRC2 for X chromosome inactivation (Casanova *et al*, 2011). *Pcl2* was shown to be uniquely expressed in ESCs and embryonic development and play a role in early commitment of ESCs and differentiation. It directly interacts with SUZ12 and PRC2 complex without affecting the stability of the complex. Pcl2 knockdown in ESCs has increased self-renewal capacity as demonstrated by increase in the number of Oct4 +ve cells in the knockdown and small compact embryoid bodies that still retain alkaline phosphatase positive cells as opposed to a differentiated morphology. ChIP-sequencing experiments demonstrated that Pcl2 binds to subset of PRC2 target genes and is required for the occupancy of Suz12 and H3K27me3 on those genes and to a lesser extent Ezh2. Among key genes, are *Tbx3*, *Foxd3* and *Klf4*, all of which have been shown to be involved in cell commitment. Therefore, it is suggested that Pcl2 maintains a check of the pluripotency network in ESCs and required to commit to a certain cell fate (Walker *et al*, 2010). The other study confirmed the same results and mapped the interaction and targeting of the complex to PHD2 domain of Pcl2. They found that Pcl2 colocalizes with Xist both *in vivo* and *in vitro* and that depletion

of Pcl2 leads to reduced Ezh2 colocalization with Xist RNA in ES cells differentiated for 3 days (Casanova *et al*., 2011). Lastly, a context dependent function of Pcl2 was proposed in gene repression with PRC2 and PRC1 on *Hox* genes during axial development but an activating function on Cdkn2a genes during replicative stress possibly by inhibition of PRC2 activity (Li *et al*., 2011).

1.43 PHF19/PCL3

hPCL3L consists of 15 exons whereas *hPCL3S* shares its first 4 exons with *hPCL3L* and contains a specific exon 5. The gene is also known as PHD finger protein 19 (PHF19) and the two isoforms as hPHF19L and hPHF19S. The two transcripts encode two different proteins. PHF19L contains a Tudor domain, two PHD fingers PHD1 and PHD2, and a C-terminal domain MTF2 factor 2. The short isoform contains only a Tudor and PHD1 domain.

Figure 16: PHF19 isoforms and their domains in Human.

Co-immunoprecipitation experiments of tagged PHF19L and PHF19S revealed that both isoforms interact with EZH2 and EED, the short isoform with much less efficiency. The Tudor domain and the PHD2 domain were implicated in binding to PRC2. It was also demonstrated that the short isoform is mainly cytoplasmic whereas the long isoform is predominantly nuclear. However, most of the experiments were performed using tagged proteins that were ectopically expressed in 293T cells and only PHF19L was shown to interact with EZH2 endogenously (Boulay *et al*, 2011).

Gainful insights came into light when it was demonstrated that PHF19 interacts with PRC2 complex endogenously as shown by mass spectrometry and endogenous co-immunopreciptation in ES cells. It was also shown that loss of Pcl3 leads to spontaneous differentiation (Hunkapiller *et al*., 2012) and

some defects during differentiation into correct lineages (Ballare *et al*., 2012). Lastly, ChIP-seq experiments showed that Pcl3 occupies most of the PRC2 targets in ES cells and depletion of Pcl3 causes global reduction of H3K27me3 and loss of Suz12 occupancy at target genes (Ballare *et al.*, 2012; Brien *et* al., 2012; Hunkapiller *et al.*, 2012). Initially, TUDOR domain of Pcl3 was implicated in this function. One should mention that Pcl2 was also found to occupy CpG rich targets along with Pcl3 although in different complexes (Hunkapiller *et al*., 2012). Indeed, the breakthrough in identifying the unique function of Polycomblike proteins came in 2012 when two independent groups demonstrated the unique ability of the Tudor domain of PHF19 to bind to and read H3K36me3. This thereby explained a transition mechanism of how PRC2 complex can be recruited to active genes in ESCs to ultimately silence them. Histone peptide arrays were employed to identify the histone binding property of different domains of PHF19. The Tudor domain of PHF19 was found to bind H3K36me3 with high affinity. NMR structures revealed that the Tudor domain of PHF19 can form a complete aromatic cage that lacks in *Drosophila* Pcl protein and this aromatic cage can efficiently bind to H3K36me3. It was further demonstrated that Phf19 can recruit histone demethylases No66 or Kdm2b that removes the H3K36me3 from the histones bound by PHF19. This then allows the PRC2 complex to deposit H3K27me3 mark that leads to gene silencing. This mechanism is required for several genes important for ESCs pluripotency as well as lineage specific differentiation. Thereby, ESCs lacking Phf19 show defects in self-renewal as well as incorrect differentiation (Ballare *et* al, 2012; Brien *et al*, 2012). These findings were further extended to PHF1, which was also shown to bind to H3K36me3 and recruit PRC2 to target genes (Qin *et al*, 2013; Cai *et al*, 2013). However, PHF1 is expressed at very low levels in ESCs and therefore may have this function in different cell systems.

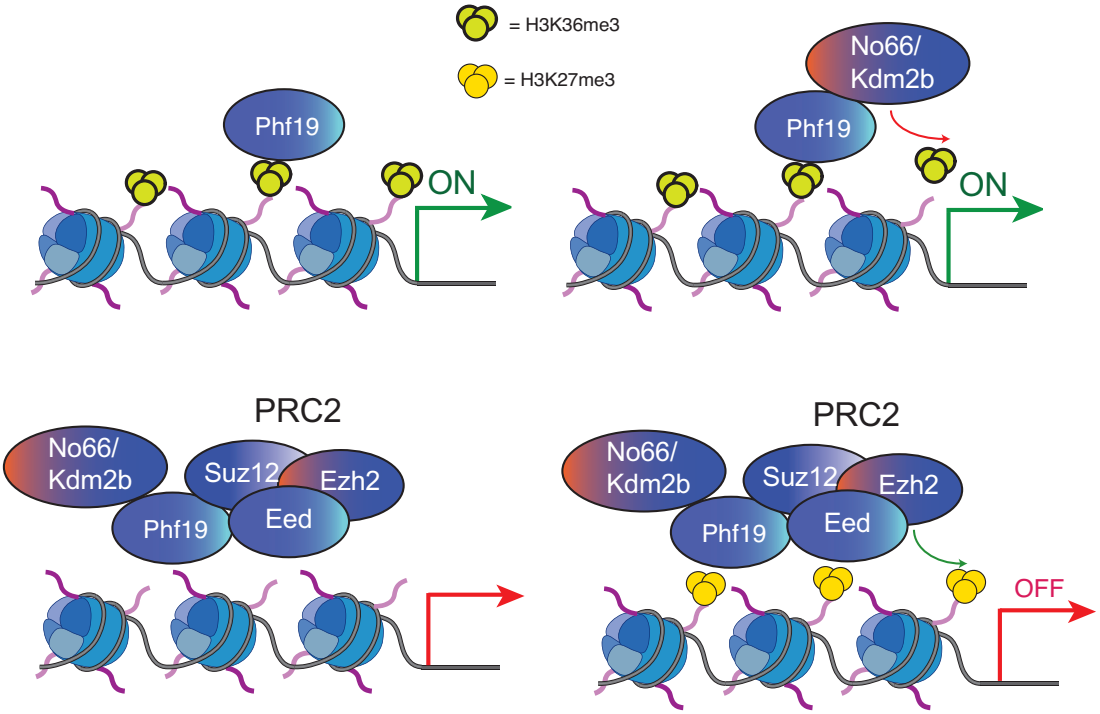

Figure 17: Model of Phf19 mediated transcriptional repression by PRC2 in ES cells. Phf19 via its Tudor domains reads H3K36me3 and binds to it. It recruits histone demethylase that removes H3K36me3 allowing PRC2 to be recruited to these genes via direct interaction with PRC2. The PRC2 complex then deposits H3K27me3 leading to transcriptional silencing. (Adapted from Ballare *et al*., 2012, Nat Struc Mol Biol).

There are few publications describing the role of PHF19 in Cancer. PHF1 and PCL3 can act as corepressors of Hypermethylated in Cancer 1 (HIC1), a tumor suppressor hat regulates cellular, growth and survival. PHF1 and PCL3 interact with HIC1 through their TUDOR and PHD2 domain whereas the opposite is mediated via BTB/POZ domain. Through interaction with Polycomblike proteins, HIC1 can recruit PRC2 complex to its target genes to repress them (Boulay *et al*., 2012). In melanoma cell lines cultured in neural crest stem culture condition, that causes them to become more invasive and less proliferative and loss their differentiated phenotype, PHF19 is downregulated and Oct4 and Nanog are upregulated. Loss of PHF19 decreases proliferation but increases the transendothelial migration capacity of melanoma cells. The mechanism was proposed via AKT pathway. In normal 2D cell culture conditions, AKT is phosphorylated and this p-AKT activates PHF19 and represses Oct4 and Nanog promoters. In neural crest

medium, the levels of p-AKT are reduced thus leading to decrease in PHF19 and increase in Oct4 and Nanog levels (Ghislin *et al*., 2012). Thus, at the present moment, there is no direct association or mechanism that explains the role of PHF19 in cancer.

OBJECTIVES

Our lab is interested in defining the different subunits of Polycomb proteins and the mechanism of recruitment in embryonic stem cells and cancer. We have already characterized the role of PHF19 in ESCs. Therefore, this project has been developed in the context of understanding the role of PHF19 in prostate cancer. The main objectives of this work are:

- Correlation of expression of PHF19 and different stages of Prostate cancer;
- Role and regulation of two isoforms in Prostate cancer;
- Gene expression changes and pathways regulated by PHF19 in prostate epithelial cells and prostate cancer cells;
- Identification of target genes of PHF19 in prostate Cancer;
- Changes in H3K27me3 to define the role of PHF19 in context of PRC2 complex in prostate cancer.

RESULTS

2. Results

2.1 PHF19 is upregulated in metastatic prostate cancer

In order to investigate if PHF19 may have a role in Prostate cancer, two previously published prostate cancer datasets were curated for the expression of the two isoforms of *PHF19*: *PHF19L and PHF19S*. The first dataset Grasso *et al.,* 2012 includes expression profiling in matched benign prostate tissues (n=12), localized prostate cancer (n=49), and metastatic castration resistant prostate cancer (CRPC, n=27). The second data set Varambally *et al*., 2005 contains expression profiling in 6 individual benign prostate, 7 primary and 6 metastatic prostate cancer samples. Scatter plot from both datasets showed no difference in expression between benign and primary/localized cancer but showed a significant increase in the expression of both the isoforms in metastatic and castration resistant prostate cancer (Figure 1 and 2). This suggests that *PHF19* may have a specific role in metastatic prostate cancer. Interestingly, *JARID2* levels did not change across the clinical samples suggesting that PHF19 may act as a specific factor for recruitment of PRC2 in metastatic prostate cancer (Figure 3).

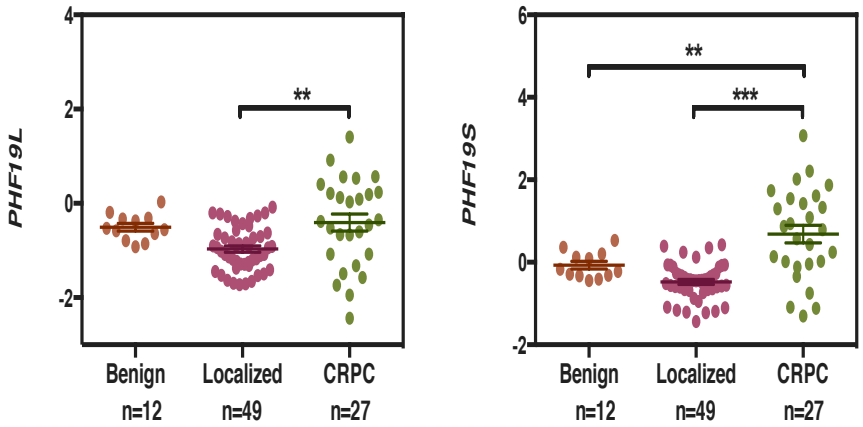

Figure 1: Scatterplot comparing the expression of *PHF19L* and *PHF19S* in Grasso *et al*, 2012 across benign, localized and CRPC. One-way ANOVA test was used to calculate significance.

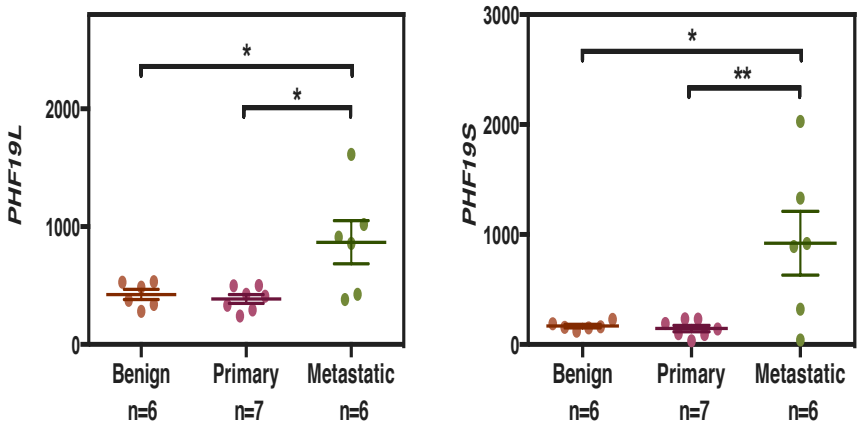

Figure 2: Scatterplot comparing the expression of *PHF19L* and *PHF19S* across benign, primary and metastatic prostate cancer from Varambally *et al*, 2005 data set. One-way anova test was used to calculate significance.

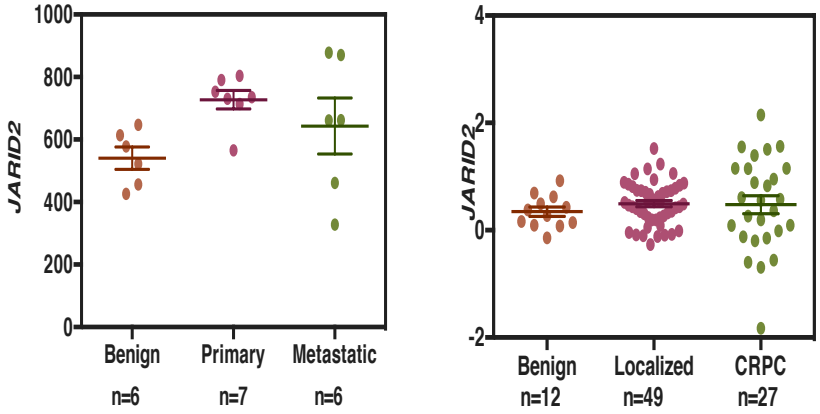

Figure 3: Scatterplot comparing the expression of *JARID2* in Grasso *et al*., 2012 (right) and Varambally *et al*., 2005 (left) data sets.

2.2 PHF19 is expressed in castration resistant androgen negative prostate cancer cells

Next, we investigated the expression of PHF19 at transcript and protein level in different prostate cancer cell lines (Figure 4). This included normal prostate cell line, RWPE1; Androgen dependent prostate cancer cell line LNCaP; and castration resistant or androgen independent prostate cancer cell lines LNCaP-abl (AR+), PC3 (AR-) and DU145 (AR-). At the transcript level, *PHF19L* was expressed at nearly the same levels in RWPE1, PC3 and DU145 cell lines with poor expression in LNCaP and LNCaP-abl cells. Similar results were observed at protein levels although there was a slight increased

expression in PC3 and DU145 cells. *PHF19S* was overexpressed at transcript levels in PC3 and DU145 cells but expressed at the same levels as *PHF19L* in RWPE1 cells. The protein level showed expression in RWPE1, PC3 and DU145 cells although at comparable levels (Figure 5). We also checked the transcript and protein expression of EZH2. As previously reported, the expression of *EZH2* gradually increases with the stage of prostate cancer and at the protein level, EZH2 is clearly overexpressed in prostate cancer cells with the highest expression in DU145 and PC3 cells. This suggests that PHF19L plays a role in normal prostate but then is specifically expressed in androgen negative prostate cancer cells whereas *PHF19S* is specifically upregulated in androgen negative prostate cancer cells. Therefore, we mainly focused on the role of PHF19L in RWPE1, DU145 and PC3 cells and the role of PHF19S in PC3 and DU145 cells.

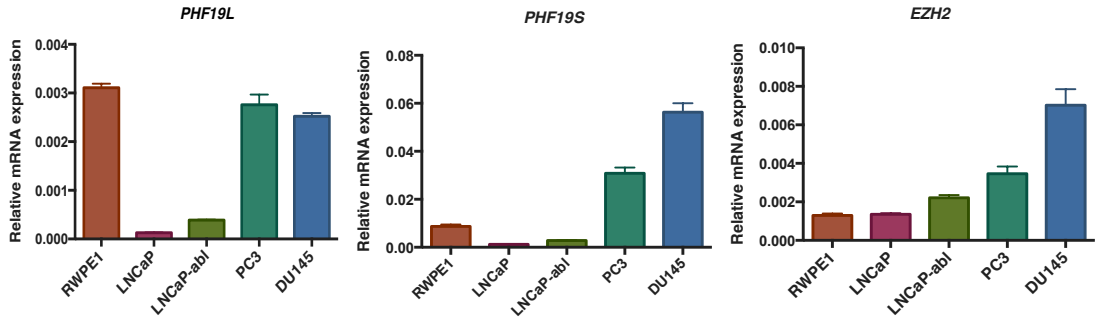

Figure 4: Expression of *PHF19L*, *PHF19S* and *EZH2* across cell lines. Error bars represent standard deviation (SD) of three independent experiments.

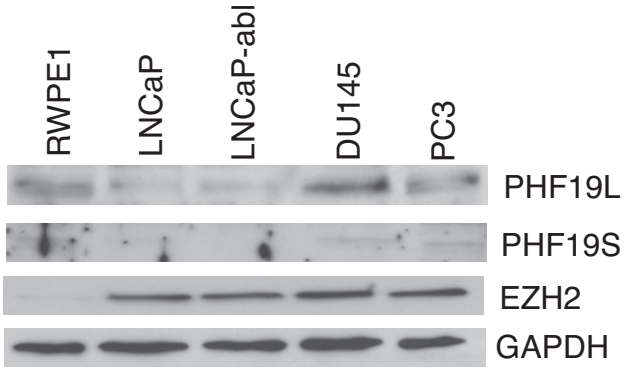

Figure 5: Western blot analysis comparing the expression of PHF19L, PHF19S, and EZH2 in different prostate cancer cell lines.

2.3 Differential interactors of PHF19L and PHF19S

Using PC3 cells as a model system to understand the role of the two isoforms, we ectopically expressed FLAG-tagged PHF19L and PHF19S followed by FLAG affinity purification and analysis using mass spectrometry. PHF19L mainly co-immunoprecipitated the PRC2 complex as has been previously described (Ballare *et al*., 2012) whereas PHF19S interacted with components of splicing and post mRNA processing machinery (Table 1). GNAI2 was identified as a common interactor. Unique peptides were found for each isoform and the two proteins did not interact with each other. This suggests an exclusive role of both isoforms in PC3 cells.

PHF19L	SCORE	PEPTIDES	PHF19S	SCORE	PEPTIDES
SUZ12	675.83	14	PHF19	251.44	7
EZH2	242.06	7	GNAI2	167.68	5
PHF19	220.95	8	RBMX	139.36	3
RBBP4	208.39	6	S10AG	112.11	3
GNAI2	158.33	4	EF2	80.68	2
RBBP7	154.35	5			
EED	150.47	4			

Table 1: Mass spectrometry score and peptides for PHF19L and PHF19S interactors in PC3 cells.

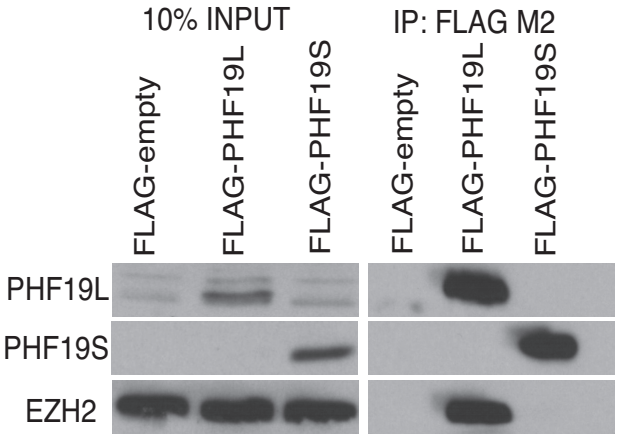

Figure 6: Co-immunoprecipitation of FLAG-empty, FLAG-PHF19L and FLAG-PHF19S with PHF19L, PHF19S and EZH2 respectively.

2.4 PHF19L is bound to chromatin and PHF19S is cytoplasmic

As most of the interactors of the short isoform were mainly cytoplasmic and involved in posttranscriptional mRNA processing, we questioned if this isoform can be recruited to chromatin. Cell fractionation revealed that the short isoform is exclusively expressed in cytoplasm whereas the long isoform is mainly chromatin bound along with EZH2 (Figure 7). GAPDH and H3 were used to assess the purity of the fractions.

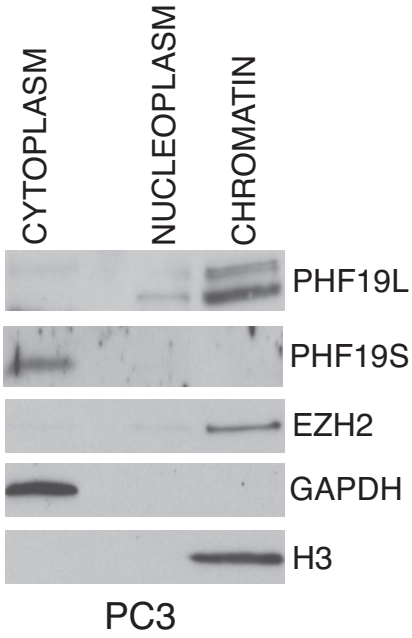

Figure 7: Western blot showing the expression of PHF19L, PHF19S and EZH2 in different cell fractions.

2.5 The two isoforms do not regulate expression of each other

Although the two isoforms do not interact with each other, they could still regulate the expression of each other. In order to verify this, we performed knockdown of both the isoforms in PC3 cells using two different shRNAs for each isoform and checked the protein expression of PHF19L, PHF19S and EZH2. The expression of PHF19S did not change upon knockdown of PHF19L and vice versa. Interestingly, the expression of EZH2 was downregulated in the knockdown of PHF19L with no change in the knockdown of PHF19S (Figure 8).

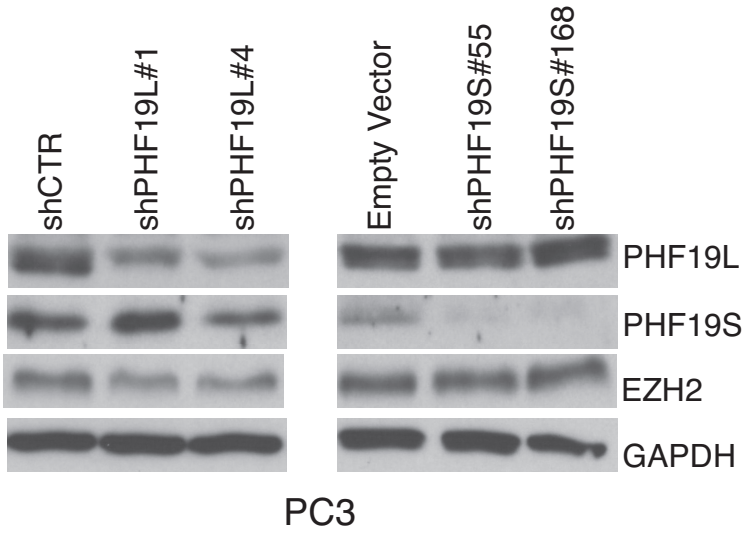

Figure 8: Expression of PHF19L, PHF19S, EZH2 and GAPDH in PC3 cells knocked down for PHF19L and PHF19S.

2.6 PHF19L knockdown does not affect the stability of the PRC2 complex in PC3 cells

We next performed co-immunoprecipitation experiments with PHF19 and EZH2 using a home made N-terminal antibody to assess if the stability of the PRC2 complex is affected in the knockdown. PHF19L interaction with EZH2 and SUZ12 is lost in both the knockdowns in PC3 cells. The stability of the PRC2 complex is not affected, as EZH2 and SUZ12 are still able to interact with each other (Figure 9). EZH2 and SUZ12 are expressed at lower levels in the knockdowns in PC3 cells as mentioned above. We also performed co-immunoprecipitation experiments of PHF19 with EZH2 and SUZ12 in DU145 cells (Figure 10). The levels of EZH2 and SUZ12 were not affected in the knockdown in these cells. The interaction of PHF19 with EZH2 and SUZ12 was lost in shPHF19L#4; however, PHF19 could still co-immunoprecipitate moderate amounts of SUZ12 in shPHF19L#1. In general, shPHF19L#4 is a stronger knockdown compared to shPHF19L#1.

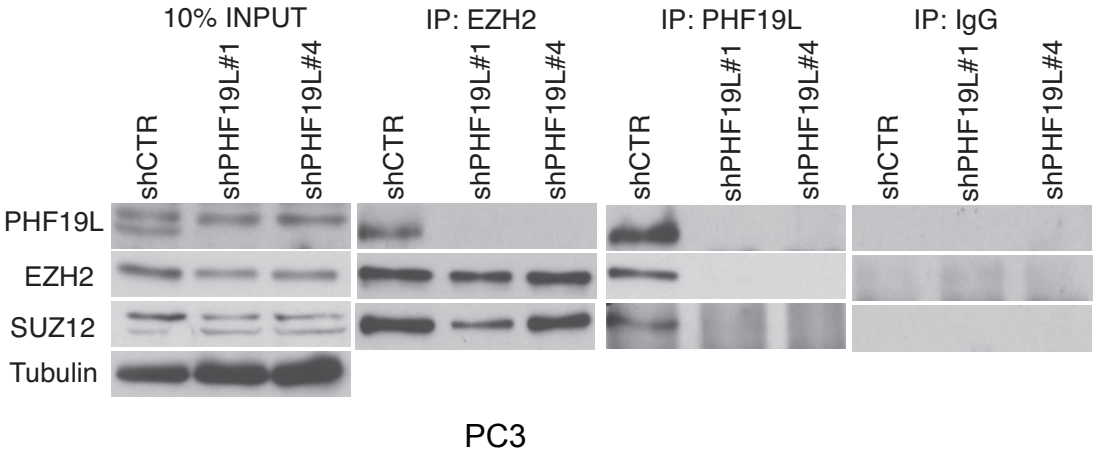

Figure 9: Co-immunoprecipitation of EZH2, PHF19L, and IgG with PHF19L, EZH2, SUZ12 in PC3 cells shCTR *versus* shPHF19L.

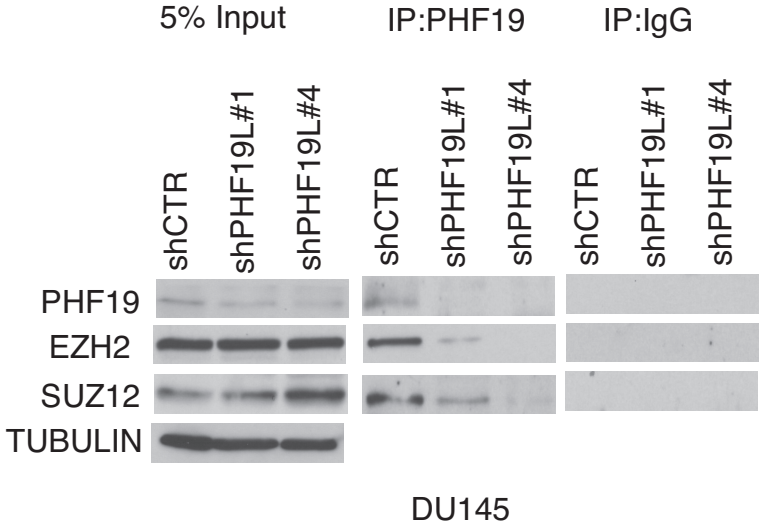

Figure 10: Co-immunoprecipitation of PHF19L and IgG with PHF19L, EZH2 and SUZ12 in DU145 shCTR *versus* shPHF19L cells.

2.7 PHF19L is required to maintain RWPE1 cells in undifferentiated state

RWPE1 cells are considered closest to transit amplifying or intermediate cells of the prostate. As the expression of PHF19L was comparable to prostate cancer cell lines, we performed RNA-seq in control *versus* knockdown to assess the function of *PHF19L* in these cells. Below is a summary of the sequencing results:

Sample	Fragments (read pairs)	Paired fragments
RWPE1 shCTR	118,275,566	75,160,086
RWPE1 shPHF19L	137,885,849	86,569,732

Table 2: Summary of total read pairs and mapped paired fragments in RWPE1 control and knockdown of the long isoform generated from paired end RNA-sequencing.

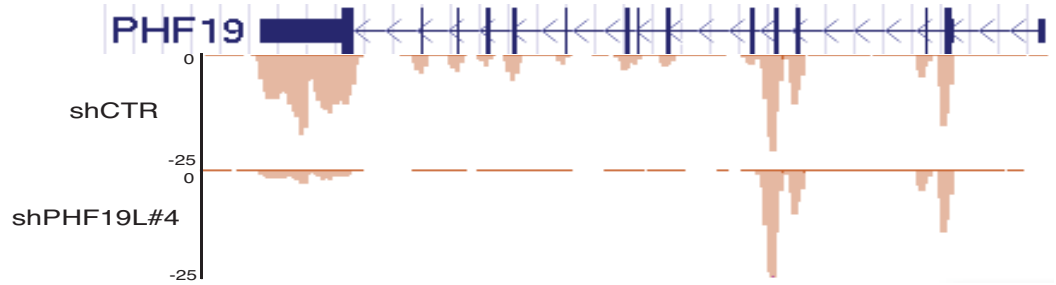

Figure 11: Screenshot from UCSC genome browser showing differences in number of reads in control and knockdown cells. The transcription from first 4 exons is attributable to the short isoform.

There were 454 genes that were upregulated and 881 genes that were downregulated. Gene ontology analysis (DAVID) suggested that genes upregulated upon knockdown were associated with differentiation whereas several transcription factors were downregulated (Figure 12).

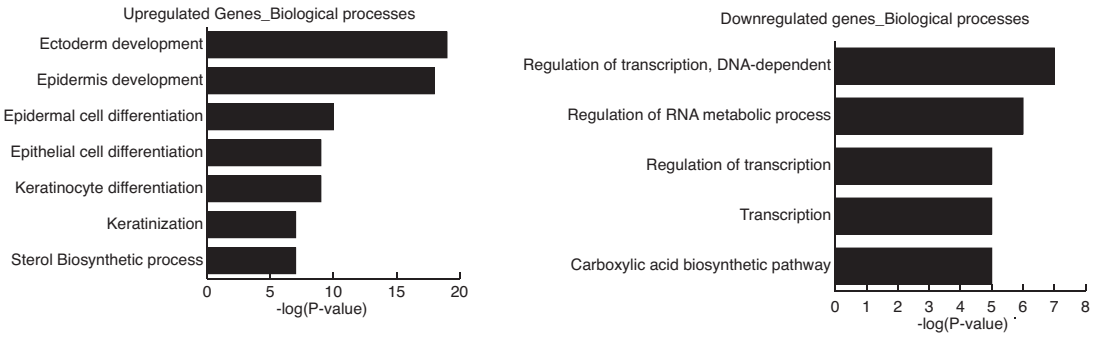

Figure 12: GO analysis of upregulated and downregulated genes in RWPE1 shCTR *versus* shPHF19L#4.

Consistent with GO analysis, differentiation markers normally associated with epithelial cell differentiation such as *IVL*, *LOR*, *CD24* and *MYC* were upregulated. It should also be noted that two actin-associated genes *ACTB* and *ACTG1* were also upregulated (Figure 13). On the other hand,

transcription factors such as *KLF4*, *TWIST1*, *and CBX4* were downregulated including *VEGFA* (Figure 13).

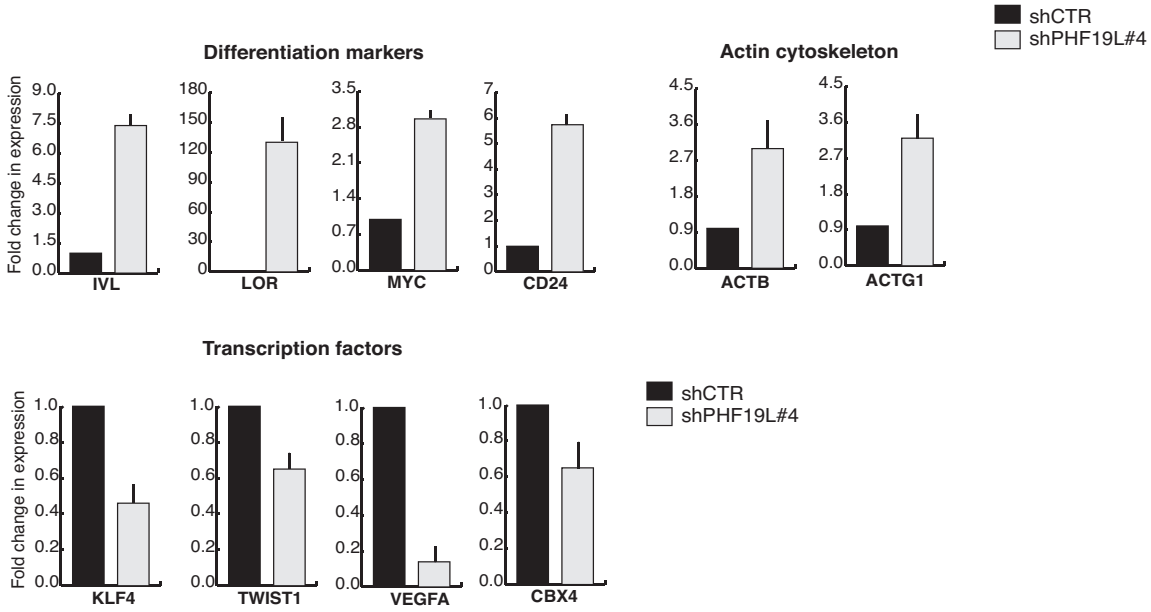

Figure 13: RT-qPCR showing differential expression of upregulated and donwregulated genes in RWPE1 shCTR *versus* shPHF19L#4. Error bars represent SD of three independent experiments.

We next compared this gene list with already published data containing differentially expressed genes upon knockdown of *EZH2* in RWPE1 cells to investigate whether the two proteins regulate the same pathways. In general, there was a poor overlap between differentially expressed genes upon knockdown of *EZH2* and *PHF19L* although *IVL* was upregulated in both the cases. This might imply a different role of PHF19L in these cells compared to EZH2.

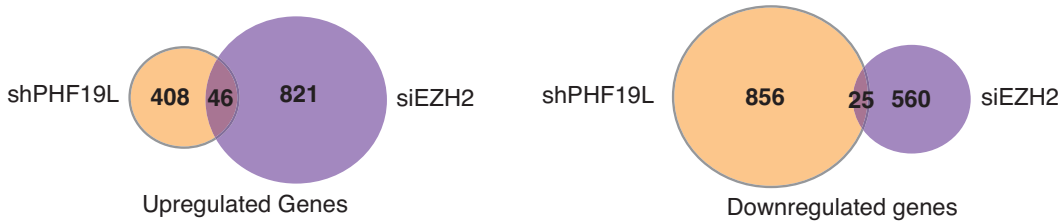

Figure 14: Venn diagram comparing differentially expressed genes in shPHF19L and siEZH2 (Gu *et al*., 2015) in RWPE1 cells.

We then looked at the morphology of the cells upon knockdown. In RWPE1 shPHF19L#4, there was a clear difference in the morphology of the cells (Figure 15). The cells had increased cell-to-cell contact and differentiated phenotype commonly observed for epithelial cells. shPHF19L#1 exhibited the phenotype to a lesser extent. These cells were then stained for Involucrin and consistent with gene expression changes, IVL was almost absent in control cells whereas the expression starts to appear in both the knockdowns (Figure 16).

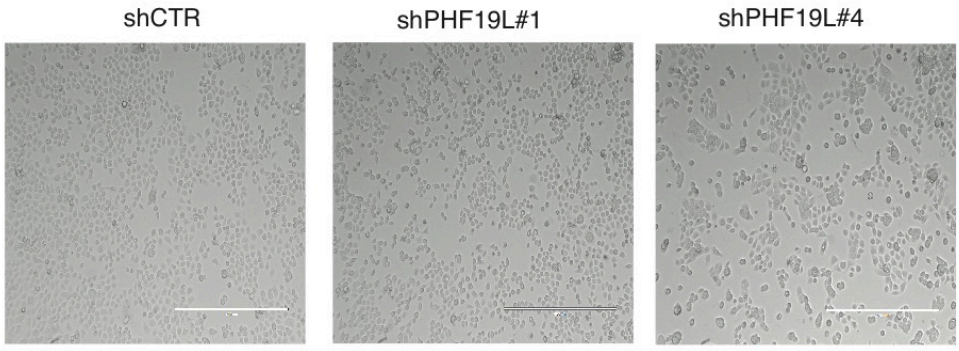

Figure 15: Phase contrast image comparing the cell morphology between RWPE1 shCTR, shPHF19L#1 and shPHF19L#4.

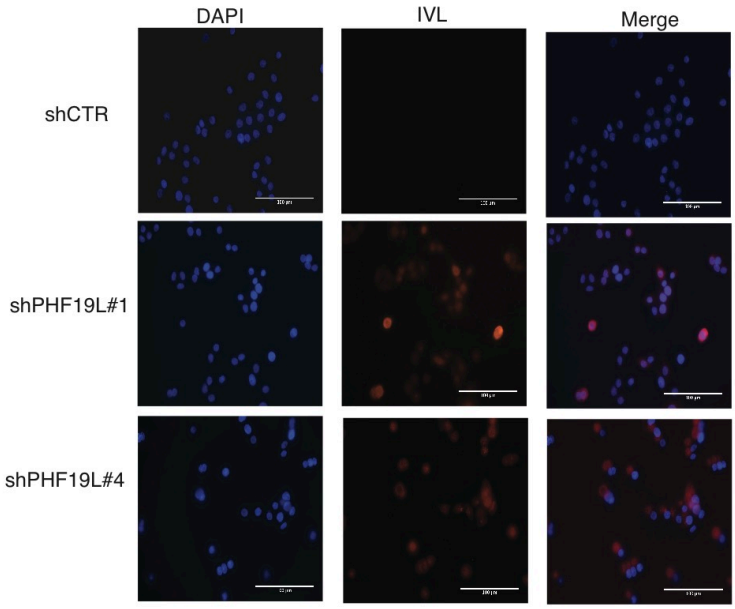

Figure 16: Immunofluorescence comparing IVL expression in RWPE1 shCTR, shPHF19L#1 and shPHF19L#4 (n=2).

As there was upregulation of *CD24*, we performed FACS analysis of control and knockdown cells using CD24 and CD44 antibodies (Figure 17-19). 61% of the cells were positive for both markers whereas 37% of the cells were only positive for CD44 (Figure 17). This is in agreement with expression profile of intermediate cells that express markers of both basal and luminal cell types. Upon knockdown, we observed a slight shift in the double stained population that is represented by a minor gain of CD24 only population (Figure 19) and loss of CD44 staining in the total population of cells (Figure 18). Although the cells are not completely differentiated, they show a tendency towards differentiation and start loosing markers of undifferentiated state.

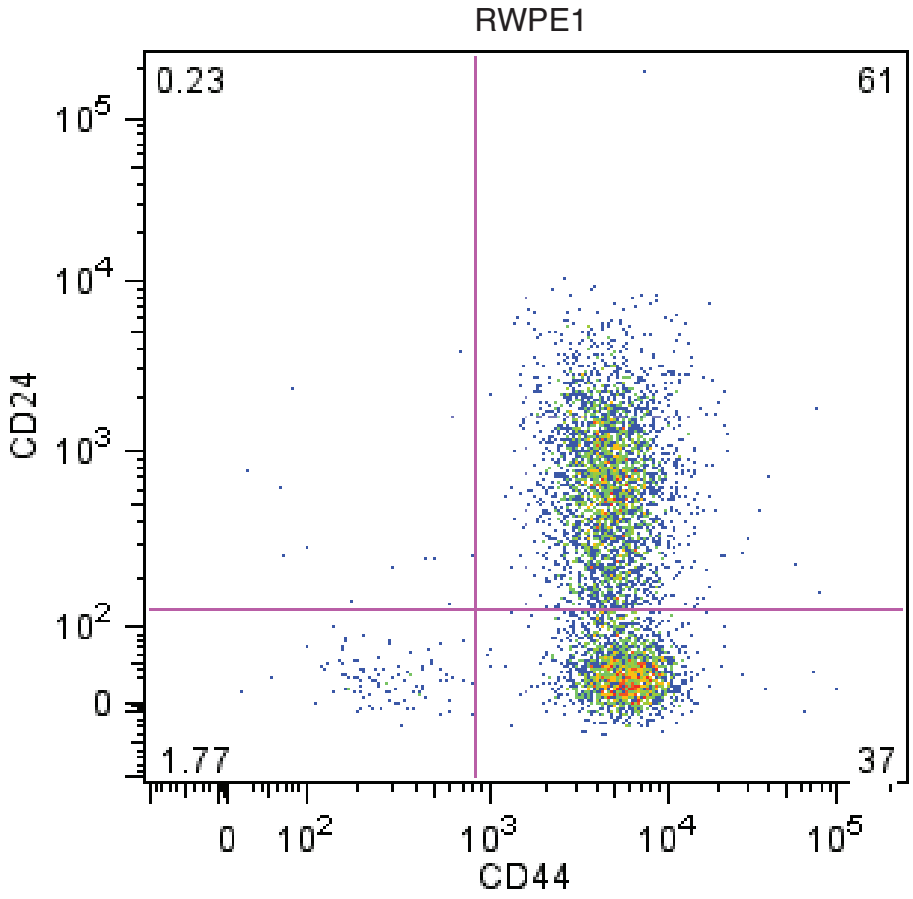

Figure 17: FACS plot showing the % of RWPE1 cells positive for CD44 and CD24

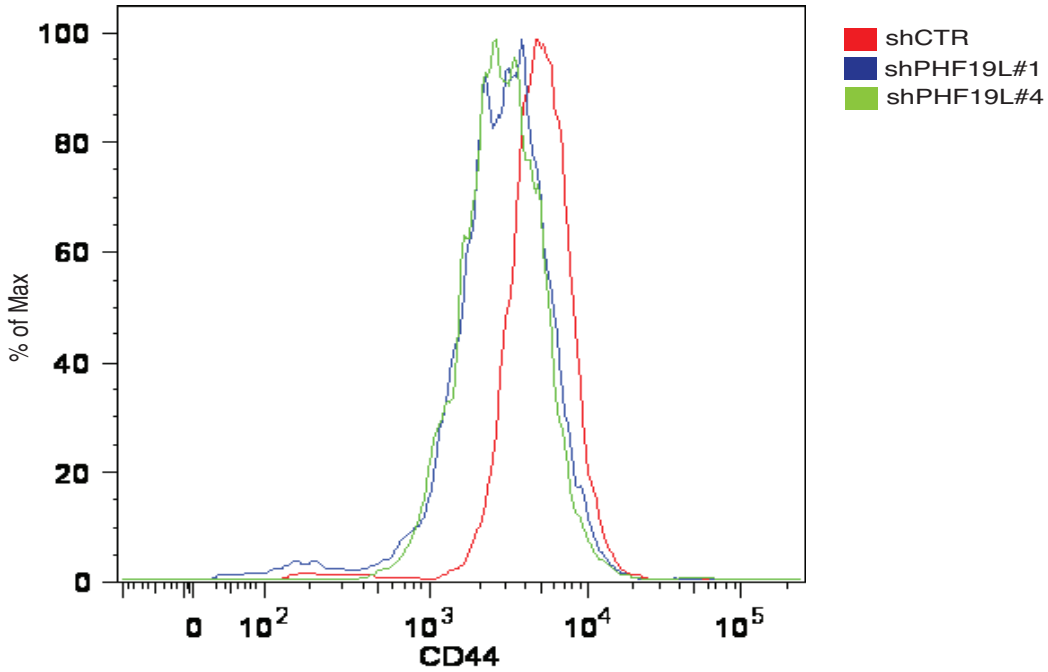

Figure 18: Histogram showing loss of CD44 surface marker in the knockdown cells. Representative image of three biological replicates.

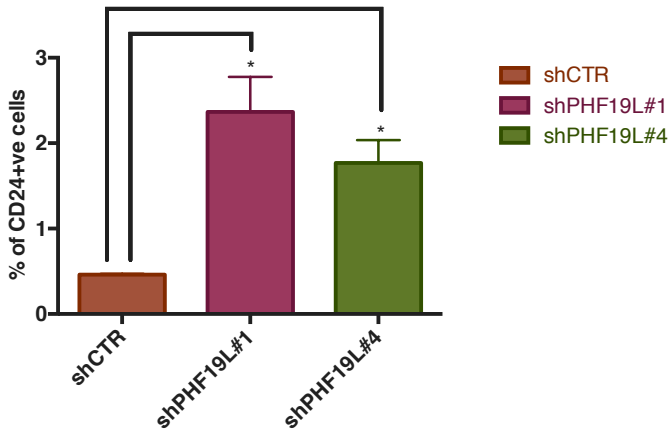

Figure 19: Column graph showing an increase in $CD24^+$ only cells in the two knockdowns in RWPE1 cells. Error bar represents SD of three biological replicates. Student t test was performed to calculate significance.

Thus in RWPE1 cells, PHF19L acts as a barrier to maintain these cells in the undifferentiated state suggesting a crucial of PHF19L in prostate epithelial cells.

As the short isoform is expressed at transcript level to a much lower level compared to prostate cancer cell lines, we next asked if the overexpression of the short isoform could provide any advantage. However, we did not observe

any changes in cell growth upon overexpression of PHF19S or PHF19L (Figure 20).

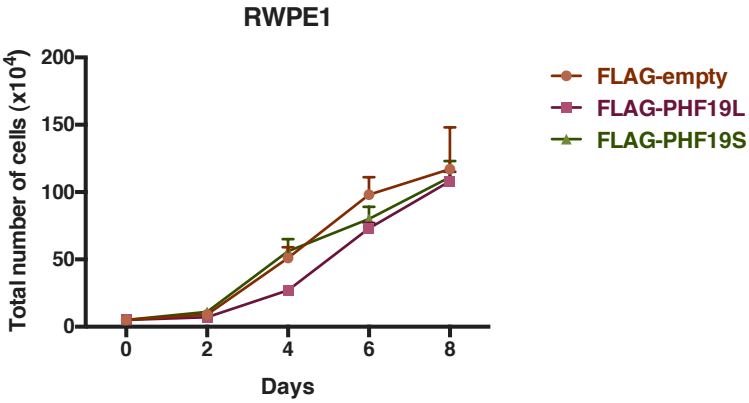

Figure 20: Growth curve showing no difference in cell growth rate over a period of 8 days upon overexpression of PHF19L and PHF19S. Error bar represents SD of three independent experiments.

2.8 PHF19L regulates different genes in PC3 and DU145 cells

As the main focus of this thesis was on prostate cancer, we next performed paired end RNA-seq for both the long and short isoform in PC3 and DU145 cells. Below is a summary of the RNA-seq results in the two cell lines for both long and short isoform.

Sample	Fragments (read pairs)	Paired fragments
PC3 shCTR	123,202,792	82,540,453
PC3 shPHF19L	113,118,884	75,678,507
PC3 shMLP	122,246,421	89,733,041
PC3 shPHF19S	158, 811, 831	108,546,468
DU145 shCTR	122,482,266	78,651,435
DU145 shPHF19L	132,258,836	85,442,208
DU145 shMLP	122,181,672	78,370,459
DU145 shPHF19S	126,118,901	79,018,923

Table 3: Summary of total read pairs and mapped paired fragments from paired end RNA-sequencing in PC3 and DU145 cells for shCTR *versus* shPHF19L and shMLP *versus* shPHF19S.

Consistent with use of specific short hairpins targeting each isoform separately without affecting the expression of the other, we obtained RNA-seq profiles showing loss of reads specific to each isoform (Figure 21-22).

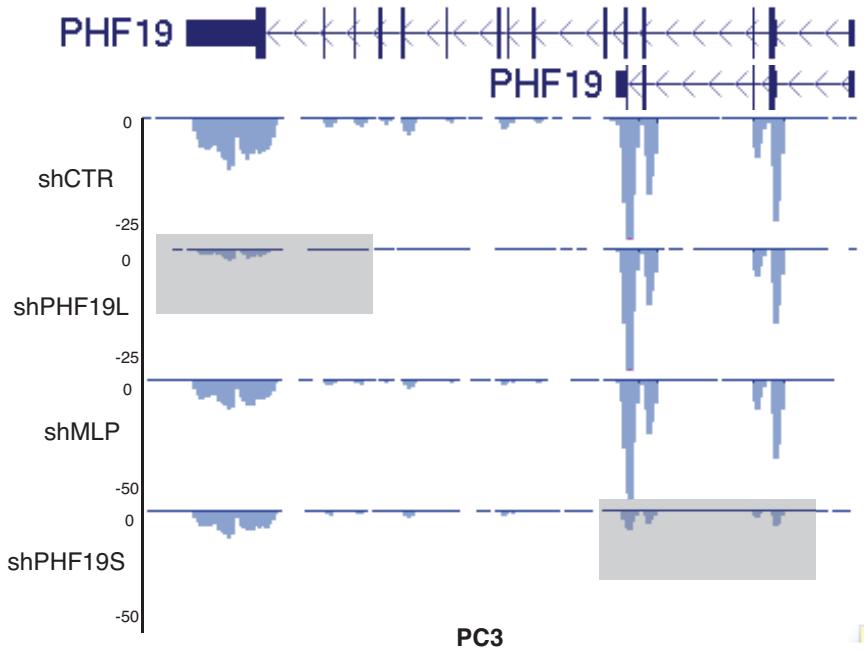

Figure 21: Screenshot from UCSC genome browser comparing RNA-seq profiles from shCTR *versus* shPHF19L#4 and shMLP *versus* shPHF19S#168 in PC3 cells.

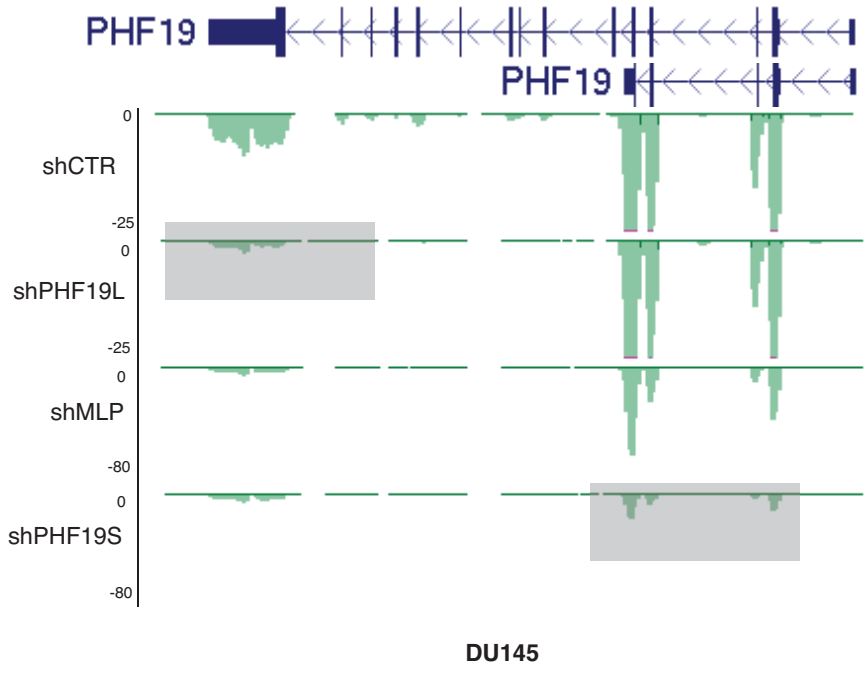

Figure 22: Screenshot from UCSC genome browser comparing RNA-seq profiles from shCTR *versus* shPHF19L#4 and shMLP *versus* shPHF19S#168 in DU145 cells.

There were 267 upregulated genes and 166 downregulated genes upon knockdown of *PHF19L* in PC3 cells, and 270 upregulated genes and 398 downregulated genes in DU145 cells respectively. However, there were only 18 genes upregulated and 26 genes downregulated upon knockdown of *PHF19S* in PC3 cells and 19 genes upregulated and 19 genes downregulated in DU145 cells respectively. Most of the genes affected by knockdown of *PHF19S* were small nucleolar RNAs. The non-significant number of genes upon knockdown of *PHF19S* suggests that the protein does not affect gene expression due to its absence from chromatin.

We therefore concentrated on the genes affected by knockdown of *PHF19L*.

In order to see if similar pathways were affected in the two prostate cancer cell lines, we overlapped the upregulated and downregulated genes (Figure 23). Among the upregulated genes, there was a poor overlap between the two cell lines although 73% of downregulated genes in PC3 cells were also downregulated in DU145 cells. Most of these common downregulated genes were associated with cell cycle and proliferation.

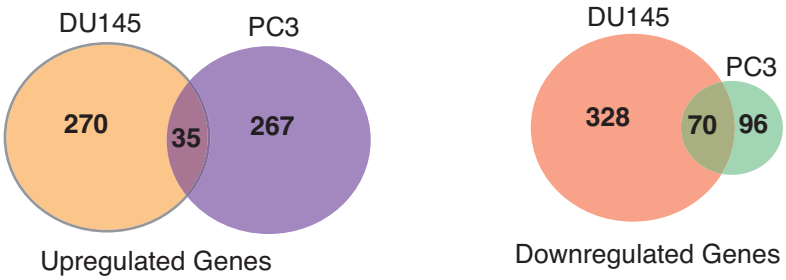

Figure 23: Venn diagram showing the overlap between upregulated and downregulated genes upon knockdown of *PHF19L* in DU145 and PC3 cells.

We therefore decided to look at differentially expressed genes in each cell line separately in PC3 and DU145 cells.

2.9 PHF19L knockdown downregulates interferon signalling pathway and causes hypoxia induced angiogenesis in DU145 cells

GO (Enrichr) analysis of upregulated genes suggested a role in inhibition serine/threonine kinases, particularly, MAP kinases as well as response to

hypoxia, and downregulated genes suggested a role in interferon signalling pathway (Figure 24).

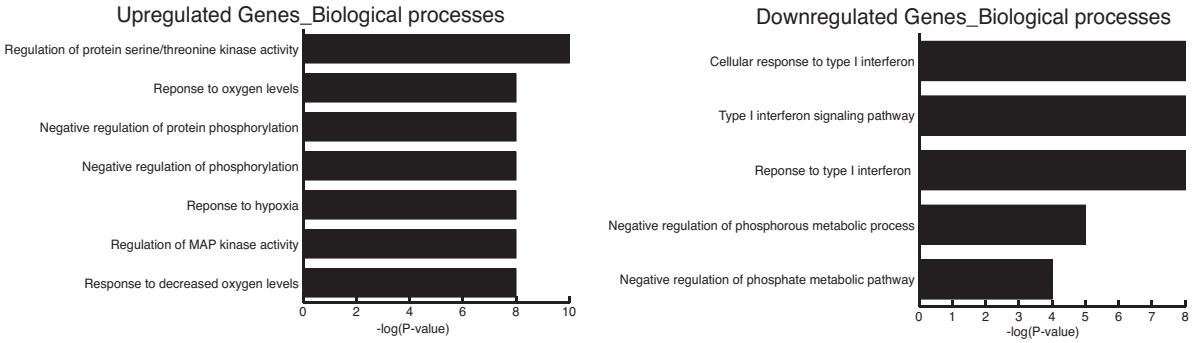

Figure 24: GO of upregulated and downregulated genes upon knockdown of *PHF19L* in DU145 cells.

Among the upregulated genes, there were two categories of genes that stood out (Figure 24). Several members of dual specificity phosphatases were induced that negatively regulate MAP kinases. In addition to this, there were several genes induced that are typically upregulated upon hypoxia but are known to drive angiogenesis and metastasis (Figure 25).

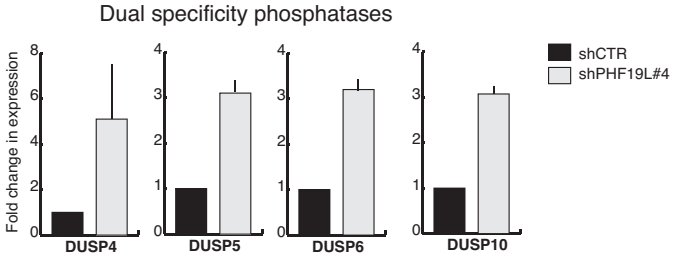

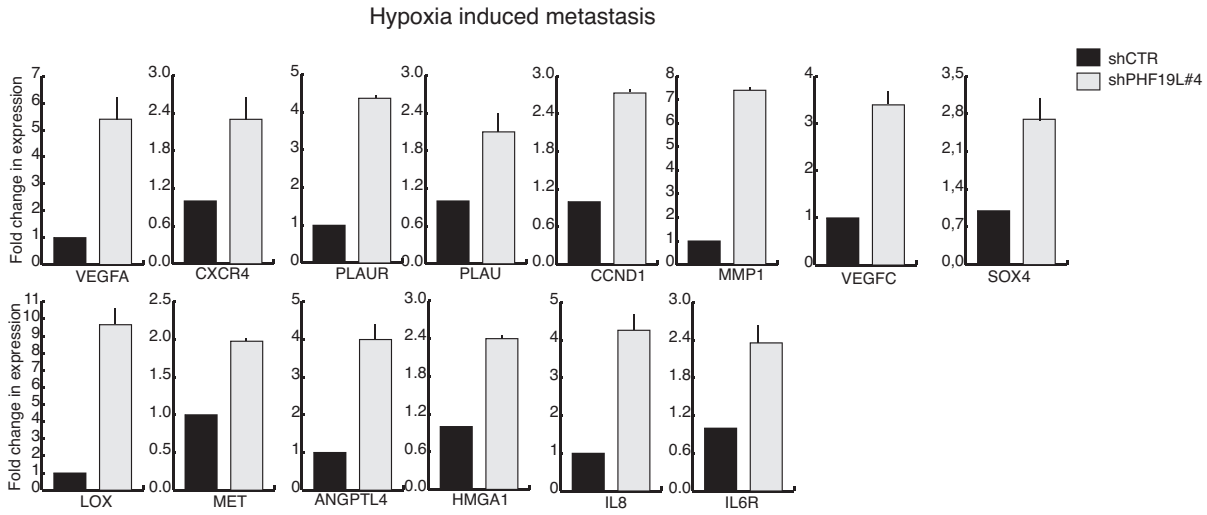

Figure 25: RT-qPCR showing upregulation of DUSPs and hypoxia induced metastasis genes in knockdown of *PHF19L* in DU145 cells. Error bar represents SD of three biological replicates.

We also validated the downregulation of several genes associated with type-I interferon pathway and two cell proliferation associated genes *CDK4* and *AATF* that were also downregulated (Figure 26).

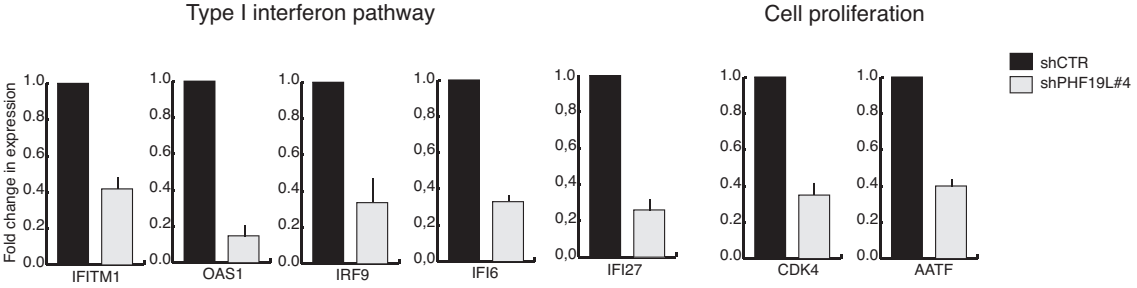

Figure 26: RT-qPCR showing genes associated with type I interferon pathway and cell proliferation downregulated upon knockdown of *PHF19L* in DU145 cells. Error bar represents SD of three biological replicates.

The DUSPs can act both to promote and inhibit cancer and there was downregulation of cell cycle associated genes such as *CDK4*, *AATF* and *CCNA2* (not shown). We therefore assessed the cell growth and proliferation of these cells upon knockdown (Figure 27). Cell growth curve showed a dramatic decrease in cell growth in shPHF19L#4. As there was only a modest decrease in protein levels in shPHF19L#1, there was only a slight decrease in proliferation in these cells.

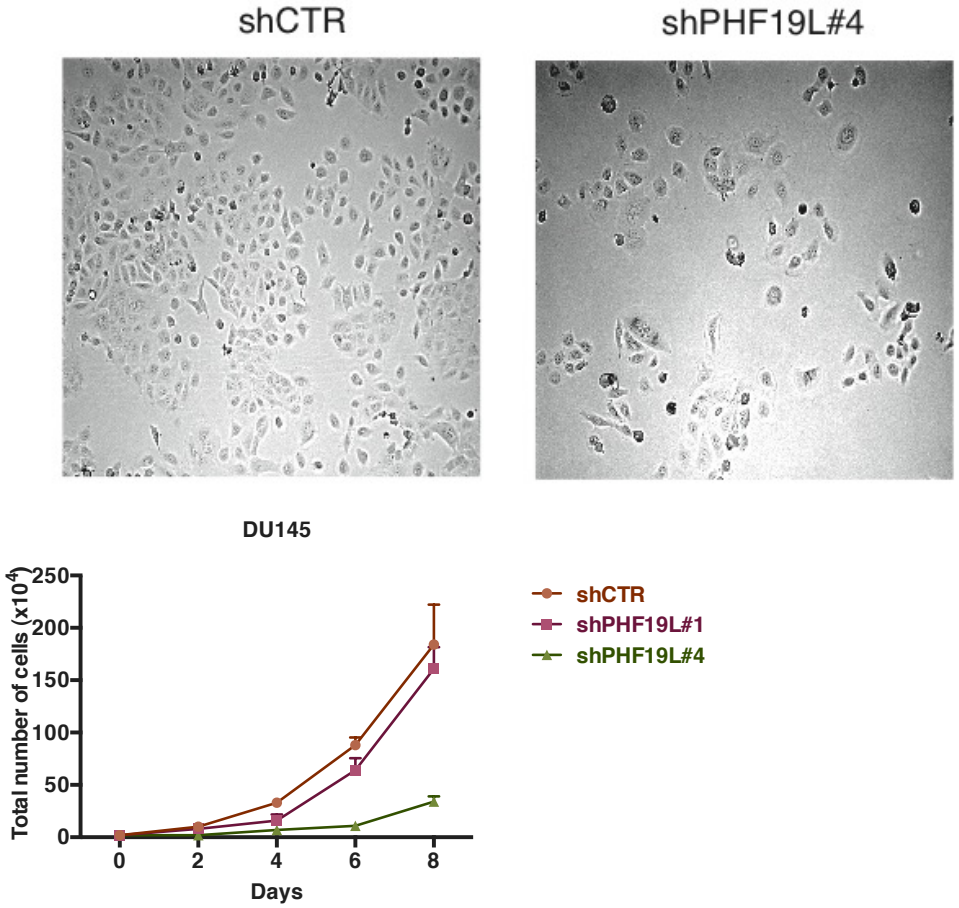

Figure 27: Cell morphology and growth curve comparing the growth rate upon knockdown of *PHF19L* in DU145 cells. Error bars represent SD of three biological replicates.

As there were no floating cells, we next assessed if this decrease in cell growth was due to decreased cell proliferation. We performed FACS analysis using BrdU that in only incorporated into cells actively progressing through the S phase (Figure 28). After 2 hours of BrdU treatment, there was a severe reduction in cell proliferation in shPHF19L#4.

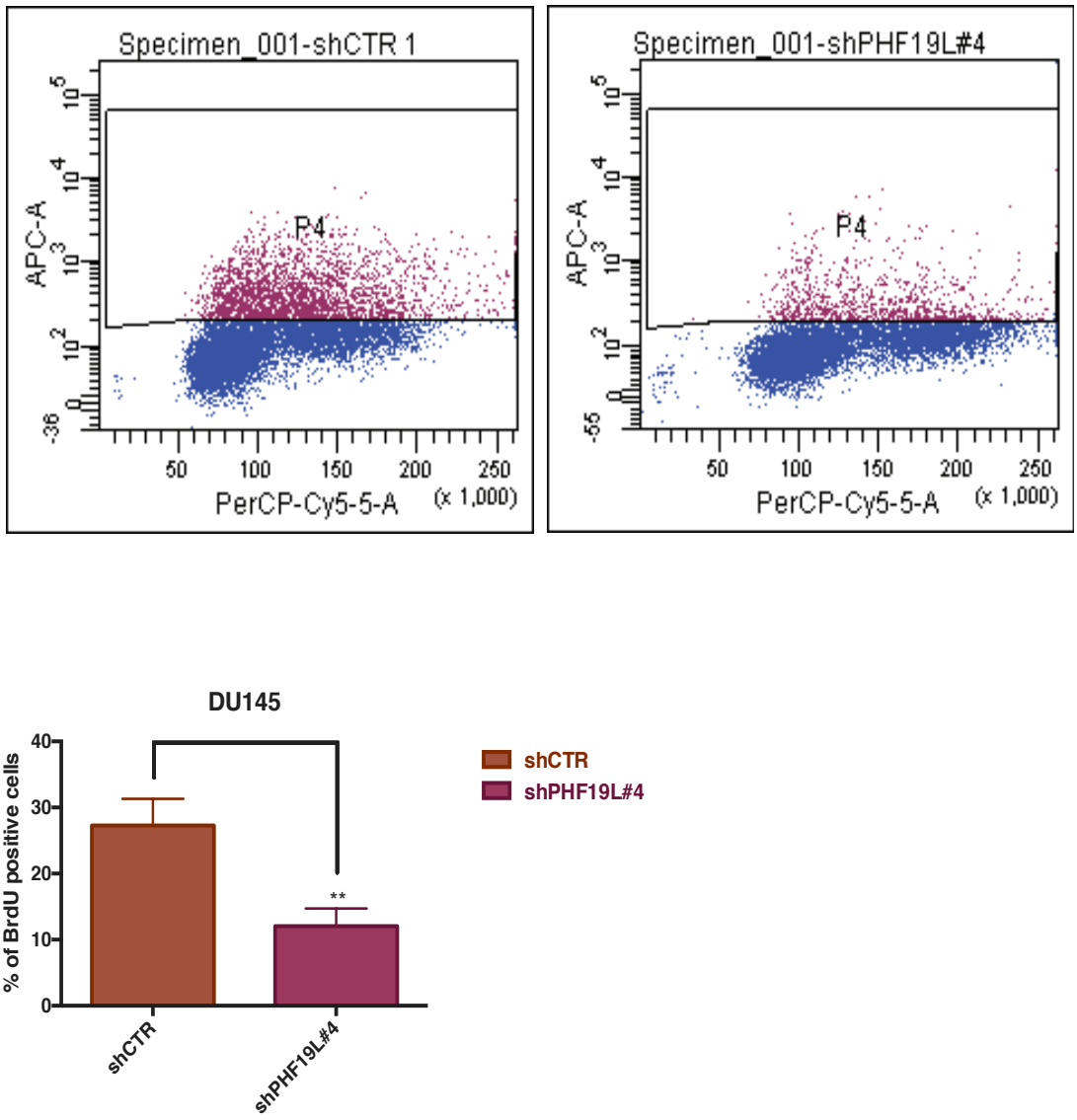

Figure 28: BrdU assay comparing cell proliferation rate between control and knockdown cells. Error bar represents standard error of deviation (SD) from three biological replicates. Student t-test was used to calculate significance.

Although these cells have decreased growth and reduced proliferation, they still exhibit upregulation of several genes associated with angiogenesis. We therefore performed *in vitro* tube formation assay on human umbilical vein endothelial cells (HUVECs) using conditioned medium without serum after 5 days of selection from DU145 shCTR and DU145 shPHF19L#4 (Figure 29). As expected there was an increased tube formation in the knockdown cells compared to control cells 6 hours after adding conditioned medium to the cells.

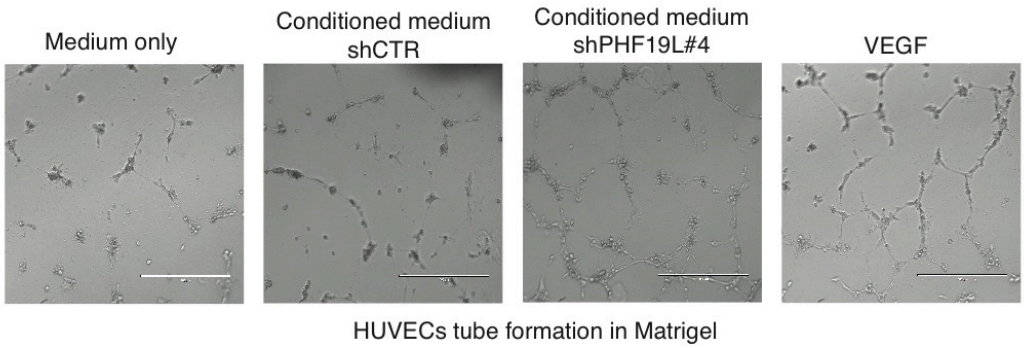

Figure 29: HUVEC tube formation assay showing increased tube formation in the knockdown cells compared to control DU145 cells. VEGF (50ng/ml) was used as a positive control and unconditioned medium was used as a negative control. Representative image of two biological replicates.

A previously published study has reported that upon knockdown of EZH2 in DU145 cells, genes associated with interferon gamma pathway are upregulated. However, in our RNA-seq the same genes were downregulated. Therefore, although the decrease in cell growth and proliferation is consistent with what is known about the role of EZH2, the upregulation of angiogenesis and metastasis associated genes and downregulation of interferon pathway associated genes seems to be a novel role of PHF19 perhaps independent of PRC2 complex or due to mistargeting of the complex.
Next, we investigated if similar phenomenon occurs in PC3 cells.

2.10 PHF19L is required for cell proliferation and growth but its downregulation switches PC3 cells to a more invasive phenotype

GO (Enrichr) of differentially expressed genes showed upregulated genes to be associated with interferon gamma pathway and downregulated genes with cell cycle (Figure 30). This was quite interesting as the same genes that were downregulated in DU145 cells were now upregulated in PC3 cells suggesting two different mechanisms of action in the two cell lines.

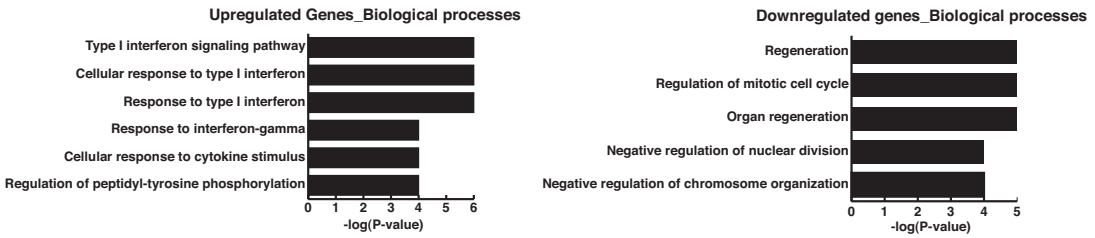

Figure 30: GO (Enrichr) analysis of differentially expressed genes upon knockdown of *PHF19L* in PC3 cells.

On a closer look, genes associated with cell cycle and proliferation such as *E2F1*, *CCNA2*, *CCNB2*, *CDK4 and AATF* were downregulated and this was concomitant with increase in levels of *CDKN1A (p21)* (Figure 31).

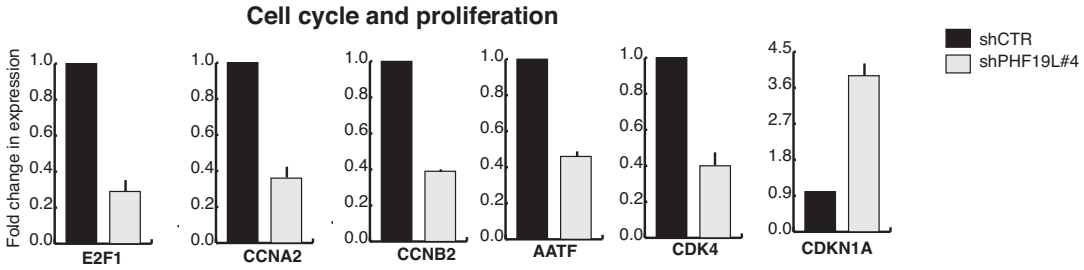

Figure 31: RT-qPCR showing dowregulation of gene associated with cell cycle and proliferation and upregulation of *p21* upon knockdown of *PHF19L* in PC3 cells. Error bar represents SD of three biological replicates.

However, there was another class of genes that was downregulated. Many of these genes were associated with RNA processing and cap-dependent protein translation (Figure 32).

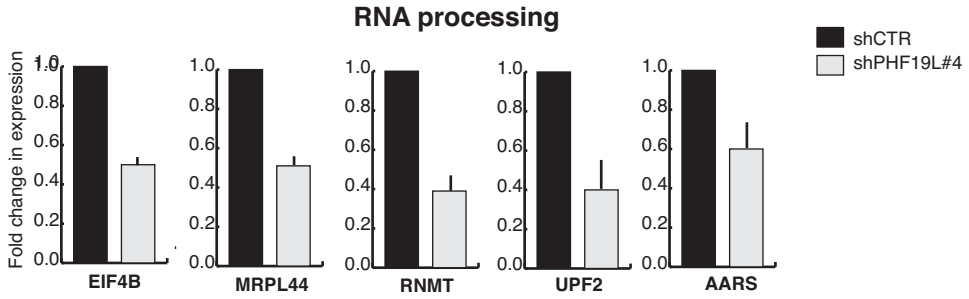

Figure 32: RT-qPCR showing downregulation of genes associated with RNA processing and translation upon knockdown of *PHF19L* in PC3 cells. Error bar represents SD of three biological replicates.

Among the upregulated genes, there were also two classes of genes. The first class was associated with type I interferon pathway and surprisingly the second class was associated with genes associated with survival and invasion (Figure 33). This included the cytokines *IL6* and *IL8*, *NOTCH3*, TGF pathway associated genes such as *TGFBR1, ACVR2B, FST, LTBP1*, the ID proteins *ID1 and ID3*, invasion associated gene *EIF5A2*, survival gene *BEX2*, and several integrin genes *ITGB6* and *ITGA1*. In addition, *CD24* was upregulated along with urokinase plasminogen activator *PLAU*.

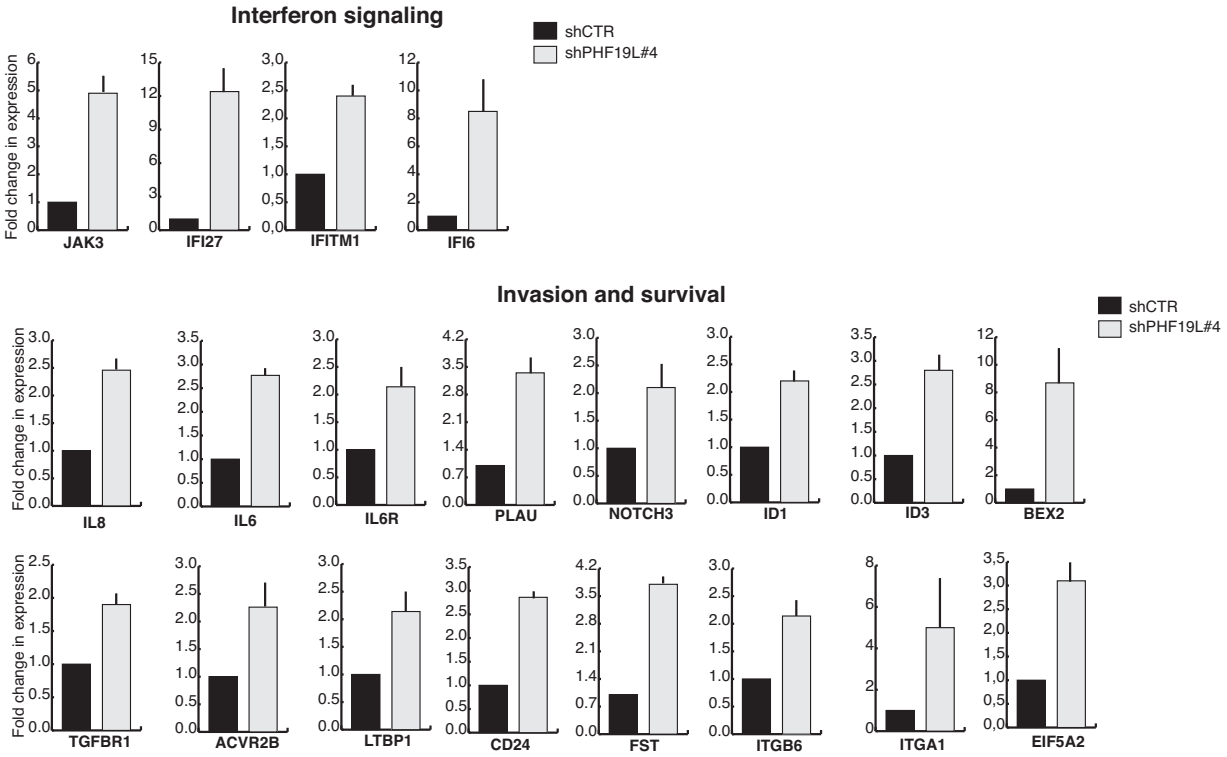

Figure 33: RT-qPCR showing upregulation of genes associated with interferon signalling, invasion and survival upon knockdown of *PHF19L* in PC3 cells. Error bar represents SD of three biological replicates.

We also compared the differentially expressed genes between the knockdown of EZH2 (previously published) and PHF19L in PC3 cells (Figure 34). Similar to RWPE1 cells, there was a poor overlap between upregulated and downregulated genes although *BEX2, CD24, CDKN1A* and *PLAU* were upregulated in both the knockdowns.

Figure 34: Venn diagram comparing differentially expressed genes in siEZH2 (Gu *et al*., 2015) and shPHF19L in PC3 cells.

Based on the gene expression changes, we went on to characterize the phenotype in these cells. Firstly, the cell morphology of these cells was quite different. The cells were more round and became bigger in size and lost the typical spindle shaped epithelial phenotype (Figure 35).

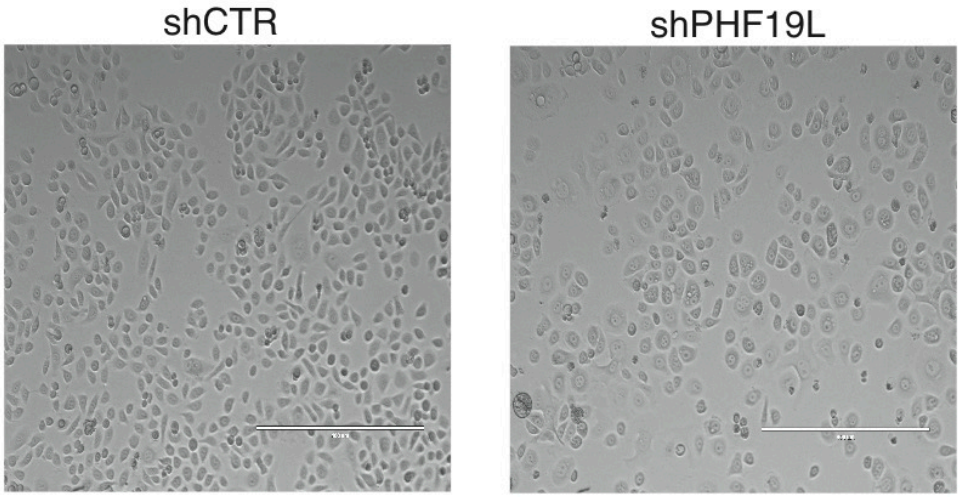

Figure 35: Phase contrast image comparing cell morphology of PC3 shCTR *versus* shPHF19L.

Next, we performed cell growth curve to monitor the cell growth over a period of 8 days (Figure 36). As expected, there was a decrease in cell growth in both the knockdowns in PC3 cells. shPHF19L#4 is a better knockdown than shPHF19L#1 and therefore the decrease was concomitant with the knockdown levels.

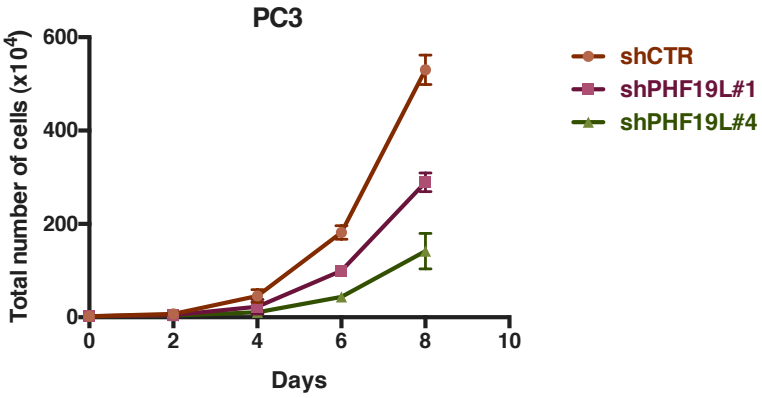

Figure 36: Growth curve comparing the growth rate of PC3 cells upon knockdown of *PHF19L* in PC3 cells. Error bar represents SD of three biological replicates.

There was no change in cell morphology or cell growth upon knockdown of *PHF19S* (Figure 37).

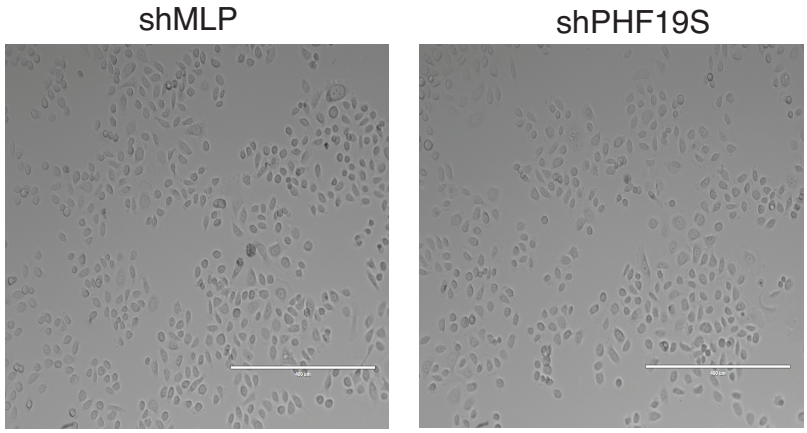

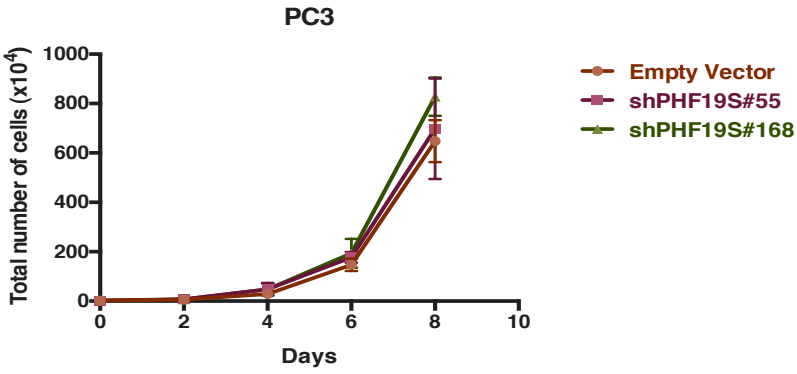

Figure 37: Comparison between cell morphology and cell growth between shCTR *versus* shPHF19S.

As there was upregulation of interferon signalling pathway-associated genes, we wanted to confirm that the reduction in cell growth was not due to

apoptosis. We performed Annexin V staining observe any apoptosis by FACS analysis (Figure 38). There were no changes in the number of viable cells upon knockdown suggesting that these cells are not undergoing apoptosis.

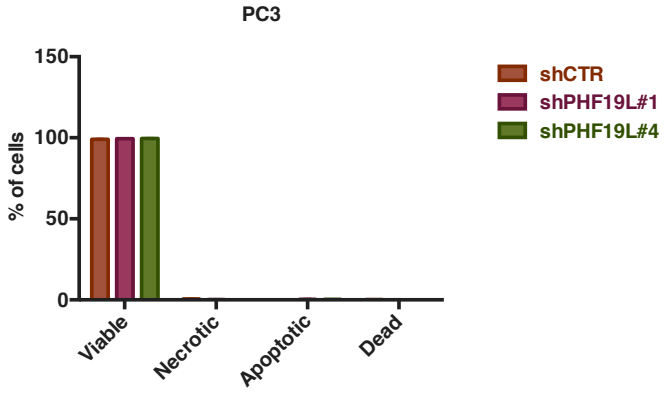

Figure 38: Apoptosis assay showing absence of apoptotic cells in the knockdowns. Error bars represent SD of three biological replicates.

We next investigated if this was due to changes in proliferation. We performed BrdU assay and confirmed that the decrease in cell growth was due to reduced proliferation in the knockdown cells (Figure 39).

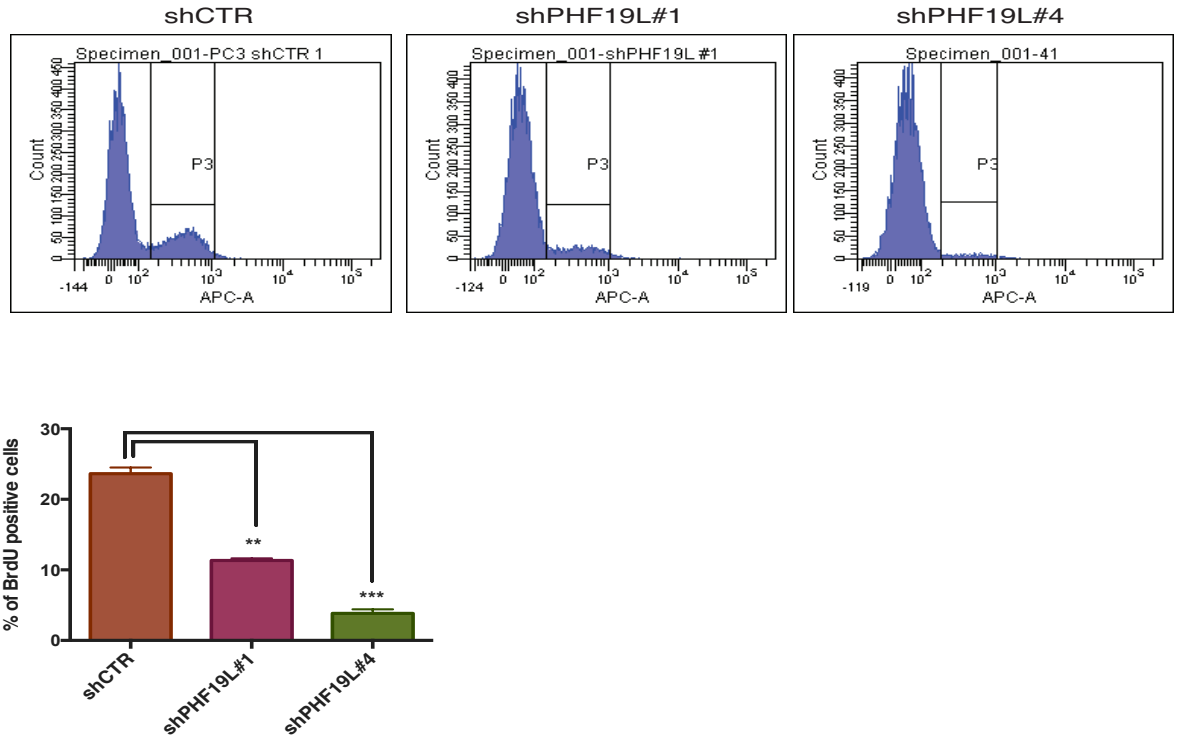

Figure 39: Changes in cell proliferation upon knockdown of *PHF19L* in PC3 cells. Error bars represent SD of three biological replicates. Student t-test was performed to calculate significance.

As there were several genes upregulated that were associated with degradation of extracellular matrix and invasion, we performed transwell matrigel invasion assay to observe if there was any increase in the invasive capacity of these cells. There was an increase in the invasive capacity of these cells to invade matrigel upon knockdown of PHF19L (Figure 40).

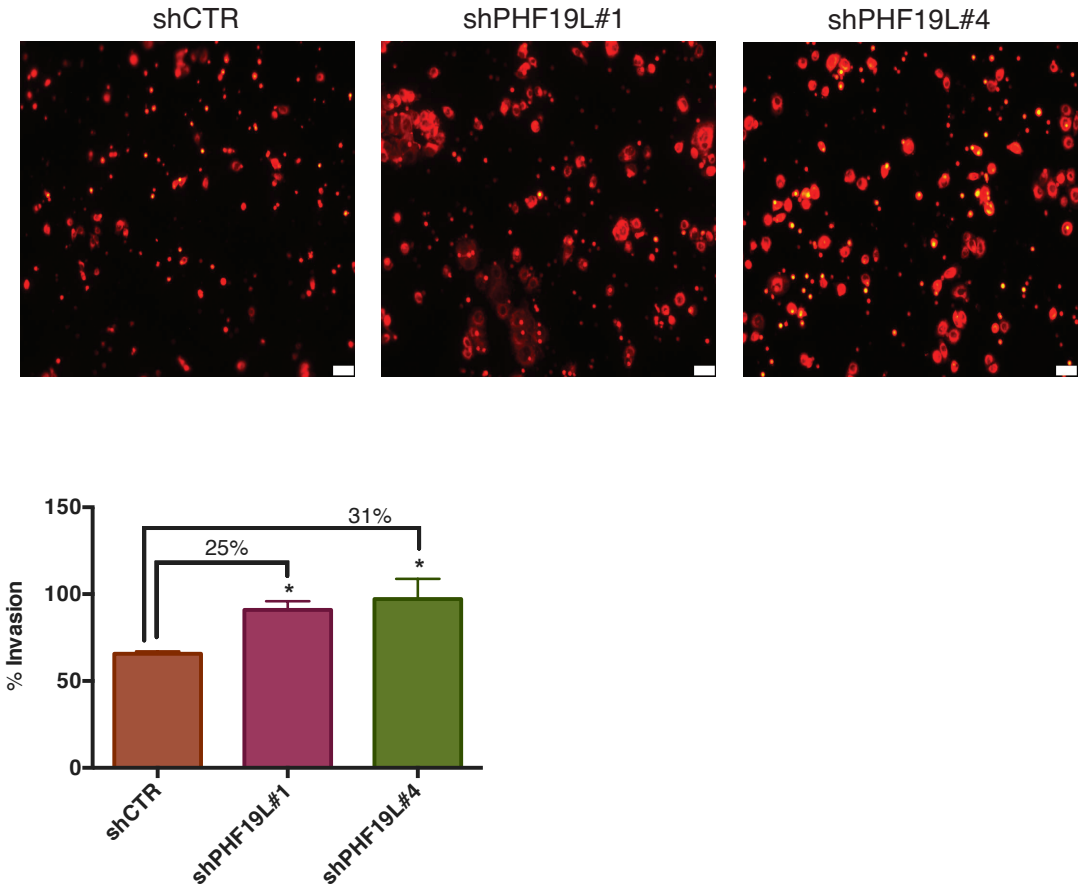

Figure 40: Representative images and column graph showing % of invasion in control and knockdown cells. Error bars represent SD of three biological replicates. Student t-test was performed to calculate significance.

We also performed three-dimensional Matrigel/Collagen cell invasion assay to assess the formation of prostaspheres over a period of 7 days and followed this with immunofluorescence staining using Laminin-5 (LAMA5), a marker of intact basal lamina that is lost upon invasion into the matrix (Figure 41). Consistent with the transwell migration assay, the knockdown cells formed invasive prostaspheres that clearly invaded the surrounding matrix compared to more round and well-differentiated prostaspheres formed by control cells.

LAMA5 was lost in the knockdowns whereas the control cells stained positive for LAMA5 showing the presence of an intact basal membrane (Figure 41).

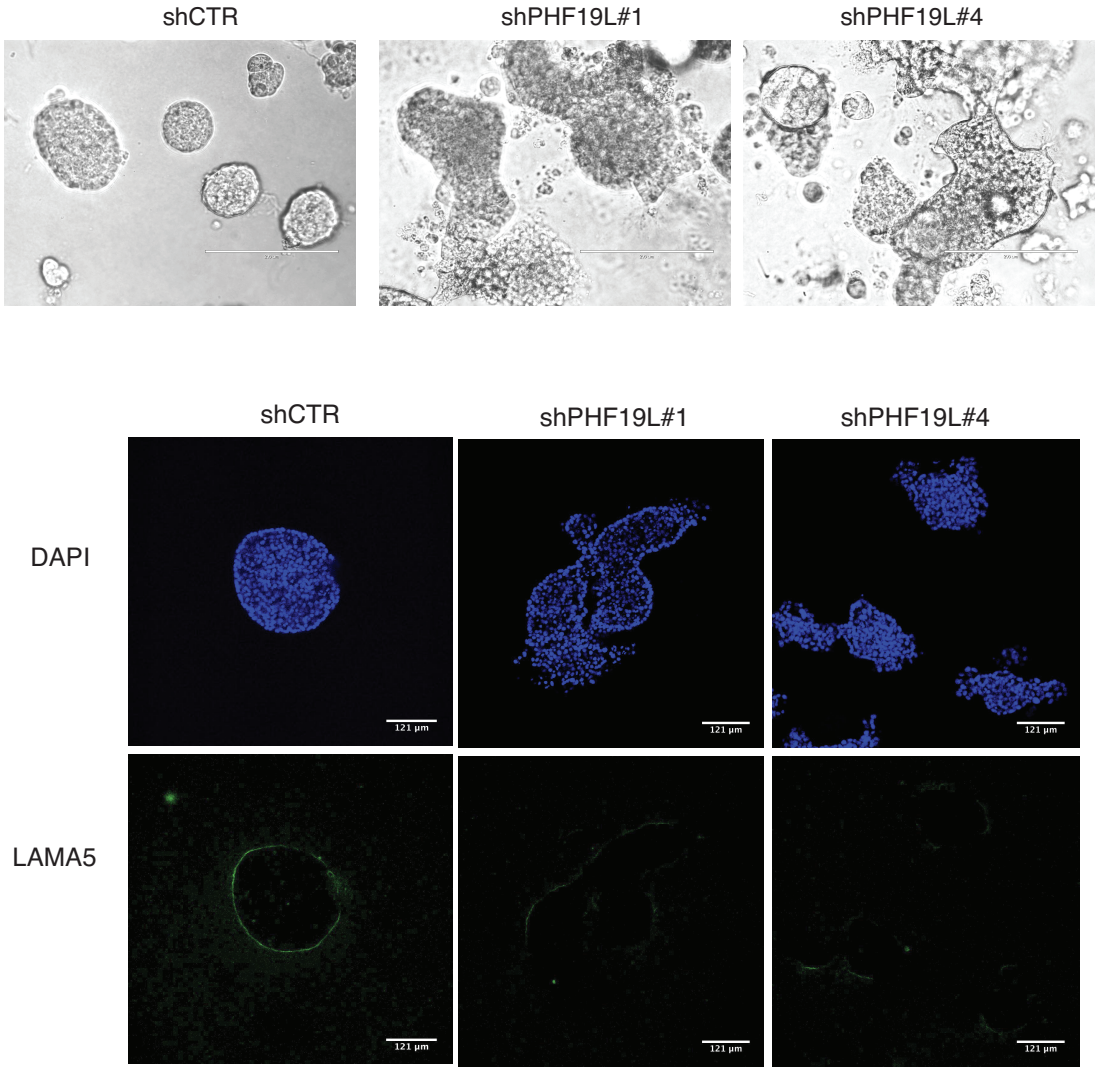

Figure 41: Phase contrast images and LAMA5 staining on the prostaspheres formed by PC3 cells in control and knockdown cells for *PHF19L*. Representative images of three biological replicates.

Therefore, on one hand, PHF19L is required for cell growth and proliferation in PC3 cells, on the other hand, it increases the invasion and survival capacity of these cells.

In summary, PHF19L is postulated to have a dual function in both DU145 and PC3 cells. In both the cancer cell lines, it is required for cell growth and

proliferation sharing several genes that are downregulated upon knockdown and are associated with cell cycle and proliferation. However, in DU145 and PC3 cells, it has an opposite function on the transcription of the genes associated with interferon type I signalling pathway. Lastly, although the final outcome might be similar, in DU145 cells the knockdown promotes survival via angiogenesis whereas in PC3 cells, the knockdown promotes survival via increased invasion. Therefore, knockdown of PHF19 in both the cancer cell lines switches the cells to a less proliferative but a more aggressive phenotype.

2.11 Expression of PHF19L in LNCaP cells leads to inhibition of growth.

As both the isoforms were expressed at very low levels in the androgen dependent cell line LNCaP, we ectopically expressed both PHF19L and PHF19S in this cell line in order to observe if there is any effect. Although the overexpression of the short isoform did not induce any effect, the overexpression of the long isoform inhibited the cell growth of these cells. This suggests that PHF19 may interfere with AR driven cell growth in these cells.

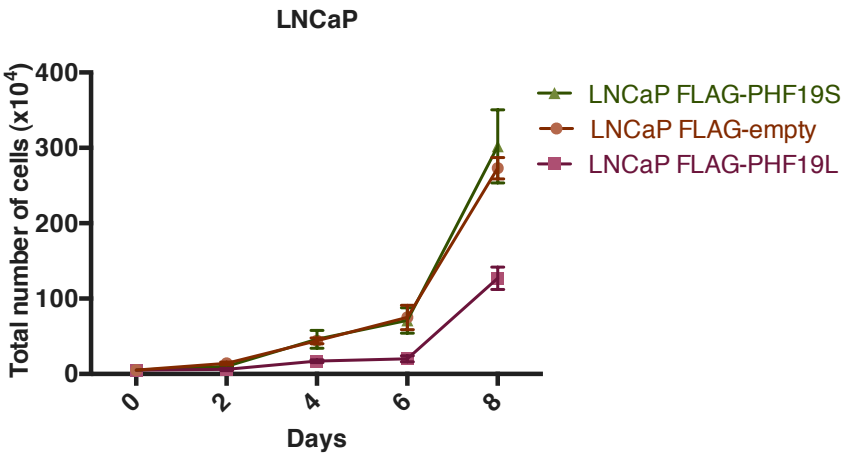

Figure 42: Cell growth curve showing inhibition of cell growth in LNCaP cells overexpressing PHF19L in LNCaP cells.

2.11 Attempts to find target genes of PHF19L.

The next step was to identify target genes that are regulated by PHF19L, and to characterize gene expression changes that are not consistent with what has been previously published for EZH2.

The first attempt was made using a homemade antibody that specifically recognized PHF19L. We tested this antibody in immunoprecipitation and the antibody was specific as it could efficiently pull down PHF19L and co-immunoprecipitate EZH2 and SUZ12 and this interaction is lost in the knockdown (Figure 43).

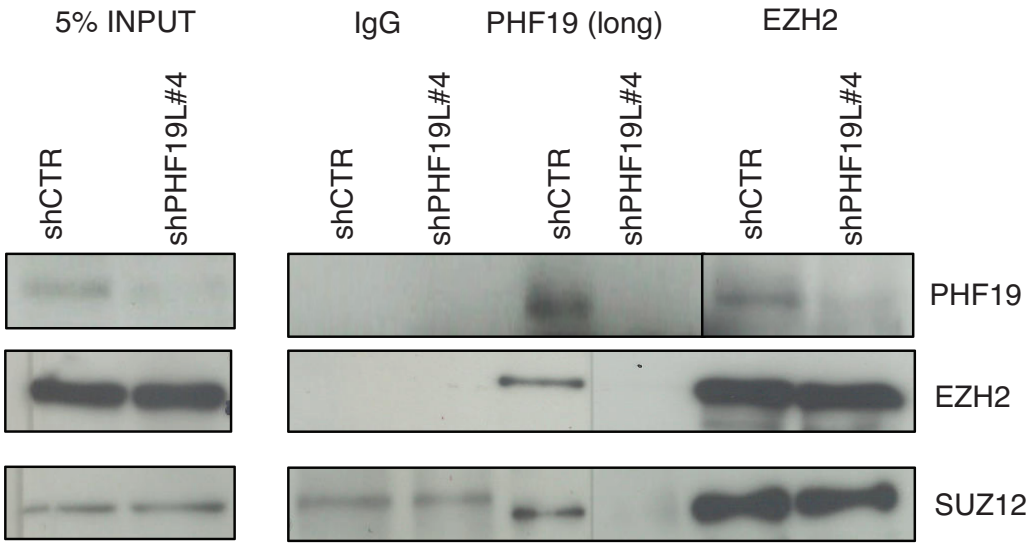

Figure 43: Co-immunoprecipitation experiment of IgG, PHF19 (long) and EZH2 with PHF19, EZH2 and SUZ12 in control and knockdown cells.

However, when we performed ChIP-sequencing using this antibody, we did not observe any specific enrichment over any region and the sample was very similar to control IgG.

We then tested another homemade antibody that recognizes both the long and short isoform of PHF19. We named this antibody as N-terminal antibody as the epitope is against the N-terminal region of the protein. This antibody performed efficiently in immunoprecipitation (Figure 8). We also performed ChIP-western using this antibody to see if it could immunoprecipitate histone H3 to test its ability to immunoprecipitate DNA. We also included the first

antibody in this analysis. A positive enrichment was seen was histone H3 using this antibody that was not observed for the first antibody (Figure 44).

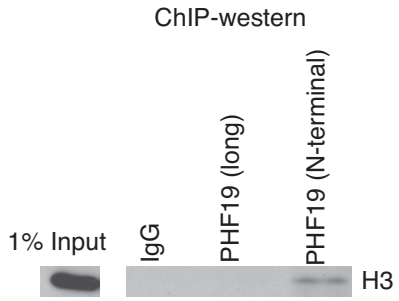

Figure 44: ChIP using PHF19 (long) and PHF19 (N-terminal) followed by Western blot to verify the co-immunoprecipitation of histone H3.

We therefore performed ChIP using N-terminal antibody in PC3 cells. Below is a summary of the ChIP-sequencing.

PHF19	2014-02-27/PHF_6417_CAGT.fastq
NR* mapped reads	35,253,877
Peaks	1,809
Genes**	1,688
PHF19_IgG	2014-02-27/IgG_6416_ACGT.fastq
NR* mapped reads	32,907,413

* NR: Non-redundant
** Peaks in the region (2.5Kb upstream of the gene, its end)

Table 4: Summary of mapped reads, peaks and target genes identified for PHF19 using ChIP-sequencing.

We identified 1688 target genes of PHF19L. PHF19L was mostly found at transcription start site (1320 genes) and a minority of peaks were found on gene body (368 genes) (Figure 45).

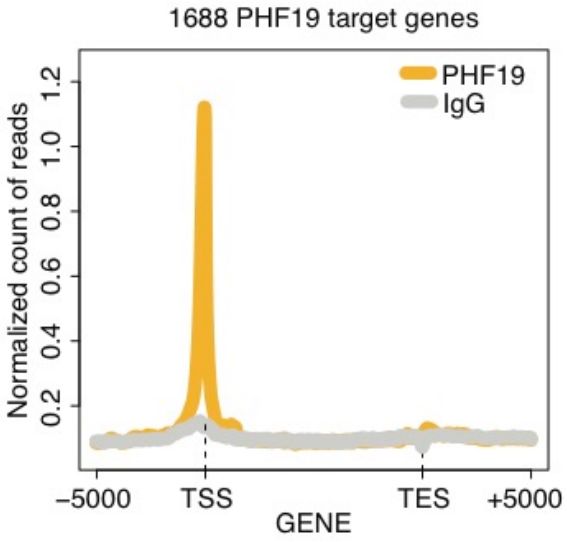

Figure 45: Graphical distribution of normalized count of reads 5 Kb upstream and downstream of TSS for PHF19L target genes.

We therefore decided to verify these peaks by ChIP-qPCR. Unfortunately, we observed that none of the peaks that we tested lost enrichment upon knockdown of PHF19. This suggested that the peaks found using this antibody were not specific for PHF19L (Figure 46).

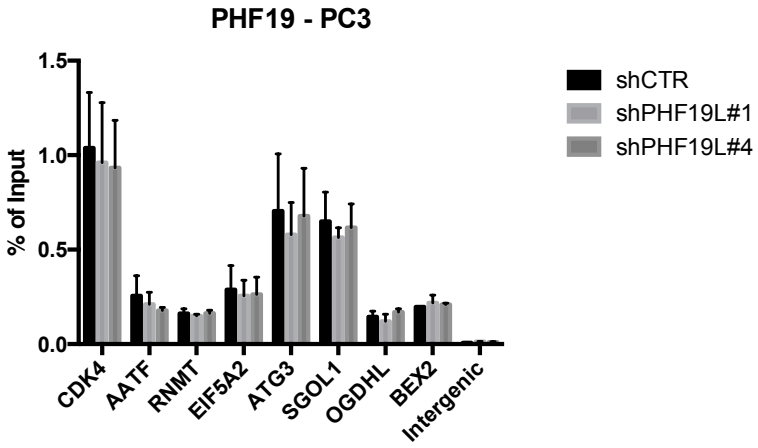

Figure 46: ChIP-qPCR validation of target genes of PHF19 in control and knockdown cells

In order to completely rule out the presence of any other isoform that could compensate for PHF19L, we performed ChIP-qPCR in PC3 cells using siRNA that abolished the expression of all the isoforms (Figure 47). However, we still

did not observe any reduction in the enrichment of signal in the knockdown (Figure 48). Therefore, we concluded that this antibody crossreacted with another chromatin protein and we could no longer use these results.

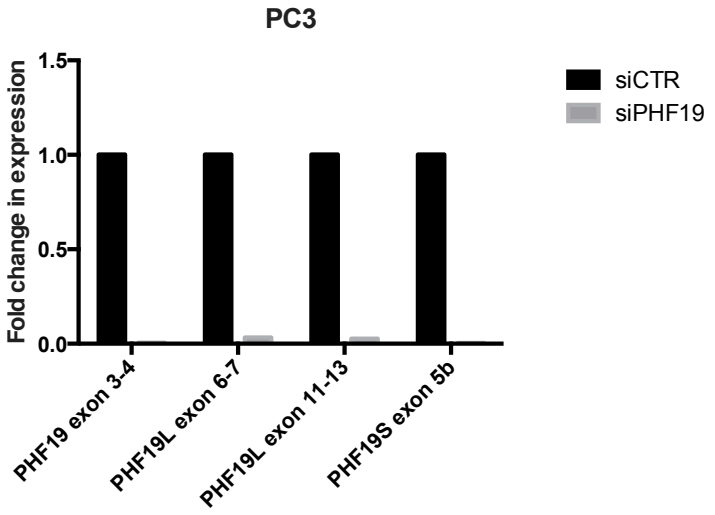

Figure 47: RT-qPCR showing the loss of expression from most of the exons of *PHF19* using siRNA.

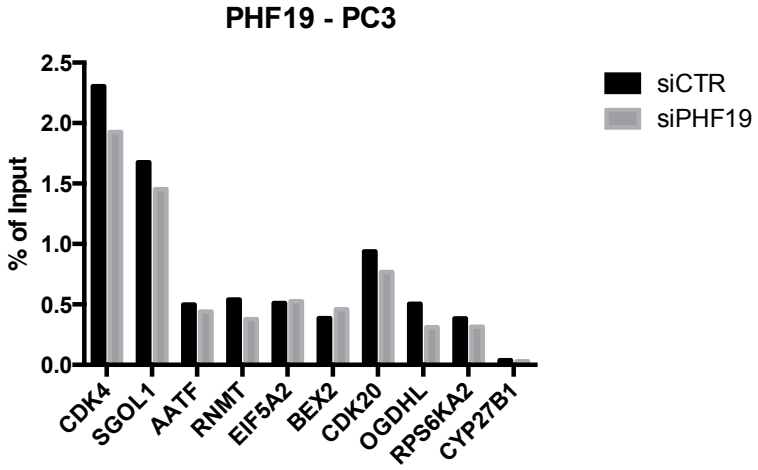

Figure 48: ChIP-qPCR validation of target genes of PHF19 in control and knockdown cells using siRNA.

We therefore decided to perform ChIP-sequencing with a commercial antibody against only PHF19L that has been previously described and verified for ChIP (Brien *et al*., 2012). We called this antibody PHF19 (Millipore). We performed cell fractionation using this antibody to ensure that the antibody recognises the chromatin bound PHF19L and this is not recognised in the knockdown. Cell fractionation showed a specific band for PHF19L that was

present in the chromatin bound fraction and was not present in the knockdown. In addition, EZH2 although present at low amounts in the cytoplasm and nucleoplasm was lost in the knockdown as described before although the chromatin bound EZH2 only showed a moderate decrease (Figure 49).

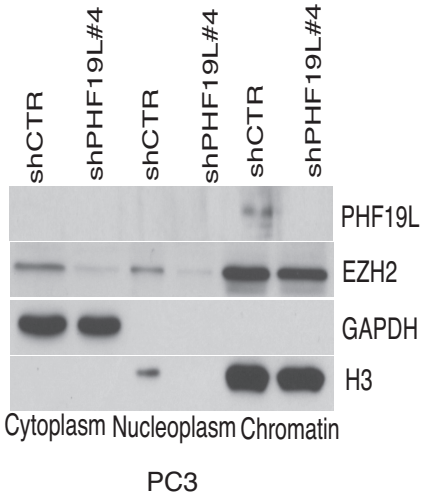

Figure 49: Cell fractionation showing a specific band for PHF19L in the chromatin fraction lost upon knockdown and loss of EZH2 expression from cytoplasmic and nucleoplasmic fraction with moderate decrease in chromatin bound fraction.

However, upon performing ChIP-sequencing, we did observe any specific enrichment of peaks using this antibody.

In the wake of none of the antibodies working for ChIP-sequencing, we employed three different approaches to find target genes for PHF19. The first approach was to generate tagged proteins and ectopically express them. We generated C-terminal triple FLAG-tagged (3X_FLAG) and C-terminal triple HA-tagged (3X_HA) PHF19 expression vectors. Next, we confirmed by co-immunoprecipitation, that upon transfection the proteins are expressed (Figure 50). We did this using nuclear extracts to ensure that the tagged protein is transported to the nucleus. In case of PHF19L_3XFLAG, we also confirmed that this tagged protein interacts with EZH2 (Figure 50).

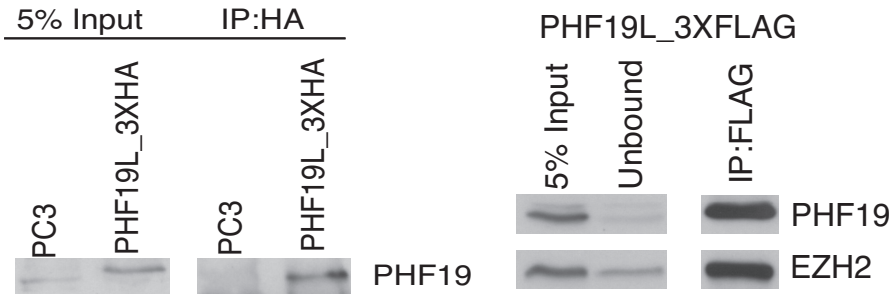

Figure 50: Co-immunoprecipitation of PHF19L_3XHA with PHF19 and PHF19L_3XFLAG with PHF19 and EZH2.

As we have a good ChIP-grade antibody available for mouse Phf19, we also decided to make use of the cell lines expressing mPhf19_3XFLAG and decided to perform ChIP-sequencing using these cell lines. We ectopically expressed mouse Phf19 in DU145 and PC3 cells. The mPhf19 expression was confirmed using mPhf19 immunoprecipitation followed by co-immunoprecipitation with mPhf19 and FLAG antibody. We also confirmed that mPhf19 interacts with endogenous human SUZ12 and EZH2 (Figure 51).

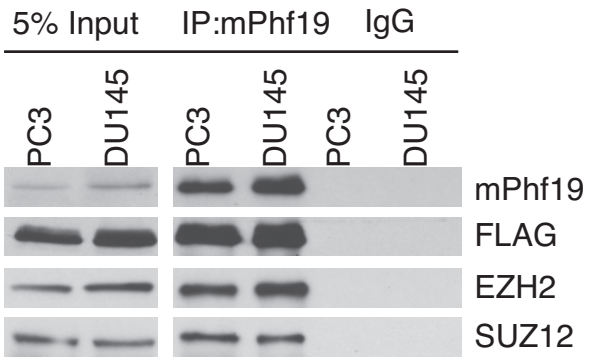

Figure 51: Co-immunoprecipitation of mPhf19 with mPhf19, FLAG, EZH2, SUZ12 in PC3 and DU145 cells.

We are currently preparing these samples for ChIP sequencing.

2.13 Changes in H3K27me3 upon knockdown of PHF19L in PC3 and DU145 cells.

As the knockdown of Phf19 leads to global reduction in H3K27me3 levels in ESCs, we performed genome wide ChIP-sequencing of H3K27me3 in control

and knockdown in both PC3 and DU145 cells to understand its function in the context of PRC2 complex. Below is a summary of the ChIP-sequencing.

Sample	Mapped reads	Peaks	Genes
PC3 shCTR	41,417,639	34,056	3,067
PC3 shPHF19L	43,091,609	51,531	4,351
DU145 shCTR	39,727,014	16,592	4,500
DU145 shPHF19L	47,143,889	20,157	4,337

Table 5: Summary of mapped reads and associated peaks and genes of H3K27me3 ChIP-sequencing in PC3 and DU145 cells in control and knockdown of PHF19L.

We first looked at H3K27me3 profile in the control samples in each cell line. We compared the H3K27me3 reads from both the cell lines and associated genes and found only moderate correlation between the two cell lines (r=0.68). 46% of the genes associated with H3K27me3 in PC3 cells were also associated with H3K27me3 in DU145 cells. On the other hand, 32% of the genes associated with H3K27me3 in DU145 also had peaks in PC3 cells (Figure 52).

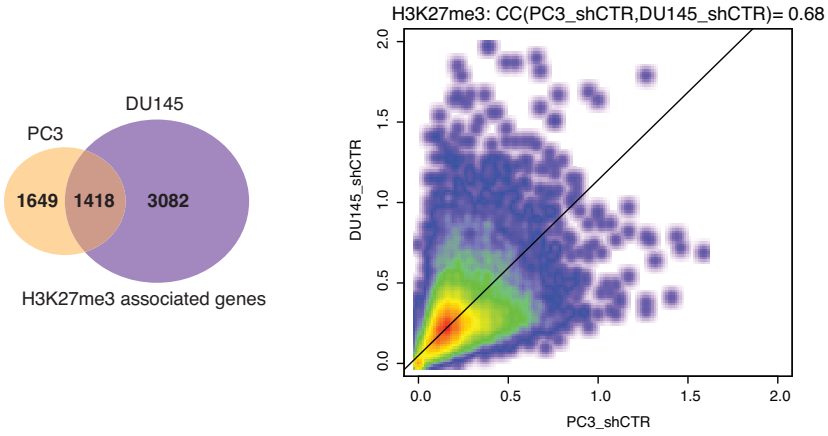

Figure 52: Venn diagram showing the overlap of H3K27me3 associated genes and scatter plot showing correlation of H3K27me3 reads in PC3 and DU145 cells.

Secondly, the profile of the peaks on target genes was very different. In DU145, the distribution was bimodal around the TSS as expected. However, in PC3 cells, although there was sharp increase at TSS, there were broad domains of H3K27me3 spreading across the body of the gene (Figure 53).

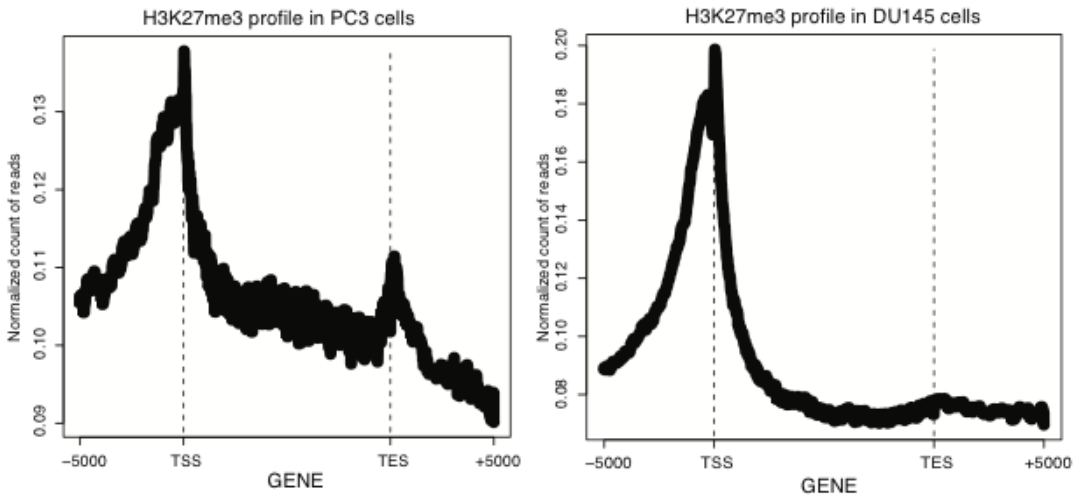

Figure 53: Graphical distribution of normalized count of reads 5kb upstream and downstream of TSS of H3K27me3 target genes.

Third, the distribution of the peaks also varied between the cell lines. Most of the peaks in PC3 cells were associated with intergenic (52%) and intronic (27%) regions with a small percentage associated with promoters (11%). On the other hand, in DU145 cells, although there were also a substantial amount of peaks associating with intergenic regions (34%) and intronic regions (20.4%), the amount of peaks associated with the promoter (31%) were almost three times as that of PC3 cells. There was no major difference in peak distribution of H3K27me3 peaks between the control and knockdown in both PC3 and DU145 cells (Figure 54).

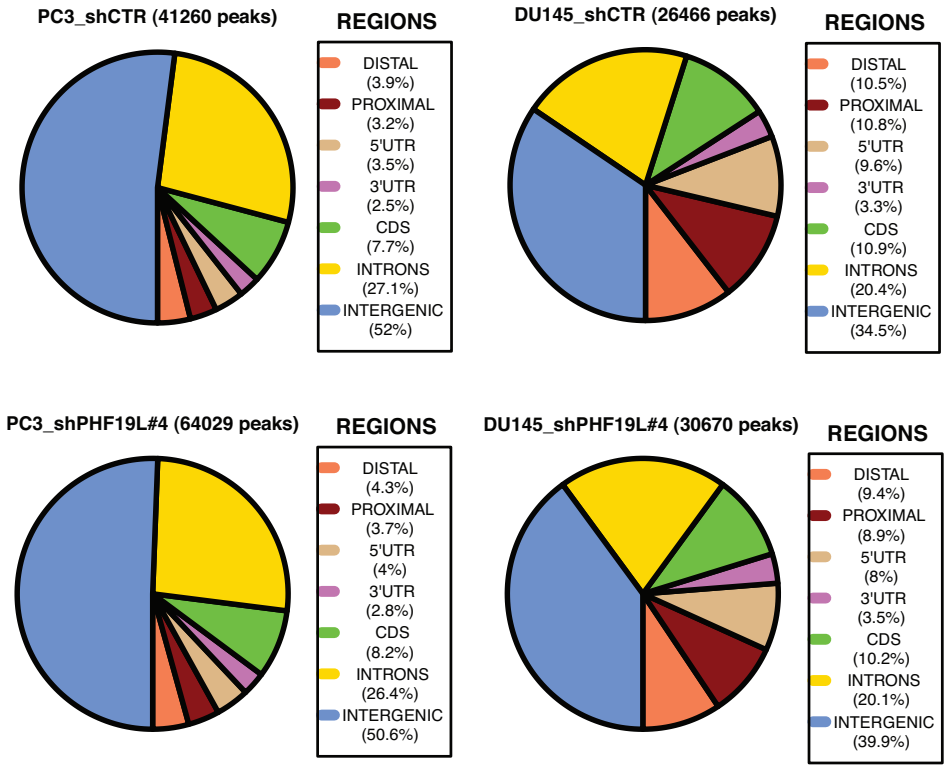

Figure 54: Pie-chart showing peak distribution of H3K27me3 across the genomic features in PC3 and DU145 control and knockdown cells.

We also asked if the differences in the profile of the peaks of H3K27me3 in PC3 and DU145 cells could be associated with changes in expression. The genes associated with broad domains of H3K27me3 in PC3 cells are more repressed compared to DU145 cells where the genes are lowly expressed. Thus, the profile of the peaks of H3K27me3 can provide an additional layer of fine-tuning of transcriptional repression in prostate cancer cells. Interestingly, this repression is slightly elevated in the knockdown in PC3 cells whereas in DU145 cells, upon knockdown, the genes on average are further repressed (Figure 55).

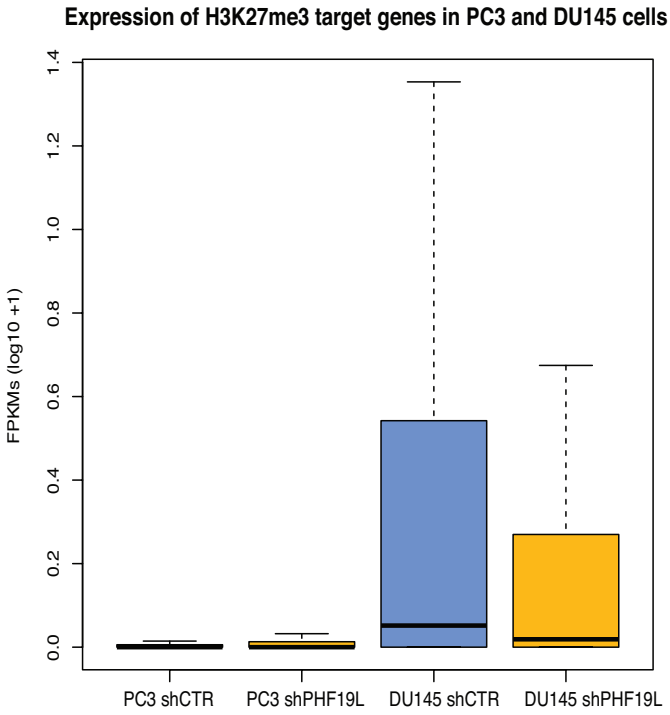

Figure 55: Box plots showing expression of H3K27me3 associated genes in control and knockdown PC3 and DU145 cells.

We next looked at the differences in H3K27me3 profile upon knockdown in two cell lines. In both the cell lines, there were no major global changes in H3K27me3 (Figure 56).

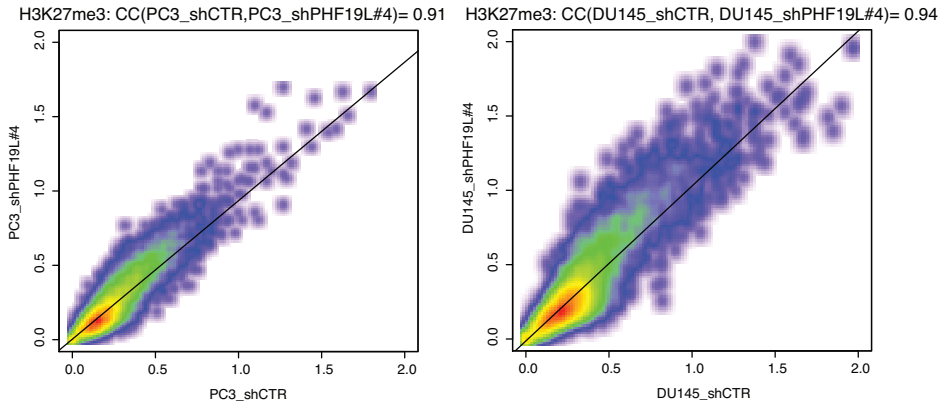

Figure 56: Scatterplot showing the correlation of H3K27me3 reads in control and knockdown samples in PC3 and DU145 cells.

However, there were few local changes in both the cell lines. There were few 100 genes that either lost or gained H3K27me3 in the knockdown of PHF19L. However, the gain or loss did not significantly change the expression of those

genes. We selected the top 100 genes based on the differences in H3K27me3 levels that either lost or gained H3K27me3 in each cell line. In PC3 cells, although the loss was mild, the gain was quite significant. On the other hand, in DU145 cells, there were significant differences in the reads both in the lost and gain genes (Figure 57).

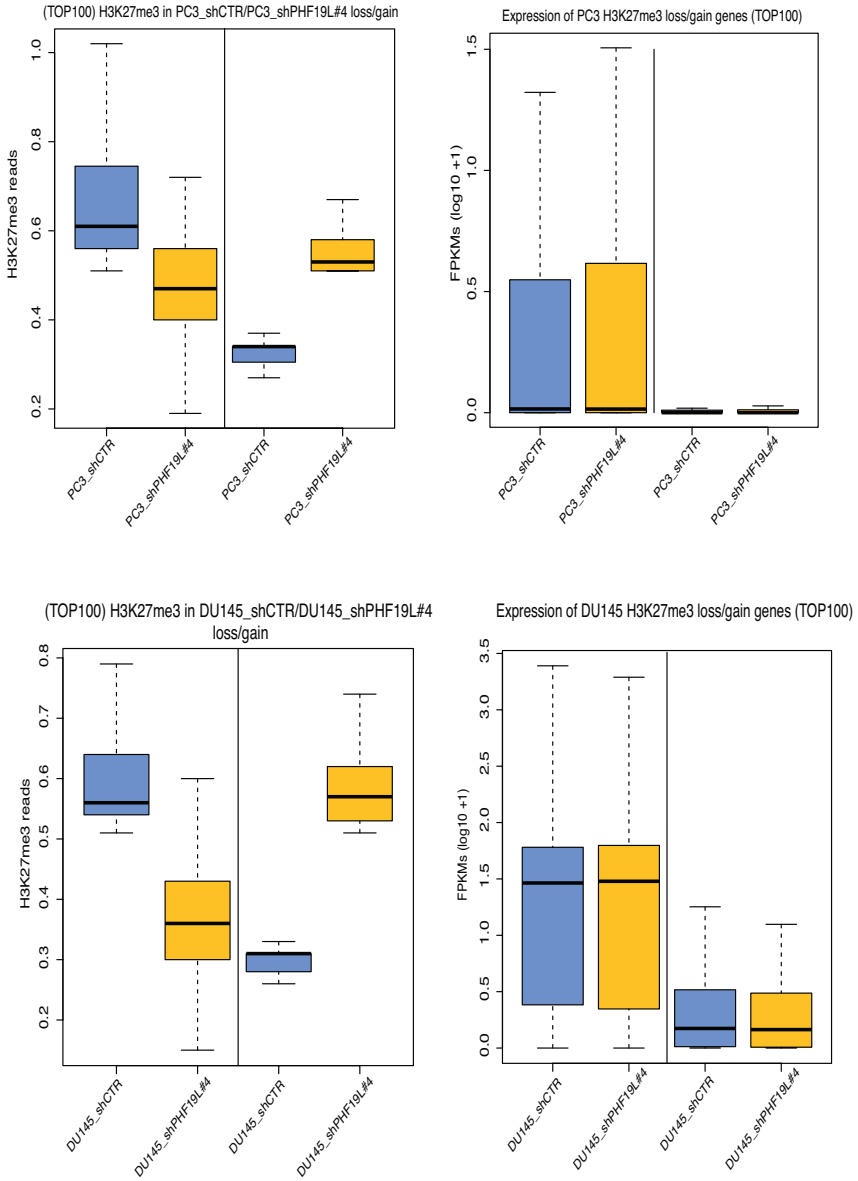

Figure 57: Box plots showing the differences in H3K27me3 reads lost or gained in the knockdown in PC3 and DU145 cells with corresponding box plots showing changes in gene expression associated with H3K27me3 reads.

We performed GO analysis to examine the role of these genes (Figure 58). In DU145 cells, the genes that lost H3K27me3 or showed a reduction in H3K27me3 levels were mostly associated with GTP metabolic process and Insulin signalling pathway. On the other hand, the genes that gained H3K27me3 were associated with synapse organization, epidermal cell differentiation, and adrenergic receptor signalling pathway.

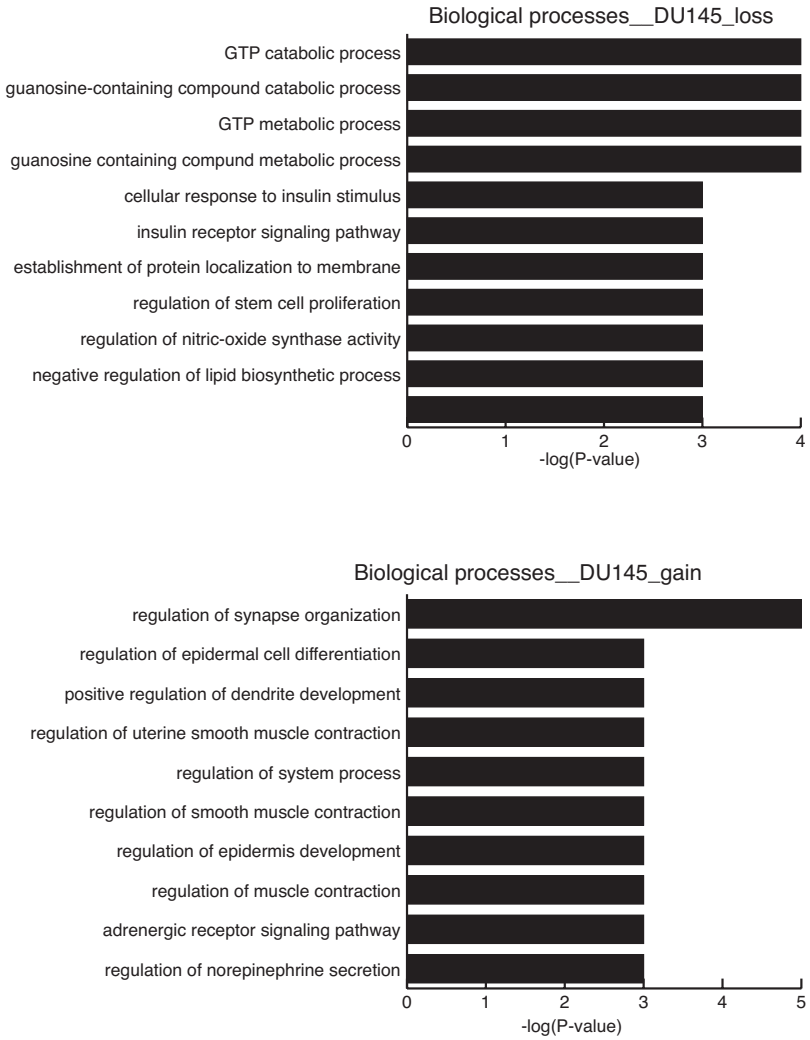

Figure 58: GO (Enrichr) of genes that loose or gain H3K27me3 in DU145 shPHF19L cells.

Below are some examples of the genes that loose and gain H3K27me3 in DU145 cells (Figure 59). However, with the exception of two genes, many of these genes do not change expression.

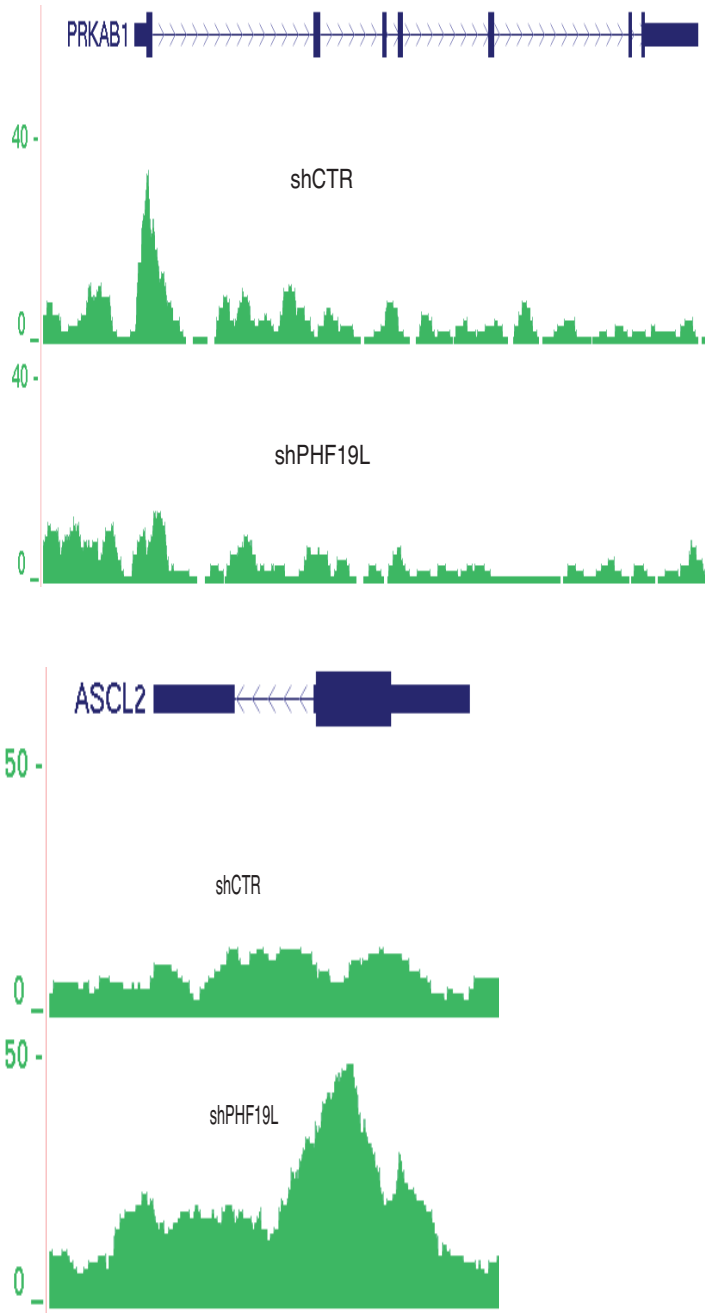

Figure 59: UCSC screenshots of PKRAB1 that looses H3K27me3 and ASCL2 that gains H3K27me3 upon knockdown in DU145 cells.

Although 20% of the upregulated genes upon knockdown of PHF19L contain H3K27me3, only four genes (*IL6R, DUSP6, CCND1, BCAR1*) show a minor reduction of this mark (Figure 62). The remaining genes although upregulated maintain the same levels of H3K27me3. These include genes such *DUSP4, DUSP8, CXCR4, LOX* and *VEGFA* (Figure 60).

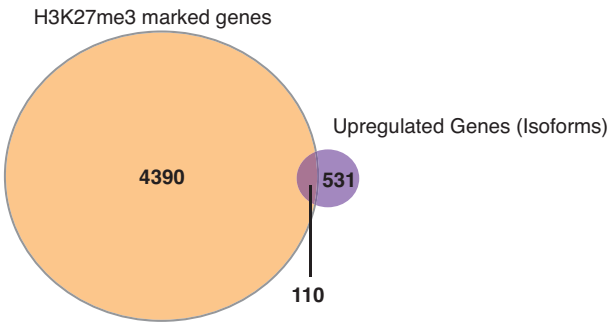

Figure 60: Venn diagram showing overlap of genes marked by H3K27me3 that get upregulated upon knockdown of PHF19L.

In addition, although the two isoforms of *OAS1* are repressed, the third isoform that is expressed and gets downregulated upon knockdown of PHF19L gains H3K27me3 (Figure 61). Below are representative examples from each scenario.

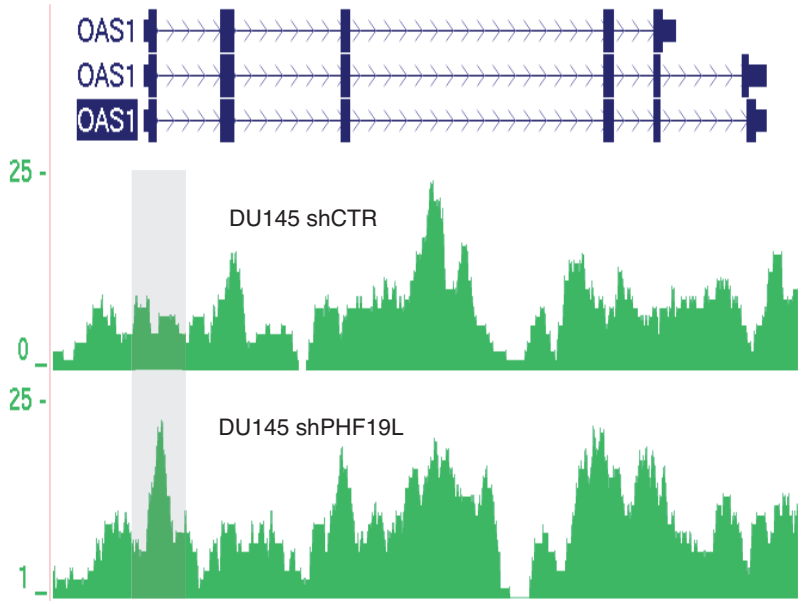

Figure 61: Screenshot from UCSC genome browser showing the gain of H3K27me3 at *OAS1* promoter in knockdown cells.

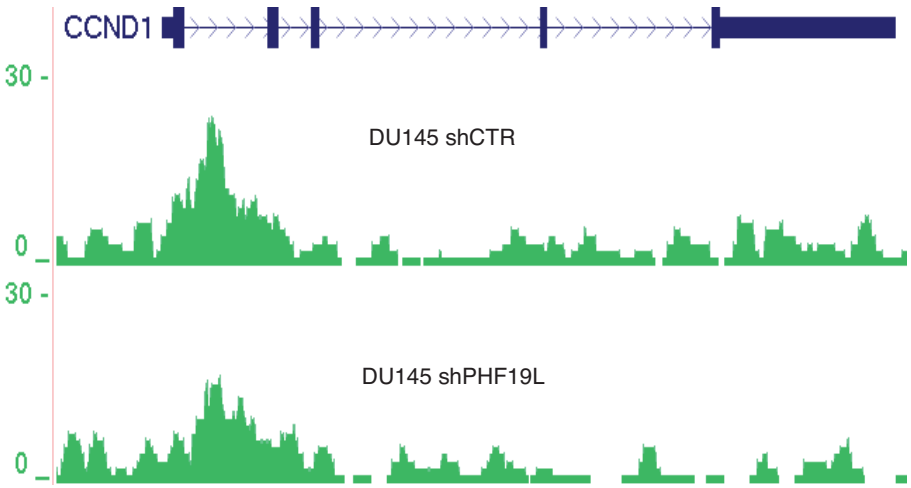

Figure 62: Screenshot from UCSC genome browser showing minor reduction in levels of H3K27me3 at *CCND1* in knockdown cells.

In PC3 cells, there is no significant loss of H3K27me3 except on handful of genes. Most of the genes show only a mild decrease in the levels of H3K27me3. On the other hand, there is a significant gain of H3K27me3 on some of the genes. The genes with mildly reduced levels of H3K27me3 are mostly associated with endothelial cell differentiation and neuron differentiation whereas the genes that gained H3K27me3 are associated with cAMP metabolic process (Figure 63). However, none of these genes change expression upon knockdown.

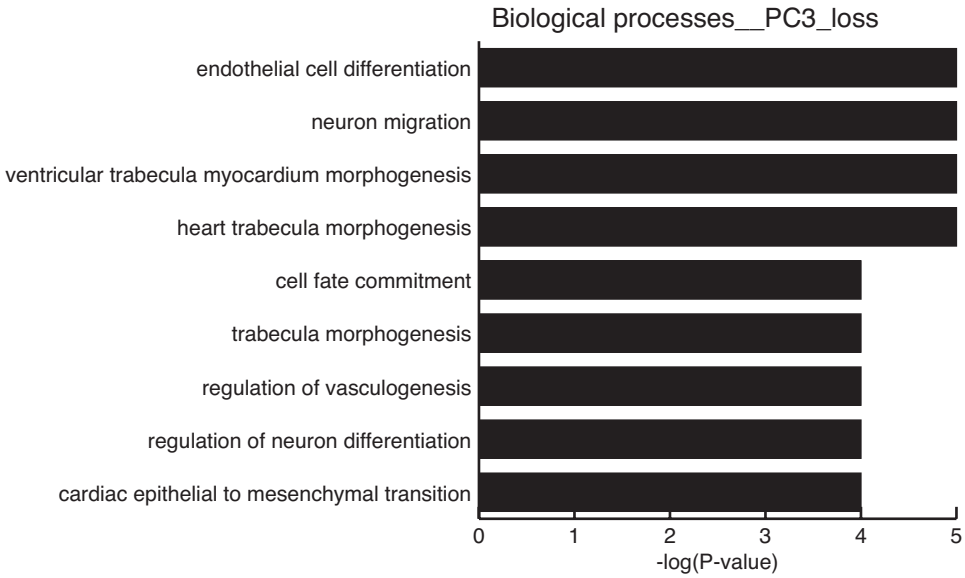

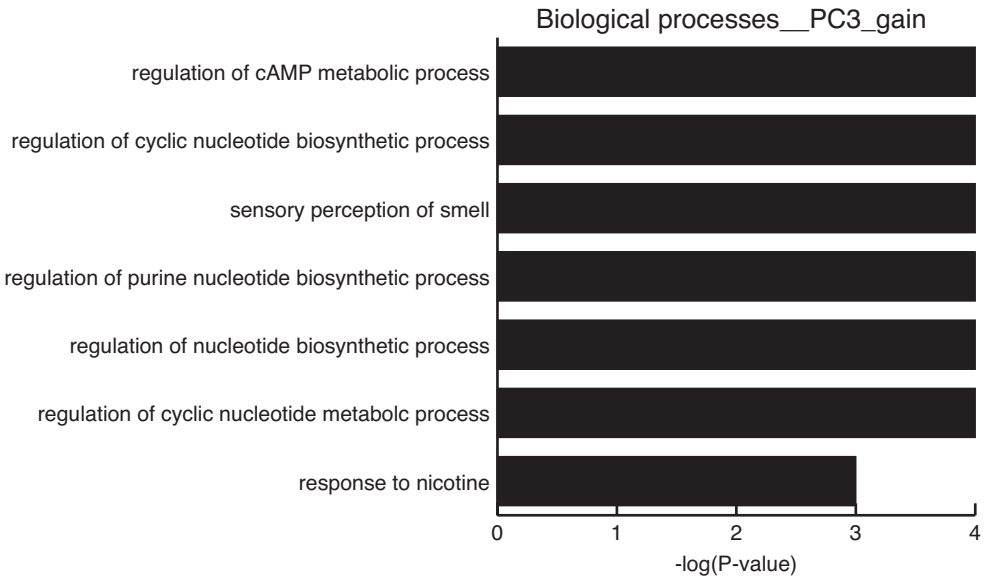

Figure 63: GO (Enrichr) of genes that loose and gain H3K27me3 in PC3 shPHF19L cells.

Below are some representative examples of genes that gain and loose H3K27me3 in PC3 cells (Figure 64).

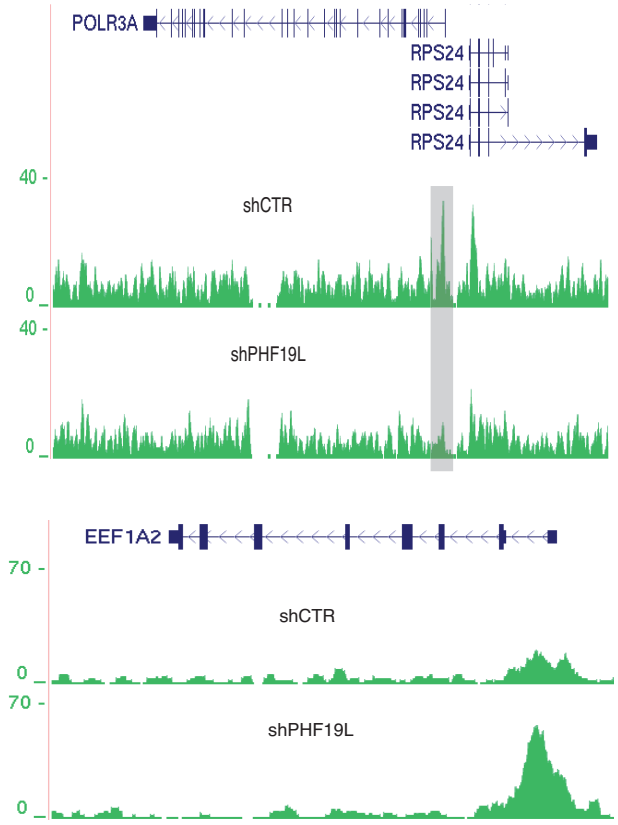

Figure 64: UCSC screenshots showing loss and gain of H3K27me3 at *POL3A* and *EEF1A2* upon knockdown in PC3 cells.

Among the genes that are associated with the phenotype, we observe a partial loss of H3K27me3 from *HIF1A* and *HEY1* (Figure 65). HEY1 is a downstream target of NOTCH3 that gets upregulated upon knockdown and HIF1A can trigger angiogenesis. However, these two genes do not change their expression and therefore it is not clear if there are additional factors required for their activation.

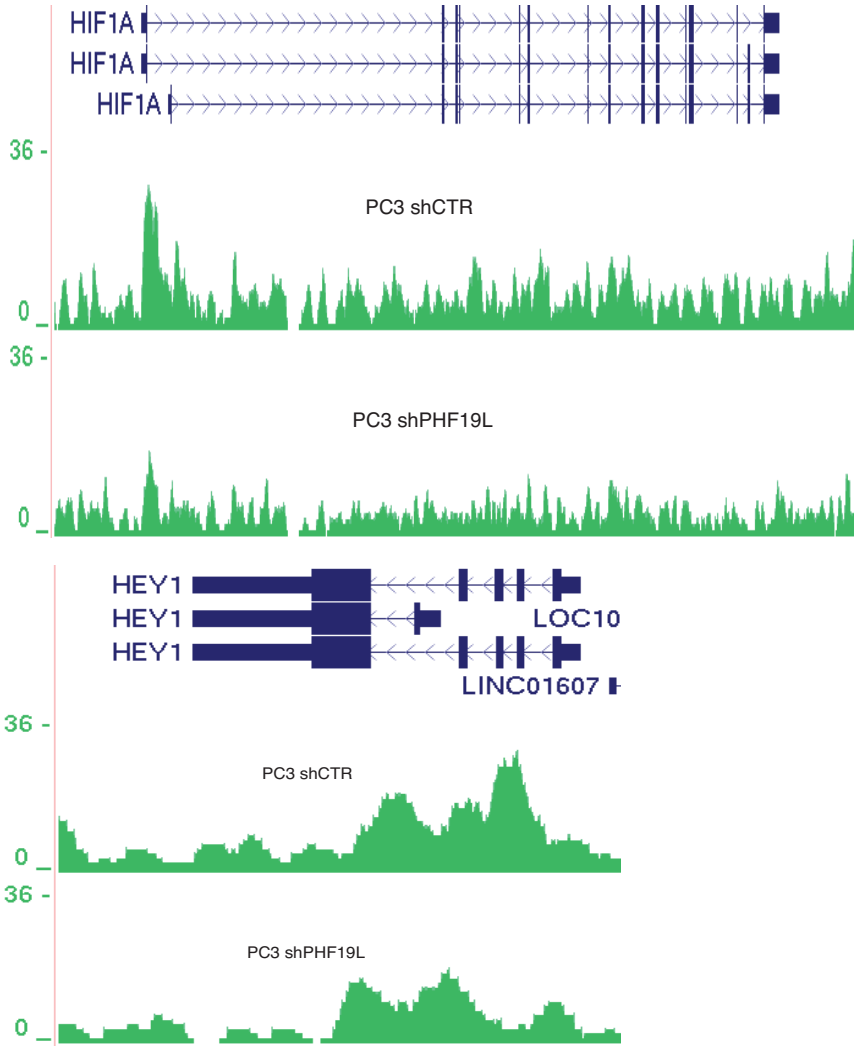

Figure 65: Screenshot from UCSC genome browser showing the loss of H3K27me3 from *HIF1A* and *HEY1* promoters and *TGFBR1* 3´UTR in PC3 shPHF19L.

Lastly, there is a very poor overlap between genes that contain H3K27me3 in wild type cells compared to genes that get upregulated upon knockdown of PHF19L in PC3 cells suggesting possibly no role of H3K27me3 in changes mediated by PHF19L in these cells (Figure 66).

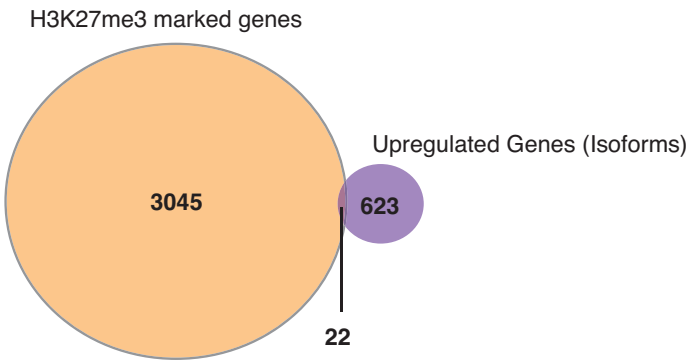

Figure 66: Venn diagram showing the overlap between H3K27me3 marked genes in PC3 cells compared to upregulated transcripts upon knockdown of PHF19.

Therefore, in both the cell lines, the genes that get upregulated upon knockdown do not necessarily loose H3K27me3 as in the case of DU145 or are not associated with this mark as in the case of PC3 cells. The handful of genes that do show significant change in the levels of H3K27me3 do not get activated or change expression upon knockdown suggesting no role of PRC2 mediated H3K27me3 in transcriptional changes induced by loss of PHF19L.

2.14 PHF19L interaction with EZH2 does not depend on posttranslational modification of EZH2

As there was a poor association of upregulated genes with H3K27me3, but the only complex that PHF19L interacts with in PC3 cells is PRC2, we investigated if PHF19L can interact with phosphorylated EZH2 that has been described to be associated with active genes and may suggest a role of PHF19L as a transcriptional activator.

PC3 cells are PTEN null and should have constitutively active AKT kinase. This phospho-AKT can phosphorylate EZH2 at serine 21, which has been postulated to be associated with actively transcribed genes and not with H3K27me3. We therefore asked if PHF19 could associate with phosphorylated EZH2 in PC3 cells. We ectopically co-expressed FLAG tagged PHF19 and HA tagged wild type (WT-EZH2), phospho-mimic EZH2 (HA-EZH2 S21D) where serine has been replaced with aspartic acid and phospho-mutant EZH2 (HA-S21A), where serine has been replaced with alanine in 293T cells. Co-immunoprecipitation experiment showed that PHF19

could interact with both phosphorylated and non-phosphoryated form of EZH2 suggesting that its interaction does not depend on this posttranslational modification (Figure 67). However, in spite of several attempts, we could not obtain a ChIP-grade antibody for EZH2 in human-derived prostate cancer cells and therefore it was difficult to explore this aspect of EZH2 in context of PHF19.

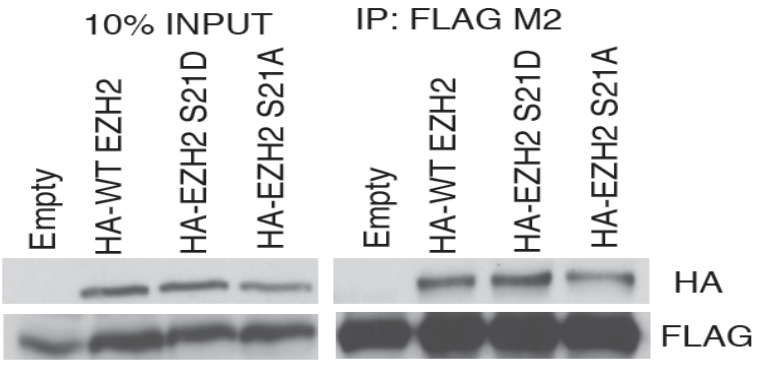

Figure 67: Co-immunoprecipitation of PHF19L_3XFLAG with Empty, HA-WT EZH2, HA-EZH2 S21D (phospho-mimic) and HA-EZH2 S21A (phospho-mutant) in 293T cells.

Therefore, to conclude, we have described in this thesis dual role of PHF19 in promoting growth and proliferation and inhibiting aggressive nature of two prostate cancer cell lines PC3 and DU145. We have also described its role in RWPE1 cells, where it promotes undifferentiated state of prostate epithelial cells. We have not been able to modulate the direct effect of PHF19L in these cells in absence of ChIP-sequencing, however, we can conclude that the mechanism of action is not via canonical role of PRC2 mediated H3K27me3 in both the prostate cancer cell lines. Thus, the mechanism of action of PHF19 remains to be explored for future work.

DISCUSSION

3 Discussion

3.1 PHF19 is specifically expressed in AR negative and metastatic prostate cancer

Based on the expression in clinical samples in two previously described datasets and expression in cell lines, PHF19L is expressed in a subset of metastatic and castration resistant prostate cancer tissues, and in androgen negative cancer cell lines and normal prostate epithelial cells. At the first glimpse, the expression of PHF19 seems to be exclusive in cell lines expressing AR and PSA. There have been conflicting reports that PC3 and DU145 cells may still express AR (Alimirah *et* al., 2006; Jarrard *et al*., 1998). We do not detect any transcripts for AR and KLK3 (PSA) in RWPE1, DU145 and PC3 cells in our RNA-seq data (FPKM = 0), confirming that there is no expression of AR and PSA in these cell lines. On the other hand, it is well described that LNCaP cells and LNCaP-abl cells express AR and PSA (Culig *et* al, 1999; Horoszewicz *et al*., 1983). Therefore, at least in cell lines, PHF19 is a feature of cells lacking expression of AR or PSA. With respect to the clinical tissues, in one of the studies that performed molecular profiling in prostate cancer progression, the authors show that genes that are overexpressed from benign to localized prostate cancer include gene ontology categories, such as protein synthesis and androgen signalling (Tomlins *et al*, 2007). This could explain why no significant change in expression of PHF19 is seen at this stage. However, these molecular pathways change between localized to metastatic prostate cancer. In metastatic cancer, the emphasis is on increased proliferation and in hormone naïve prostate cancers as opposed to hormone-refractory, there is downregulation of androgen signalling and protein synthesis concepts (Tomlins *et al*., 2007). This is quite interesting as PHF19 expression increases specifically in metastatic prostate cancer and assuming negative correlation with AR in prostate cancer cell lines, this increase could be specific to hormone-naïve prostate cancers. This is also in agreement with the role of PHF19 in proliferation of prostate cancer cells that are AR negative and suppression of growth of LNCaP cells upon expression of PHF19L that is AR+.

AR and PSA drive differentiation in prostate cancer and high-grade prostate cancers are usually associated with dedifferentiation. Phf19 is expressed in mouse embryonic stem cells and its expression is downregulated upon differentiation. RWPE1 cells are undifferentiated (no expression of CD24 only population), and PC3 and DU145 cells both form poorly differentiated tumours in xenograft experiments (Gilloteaux *et* al, 2012; Tai *et al*, 2011). Therefore, PHF19 may negatively correlate with degree of differentiation in prostate cancer and thus could serve as a biomarker for detecting dedifferentiation.

3.2 The role of short isoform of PHF19 and common interactor GNAI2

There is overexpression of the short isoform at transcript level in prostate cancer cell lines, specifically in PC3 and DU145 cells. However, knockdown of this isoform does not produce changes in phenotype or gene expression. In addition, this isoform although has the TUDOR domain – that is implicated in binding to H3K36me3 – is not present in the chromatin, but rather interacts with components of mRNA processing complex as opposed to PRC2 complex. The predicted nuclear localization signals in the long transcript are located after the PHD2 domain (Wang *et al*, 2004), which could explain the absence of this isoform in the nucleus. Further, the C-terminal part of the protein has been shown to interact with PRC2 complex (Ballare *et al*., 2012), which could explain why this isoform does not interact with PRC2 complex. The short isoform is absent in mouse and therefore the emergence of this transcript and specifically its overexpression in cancer might be of some biological value. However, in our system we could not detect any changes upon knockdown of this isoform. Among the interactors in PC3 cells, we found one interactor that was shared by both PHF19L and PHF19S. GNAI2 codes for a protein that is an alpha subunit of guanine nucleotide binding proteins (G proteins). This protein contains guanine nucleotide binding site and is involved in hormonal regulation of adenylate cyclase. Interestingly, GNAI2 has been shown to be required for migration of PC3 cells and is overexpressed in prostate cancer. The oxytocin receptor (OXTR) induces migration in PC3 cells along with EGF; however, this function requires coupling to G protein and is

dependent on GNAI2 dependent signalling in PC3 cells (Zhong *et al*, 2012). How PHF19 fits into this is still an open question. It is curious to observe though that upon knockdown of PHF19L, this receptor gains H3K27me3 in DU145 cells although no significant change is observed in PC3 cells (Figure 1). However, we observe an opposite effect on cell migration upon knockdown of PHF19L and therefore most likely PHF19L is not regulating this function of GNAI2. We did not conduct the transwell migration assay for PHF19S and therefore we cannot conclude if there will be an effect. Nevertheless, GNAI2 has also been implicated in regulation of cell growth, proliferation and transformation of fibroblasts through cAMP signalling pathway and the downstream MEK-ERK pathway (Dhanasekaran *et al*, 1998) and therefore the role of PHF19L in cell growth and proliferation could be associated with GNAI2. However, this was not explored in this thesis.

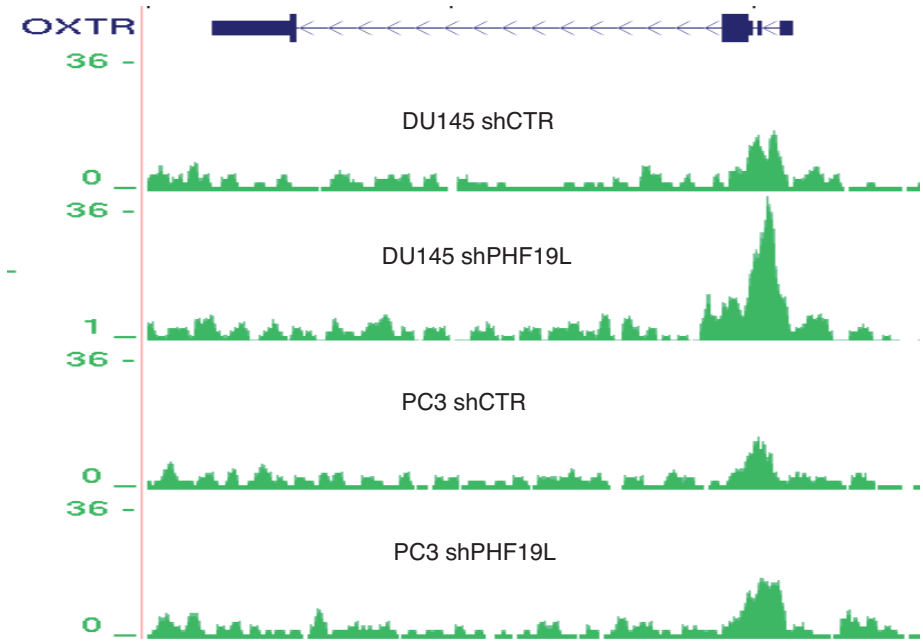

Figure 1: Screenshot from UCSC genome browser showing the H3K27me3 profile in PC3 and DU145 control and knockdown cells at *OXTR*.

The specific interactors of the short isoform included RBMX, S10AG and EF2. RBMX is a heterogenous nucleus ribonucleoprotein that has been shown to interact with members of splicing complex although this is tissue specific (Kanhoush *et al*., 2010). It has been also shown to colocalize to DNA lesions and to facilitate recombination in PAPR1 dependent manner (Adamson *et al*.,

2012). Apart from its functions as RNA binding protein, it can also associate with chromatin and maintain proper cohesion of sister chromatid (Matsunaga *et al*., 2012). On the other hand, S10AG also known as S100A16 is a Ca^{2+} binding protein whose expression is found to be elevated in several tumors (Sturchler *et al*., 2006). Overexpression in 3T3-Li preadipocytes leads to increased proliferation. It also interacts with p53 and increases the response of p53 dependent genes (Liu *et al*., 2011). Lastly, EF2 is an elongation factor that catalyzes the translocation of elongated peptidyl-tRNA from A-P sites of ribosome and promotes G2/M progression mainly by translating RNAs such as *MYC*, *VEGF* and *CCND1* (Nakamura *et al*., 2009). Thus, the interactors of PHF19S are involved in several diverse biological processes; however, absence of any obvious change makes it difficult to analyse how the protein might be involved in mediating these processes in prostate cancer. Since two of its interactors are involved in interaction with RNA, one cannot rule out that the protein might have a function with RNA binding. In addition, it is also not clear if PHF19S can elicit any response in the absence of PHF19L that can help explain the phenotype observed.

3.3 PHF19L is required to maintain undifferentiated state of intermediate cells of the prostate.

The knockdown of *PHF19L* in RWPE1 cells leads to differentiation and some changes associated with actin cytoskeleton. As observed by FACS, RWPE1 cells contain both CD44+ and CD44+/CD24+ population. However, there is absence of CD24 only population suggesting that these cells closely resemble intermediate and transit amplifying cells of the prostate epithelium.

The human chromosome locus 1q21 contains many genes that encode for proteins of late epidermal differentiation across a 2-Mb region. This is called the epidermal differentiation complex (EDC). EDC consists of group of precursor proteins of the cornified envelope such as involucrin and loricrin, the SPRRs proteins and late cornified envelope proteins (Kypriotou *et al*., 2012). Several members of this epidermal differentiation are upregulated upon knockdown of *PHF19L* in RWPE1 cells. These include the precursor proteins *IVL* and *LOR* and several members of the SPRR family including *SPRR3,*

SPRR2A, SPRR1A and *SPRR1B* among others. This clearly demonstrates a crosstalk between PHF19L and transcription factors that may regulate transcription of genes associated with this locus. Indeed, Ezh2 has been shown to be associated with basal cells of developing epidermis where it represses specific EDC genes. In P0 *Ezh2* conditional knockout animals, the epidermis displays hyper thickened stratum corneum and granular layer that is accompanied by expression of granular markers loricrin and filaggrin (Ezhkova *et al*, 2009). Although, there is a poor overlap of differentially expressed genes between *siEZH2* and *shPHF19L* in RWPE1 cells, the pathways regulated by the two proteins seem to be alike. Further, Ezh2 inhibits Ap1 transcription factor recruitment to epidermal differentiation genes (Ezhkova *et al*, 2009) due to the presence of H3K27me3. Using Enrichr position weight matrices (PWMs), that identifies transcription factor that are enriched for target genes within the input list, AP1 is the first transcription factor that is enriched in list of upregulated genes in RWPE1 sh*PHF19L* with a p value of 2×10^{-5} in our RNA-seq. Therefore, most likely the function of PHF19L in the prostate epithelium is to repress the epithelial differentiation genes through EZH2 inhibition of AP1.

CD24 is marker of luminal secretory cells and this marker is upregulated upon knockdown of *PHF19L*. FACS analysis of both CD44 and CD24 clearly showed a loss in staining of CD44 in the population suggesting the loss of basal cell marker in the cell and progression towards luminal cell lineage. Although the gain in CD24 population was very small, achieving complete luminal differentiation is usually challenging in cell culture and may also require co-operation of other factors that are required for complete differentiation. The role of MYC in prostate differentiation is not well understood. In general, overexpression of MYC is associated with proliferation; however, a modest increase in MYC over a brief period is associated with differentiation (Frank and Miranti, 2012). We also observed only a modest increase in the levels of *MYC* and therefore this could either be an indirect effect of consequent differentiation or could imply a crosstalk with other transcription factors.

The two cytoskeletal proteins *ACTB* and *ACTG1* are also upregulated. ACTB commonly drives cell migration by polymerization of actin filaments providing

forces that push the cell membrane forward. Actins are required for maintenance of cell shape (Bunell *et al*, 2010) and *Actb* is required to maintain total actin and specifically G-actin pool (Bunell *et al*., 2011). Cell adhesion is tightly coupled to actin polymerization and we observe an increased cell-to-cell contact and change in shape of the cells in the knockdown of *PHF19L*. It must also be noted that increased levels of ACTB are observed in prostate cancer tissues compared to normal tissues (Mori *et al*., 2008) and therefore the long-term consequences of this increase could be linked to development of cancer. While Actb is usually enriched at the leading edge of migrating cell, gamma actins are uniformly distributed in the cell. *Actg1* knockout MEFs do not shown any problems with cell migration, however, they have reduced cell growth and viability (Bunell *et al*., 2010). Thus, the increase in *ACTG1* in RWPE1 could promote cell viability.

We also observed a downregulation of *KLF4*, *CBX4*, *TWIST1* and *VEGFA* among other transcription factors. Cbx4 has been shown to inhibit epidermal stem cell differentiation and its expression negatively correlates with early precursors of epidermal differentiation and c-Myc (Luis *et al*., 2011). Therefore, a decrease in the levels of CBX4 are as expected. However, what is not clear is the downregulation of *KLF4*. Klf4 is usually required for epithelial differentiation (Segre *et al*., 1999) and therefore the role of KLF4 in this context is contradictory. However, in embryonic stem cells, Klf4 represses the transcription of endodermal genes that are committed to endodermal differentiation (Aksoy *et al*., 2014). Prostate is derived from endoderm and therefore in these cells, KLF4 might have a different function as that of keratinocytes. Additionally, *Spr22a* promoter is regulated by Klf4 in epidermal differentiation (Segre *et al*., 1999), however, in RWPE1 cells, this is upregulated inspite of downregulation of *KLF4* in the knockdown thus favouring a different mechanism of action of KLF4 in these cells. TWIST1 is usually associated with epithelial to mesenchymal transition in prostate cancer cells and many other cancers (Kwok *et al*., 2005). TWIST1 also promotes angiogenesis by upregulating VEGFA (Mironchik *et al*., 2005). It has been shown that expression of EMT markers such as TWIST1 can convert luminal differentiated cells into mammary epithelial stem cells (Mani *et al*., 2008) and therefore downregulation of both these factors will most likely promote the

reverse scenario of conversion of stem-like or progenitors cells of the prostate to luminal differentiated cells and could also explain the loss of CD44 surface marker in the knockdown cells.

Therefore, in conclusion PHF19 regulates the maintenance of intermediate cells of the prostate in undifferentiated state and its subsequent knockdown initiates differentiation into the luminal phenotype mediated via crosstalk between actin cytoskeleton rearrangement and transcription factors and possibly via EZH2 and its role in epidermal differentiation.

3.4 Role of PHF19L in proliferation of prostate cancer cells

In order to understand the role of PHF19L in cell growth and proliferation, it is important to understand the two central pathways that play a role in cell growth and proliferation.

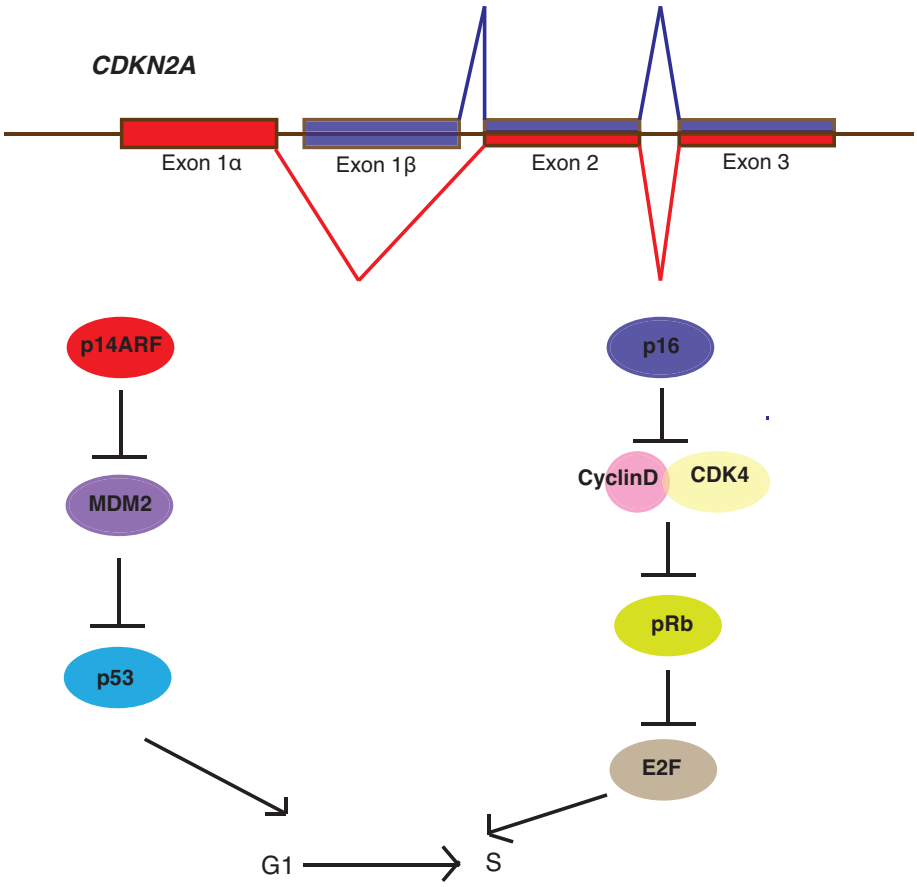

Figure 2: CDKN2A locus (Adapted from Lin *et al*., 2008, British Journal of Dermatology). CDNK2A encodes two proteins p16INK4A and p14ARF as denoted by separate exons and share exon 2 and 3. Loss of p16INK4A leads to inactivation of Rb pathway and inactivation of p14ARF leads to abrogation of p53 pathway.

In both the prostate cancer cell lines, there is an inhibition of growth and decreased proliferation upon knockdown of PHF19L. *CDKN1A* is upregulated and *CDK4, CCNA2* and *AATF* are downregulated in both the cell lines. In addition, *E2F1* is downregulated in PC3 cells. The *CDKN2A* gene encodes two isoforms *p16INK4A* and *p14ARF* in humans. Based on our RNA-seq data, in PC3 cells only *p14ARF* is expressed whereas in DU145 cells, both *p16INK4A* and *p14ARF* are expressed. Thus in PC3 cells, in absence of p16, there is constitutive activation of CDK4. Therefore, its inhibition is independent of *CDKN2A* locus. In PC3 cells, we also observe an upregulation of genes associated with both type I and type II interferon signalling. IFNAR1 is silenced in PC3 cells and we do not observe any changes in expression of other receptors including IFNAR2, IFNGR1 and IFNGR2. It is not clear what leads to activation of this signalling. IFITM1, member of IFN-inducible transmembrane protein family has been shown to reduce growth rate in hepatoma cell lines by inhibiting ERK and reducing the Thr55 phosphorylation of p53 leading to upregulation of *CDKN1A (p21)* (Yang *et al*., 2007). However, PC3 cells are null for p53. Therefore, this effect has to be independent of p53. We observe 1.7-fold upregulation of downstream effector of IFN signalling, *STAT1* as well as upregulation of *JAK3* in these cells. It has been shown that IFN-gamma can induce STAT1 that binds to promoter of p21 and activate it that typically leads to growth arrest (Chin *et al*., 1996). Therefore, the upregulation of several members of interferon signalling could activate the expression of p21. Similarly, IFN alpha has been shown to inhibit H1 kinase activity of CDK4 via p21 (Mandal *et al*., 1998). p21 can also both inhibit and act as a substrate for CDK4 thus presenting a feedback loop between the two proteins mediated by phosphorylation of p21 (Bisteau *et al*., 2013). Therefore, most likely the downregulation of CDK4 is a consequence of upregulation of p21, which is in turn activated by IFN signalling. Which of these genes is a direct target of PHF19 is still a question in the absence of a ChIP-seq. The mild changes in H3K27me3 suggest that PHF19 may be an activator and CDK4 could be a direct target since this gene is downregulated in all the cell lines tested. Inhibition of CDK4 will lead to hypophosphorylation of RB1, which in turn will inhibit E2F1. Consequently, we see a downregulation of *E2F1*. Interestingly, it has been shown that AATF can bind to pocket region of RB1

and compete with HDACs thus preventing HDACs from being recruited to E2F1 responsive promoters and allowing transcription (Bruno *et al*., 2002; Passananti *et al*., 2007). Downregulation of *AATF* would thus further augment the RB1 mediated deposition of HDACs and affect the transcription of E2F activated genes, which we see in downregulation of E2F1 target gene *CCNA2*. As mentioned in the introduction E2F proteins also regulate the expression of Polycomb components EZH2, SUZ12 and EED and subsequently we also see a downregulation at protein levels for both EZH2 and SUZ12.

Thus, PHF19L regulates a very important cascade involved in cell growth and proliferation by regulating transcription of several genes involved in this process. As mentioned above, it is important to know which of these are direct targets or if this action is mediated by an upstream regulator.

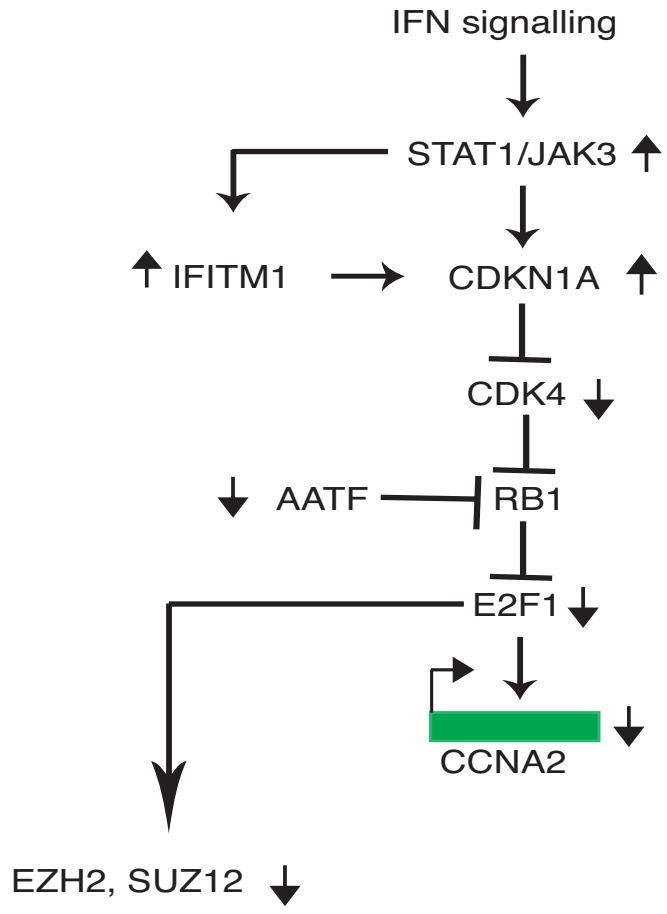

Figure 3: PHF19L mediated transcriptional changes leading to growth arrest in PC3 cells.

In addition to the genes associated with cell growth, we also observe a downregulation of genes involved in RNA processing such as *EIF4B*,

MRPL44, *RNMT*, *UPF2*, and *AARS*. RNMT is RNA guanine -7 methyltransferase that is recruited to transcription initiation site where it methylates nascent transcript in mRNA cap methylation. This methylation is necessary for stabilization of mRNA, its export and cap dependent translation initiation. Two transcription factors MYC and E2F1 have been implicated in increasing cap depedent methylation by recruiting transcription factors that phosphorylate paused RNA polymerase that can then recruit RNMT (Cole *et al*, 2009). Several differentially expressed genes associated with RNA processing in our RNA-seq in PC3 cells contain the MYC:MAX motif including RNMT and therefore this implies a link between PHF19 regulated transcription and MYC. EIF4B is a translation initiation factor that binds to 5´UTR of mRNA in a cap dependent or cap independent manner and is required for ribosome entry at the 5´UTR. EIF4B is also required for survival and proliferation of HeLa cells due to translation of important mRNAs linked to these processes (Shahbazian *et al*., 2010). AARS is the alanyl-tRNA synthetase that links cognate amino acid to transfer RNA. This process is essential for correct translation of the genetic code into the protein sequence. UPF2 is a regulator of nonsense transcripts and is part of post-splicing complex that is involved in mRNA nuclear export and mRNA quality control. It detects and degrades mRNA with premature stop codons and protects from deleterious effect of C-terminally truncated proteins (Clerici *et al*., 2014). However, its depletion does not affect the growth of HeLa cells (Wittmann *et al*., 2006). Lastly, MRPL44 is a ribosomal protein that is encoded by nuclear genes and helps in protein synthesis within the mitochondrion. Thus, an inhibition in transcription of these components will eventually lead to reduced cap methylated mRNAs, export of nonsense transcripts, inefficient cap dependent translation initiation, and a decreased abundance of amino acids linked to tRNA. Eventually, this will effect translation of mRNA and protein synthesis. This is also reminiscent of the mTOR pathway that is closely linked to protein synthesis and it remains to be elucidated if PHF19 may directly regulate an important component of this pathway. We did not check abundance of non-sense transcripts or methylated *versus* non-methylated mRNAs as this was outside the scope of the lab. However, several downregulated transcripts could be a direct effect of this

process. Lastly, the gene expression changes associated with these genes are specific to PC3 cells, and are absent in DU145 cells.

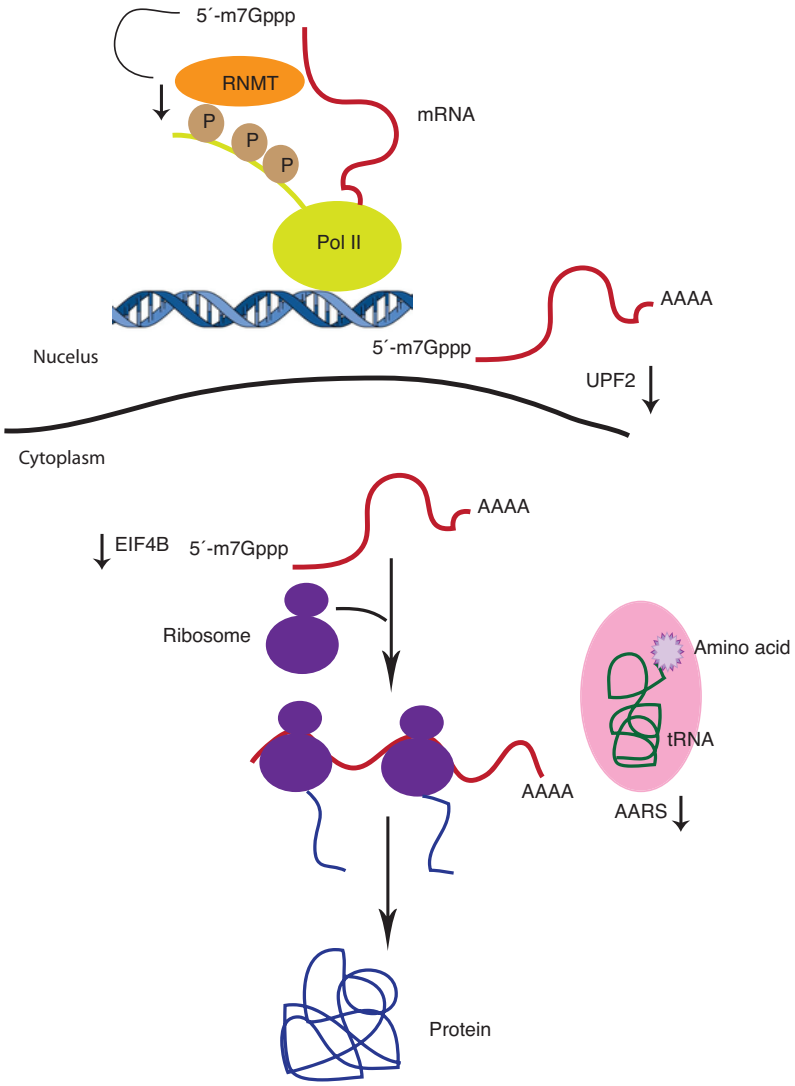

Figure 4: PHF19 transcription regulation of genes encoding proteins involved in various steps of RNA processing and protein translation. Adapted from Cole *et al*., 2008, Nat Rev Mol Cell Biol).

The scenario in DU145 cells is slightly more complicated. Although, we see an upregulation of *CDKN1A* and downregulation of *CDK4* and *AATF*, no changes are observed in the expression of *E2F1*. In addition, we see an upregulation of *CCND1* that is usually in complex with CDK4. Lastly, the same interferon responsive genes that are upregulated in PC3 cells are now downregulated in DU145 cells. This suggests that although there is some convergence in the pathways leading to cell growth and proliferation in two cell lines, there is also a divergence suggesting a different set of target genes.

One must note that DU145 cells have heterozygous PTEN, which is absent in PC3 cells, and thus this can affect the outcome of the transcriptional response mediated by PHF19. We also do not see any change in the expression of EZH2 and SUZ12 in the knockdown, which could be explained by no change in the levels of E2F1.

In DU145 cells, on one hand we see an upregulation of several members of dual specificity phosphatases (DUSPs) that will dephosphorylate and inactivate all the three different types of MAP kinases including ERK1/ERK2, p38 and c-Jun NH2 terminal kinase (JNK). At the same time, we see a downregulation of several genes associated with IFN signalling that will lead to suppression of immune response and make these cells insensitive to IFN mediated apoptosis. Thus, two integral pathways are deregulated that can result in a wide range of phenotypic alterations.

The ERK pathway regulates survival and cell growth. It has been shown to be required for prostate cancer tumorogenesis by regulating cellular proliferation, DNA synthesis and development of androgen independence in prostate cancer cells (Arnoldussen and Saatcioglu, 2009). DUSP6 can inactivate both ERK1 and ERK2 thus affecting the survival and growth of these cells. It prevents the cytoplasmic ERK to translocate into the nucleus (Caunt and Keyse, 2012). It has been shown that DUSP6 inhibits the proliferation and metastasis of DU145 cells (Zhai *et* al., 2014). Additionally, there is upregulation of DUSP4 and DUSP5 that dephosphorylate nuclear ERK1/ERK2 in response to mitogenic and stress signals (Cagnol and Rivard, 2013; Caunt and Keyse, 2012). p38 has been shown to be required in early stages of prostate cancer and well-differentiated carcinomas. However, its expression is reduced in advanced prostate cancer. Further, the ratio of ERK/p38 can either favour prostate cancer cell growth *in vitro* and *in vivo*, or the reverse can induce growth arrest (Arnoldussen and Saatcioglu, 2009). Among the DUSPs that increase their expression upon knockdown of PHF19L, several of them target ERK with few targeting p38 and JNK which can affect the ratios of these kinases and lead to growth arrest in DU145 cells as seen by cell growth curve and BrdU assay. The role of JNK is controversial in prostate cancer; however, most of the studies support its role in promoting apoptosis in prostate cancer cells. DUSP10 is upregulated and had been

shown to inhibit p38 and JNK. Expression of DUSP10 leads to reduced invasion, decreased prostate cancer cell growth and anti-inflammatory effects in various prostate cancer cell lines. Thus, on one hand it has been reported to act as a tumor suppressor whereas on the other hand, its inhibition of pro-inflammatory signalling in response to chemicals suggest a protective role in prostate cancer (Arnoldussen and Saatcioglu, 2009). DUSP8 also targets both p38 and JNK, however, there is little known about its role in prostate cancer.

Among the IFN-regulated genes, we observe a downregulation of *IFITM1*, *OAS1*, *IRF9*, *IFI6* and *IFI27*. IRF9 is essential for mediating transcriptional response of Type I and Type III IFN signalling as it forms the ISGF3 complex with tyrosine-phosphorylated STAT1 and STAT2 which binds to interferon stimulated response element (ISRE) to activate gene expression (Platanias, 2005). It is also a key factor for antiproliferative activity mediated by IFN-alpha (Tsuno *et al*., 2009). It has also been shown that oxidative stress (discussed later) inhibits IFN alpha induced transcription by inhibition of JAK1 and Tyk-2 (Di Bona *et al*., 2006). Consequently, we observe a downregulation of other genes as well as gain of H3K27me3 on the isoform of *OAS1* that is expressed. In addition, it has been shown that this pathway and the associated genes are downregulated upon transformation of normal prostate epithelial cells RWPE1 with MYC or PI3K/AKT, and therefore its further downregulation in DU145 cells upon knockdown of PHF19 could imply a crosstalk with these two oncogenic pathways that are also related to MAPK pathway.

Lastly, inhibition of p38 has been linked to inactivation of IFN-alpha mediated transcription regulation via ISRE binding as well as GAS element for IFN-gamma (Platanias, 2005) and therefore there could a crosstalk between activation of DUSPs that inhibit p38 and downregulation of interferon mediated transcription.

Thus, the most likeable outcome from these changes will be suppression of cell growth and survival on one hand, which in turn is balanced by downregulation of Interferon signalling as well as inhibition of JNK and p38, which can make the cells more resistant to apoptosis.

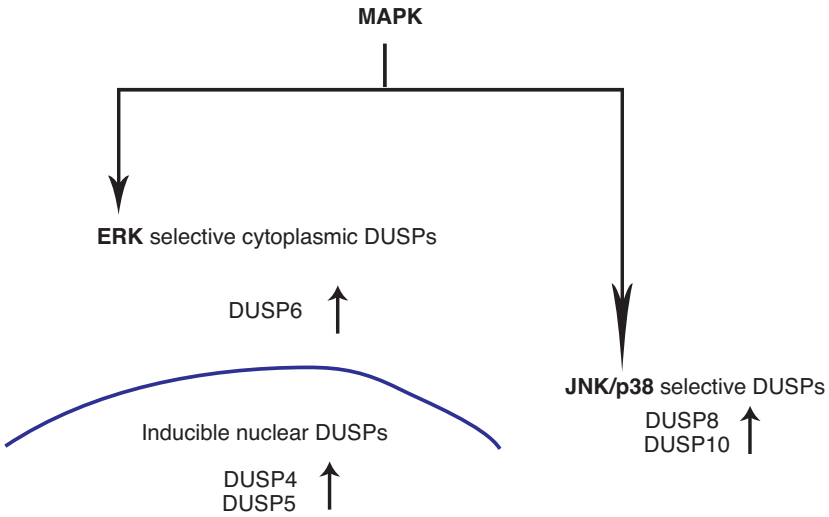

Figure 5: Transcriptional regulation of Dual specificity phosphatases by PHF19L in DU145 cells. Adapted from Caunt and Keyse, 2013, FEBS J.

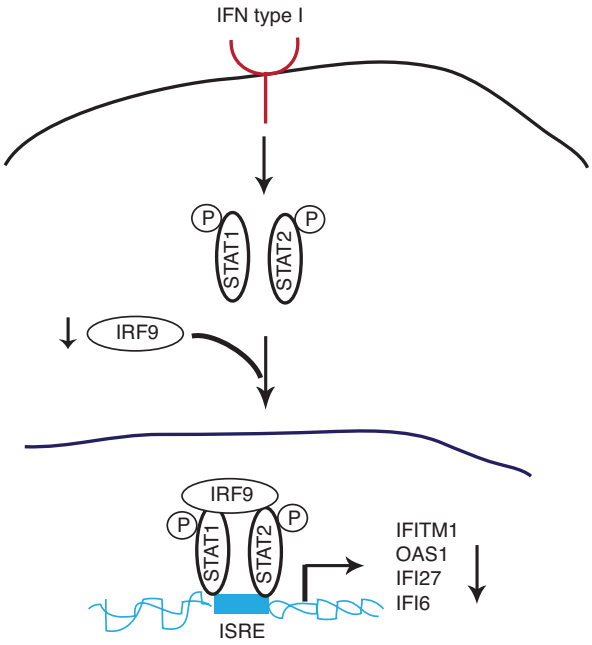

Figure 6: Transcriptional regulation of IFN signalling pathway by PHF19L in DU145 cells. Adapted from Platanias, 2005, Nat Rev Immunol.

3.5 Role of PHF19L in angiogenesis and invasion of prostate cancer cells

PC3 cells

In PC3 cells, the knockdown of PHF19L leads to upregulation of genes that are associated with survival, angiogenesis, and invasion and this in turn can be observed by increased invasion through matrigel in both transwell matrigel invasion assay and in three dimensional cultures of prostaspheres that clearly invade the extracellular matrix upon knockdown of PHF19L. Further, in spite of growth arrest and reduced proliferation, the cells do not undergo apoptosis suggesting activation of survival genes. BEX2 prevents mitochondrial apoptosis in breast cancer cells by regulating phosphorylation and activation of anti-apoptotic protein BCL2; and phosphorylation and inactivation of proapoptptic protein BAD (Naderi *et al*., 2010). In addition, it increases migration and invasion of glioma cells (Zhou *et al*., 2013). Although, there is no report of its role in prostate cancer, it is possibly mediating the same function in PC3 cells. EIF5A2 although less described in prostate cancer is frequently amplified and overexpressed in a wide variety of cancers and promotes invasion and poor prognosis in patients with gastric cancer, bladder cancer, melanoma and hepatocellular carcinoma. It is also a hypoxia responsive gene in esophageal squamous cell carcinoma (Li *et al*., 2014) and activates TGF-beta driven EMT in bladder cancer (Wei *et al*., 2014). Upregulation of several genes associated with degradation of ECM and poor prognosis is also observed. These include the serine protease PLAU (uPA) and its receptor PLAUR (uPAR) that has been shown to be required for *in vitro* invasion through matrigel in LNCaP, DU145 and PC3 cells (Forbes *et al*., 2004). Urokinase-type plasminogen activator (PLAU) is activated by binding to its cell surface receptor (PLAUR). The activated urokinase converts plasminogen to plasmin, which can directly degrade several ECM proteins as well as activate growth factors and MMPs that degrade ECM.

In addition, we observe an upregulation of adhesion receptors integrins *ITGB3* and *ITGB6* that induce prostate cancer via focal adhesion pathway (Li *et al*., 2013). ITGB6 is associated with poor survival in many cancers (Moore *et al*., 2014), and bind to FN1, its ligand and induce motility of prostate epithelial

cells (Azare *et al*., 2007). Consequently, we see an upregulation of *FN1*. ITGB6 has also been shown to mediate expression of PLAU via phosphorylation of p38 MAPK and PI3K/AKT pathway that leads to upregulation of uPA (Xue *et al*., 2013). It can also activate endogenous latent TGFβ1 and indeed we see an upregulation of *LTBP1* that targets latent complexes of TGFβ to the extracellular matrix (Munger *et al*., 1999). It must also be noted ITGB3 is associated with CD44+/CD133+ cancer initiating cells isolated from DU145 cells (Rentala *et al*., 2010). TGFβ also induces the expression of inhibitor of DNA binding proteins ID1 and ID3 which are required for TGFβ induced migration of PC3 cells (Strong *et al*., 2013). Both *ID1* and *ID3* are upregulated upon knockdown of PHF19L. ID1 has also been shown to be overexpressed in highly aggressive prostate cancer cell lines (Coope *et al*., 2004). Additionally, we see an upregulation of *NOTCH3*, associated with prostate cancer cells with high metastatic potential (Ross *et al*., 2011) and subsequent loss of H3K27me3 and possible activation of its downstream target HEY1.

Two pro-inflammatory cytokines *IL6* and its receptor *IL6R*, and *IL8* are also upregulated. Both IL6 and IL8 are increased upon hypoxia in prostate cells (Watson *et al*., 2009). IL8 enhances angiogenesis in tumor cells and mediate Ras induced tumor promotion and metastasis. It is also increased in advanced prostate cancer when tumor does not respond to anti androgens (Araki *et al*., 2007). Further, it is required for angiogenic activity of PC3 cells and tumorigenicity *in vivo* (Inoue *et al*., 2000). IL6 expression is also higher in androgen independent prostate cancer cell lines which show enhanced metastatic potential. This cytokine is activated by TGFβ and mediates resistance to chemotherapy. It can also lead to neuroendocrine differentiation in prostate cancer cell lines. Further, it plays a role in survival through PI3K/AKT pathway that is usually mediated by CCNA1 (Culig, 2014) and in our RNA-seq data, we see an upregulation of *CCNA1*. IL6 also mediates its effect via STAT3, however, PC3 cells are null for STAT3.

Further, we see an upregulation of *CD24*. CD24 has been described as a prognostic marker strongly linked to significantly earlier disease progression in prostate cancer (Kristiansen *et al*., 2004). Lastly, we see an upregulation of Follistatin (*FST*) that has been associated with tumor angiogenesis,

metastasis and as a prognostic marker in prostate cancer progression (Sepporta *et al*., 2013).

This is not an exhaustive list and we observe several other gene expression changes that can explain the metastatic phenotype that we observe upon knockdown of PHF19L in PC3 cells. There seems to be a crosstalk between PHF19 and TGFβ pathway as its knockdown activates several gene expression changes that are associated with activation of TGFβ1. We also see upregulation of *ACVR2B*, activin type II receptor that also binds ligands that belongs to TGFβ family. It must also be noted that although we do not observe any gene expression changes of HIF1A, we observe a loss of H3K27me3 at this gene which could explain the induction of IL6 and IL8 as a response to hypoxia mediated angiogenesis.

DU145 cells

In a similar fashion although via similar and different gene expression changes, we observe a hypoxia induced metastatic gene signature in DU145 cells upon knockdown of PHF19L. These genes act through several steps of metastasis and their overexpression in malignant cells will render the cancer cells even more aggressive. As a consequence, we see increased tube formation of HUVECs on matrigel when we use conditioned medium from knockdown cells.

Similar to PC3 cells, we see an upregulation of cytokines *IL8* and *IL6* receptor. Intriguingly, we do not see an overexpression of *IL6*. Repression of PTEN is associated with activation of IL8 under hypoxic conditions and induces hypoxia-mediated transcription required for survival. DU145 cells are heterozygous for PTEN allele and PC3 cells are null for PTEN and thus this activation can support survival under hypoxia in both the cell types (Maxwell *et al*., 2013). IL8 is also associated with increase of cyclin D1 expression in prostate cancer cells via mTOR pathway. Consequently, we see an upregulation of *CCND1* (Waugh and Wilson, 2008). IL6 and IL8 also play an important role in induction of bone metastasis driven by hypoxia and act via different downstream pathways to regulate angiogenesis, migration, tumor self-seeding and osteolysis during bone metastasis (Xin and Kang, 2010).

Hypoxic cells are required to have high motility in order to move to organs and tissues where there is more abundant oxygen and nutrients supply. This is usually facilitated by scatter factors called hepatocyte growth factor which signals through a high affinity HGF receptor tyrosine kinase encoded by *MET*. *MET* is upregulated upon knockdown suggesting increased motility of knockdown cells. MET has been shown to be induced by hypoxia both *in vitro* and *in* vivo where it synergizes with HGF in inducing invasive growth (Pennacchietti *et al*., 2003). The MET receptor can act as docking site for several signalling pathways such as MAPK, PI3K and JAK/STAT signalling and had also been involved in loss of cell-to-cell adhesion leading to breakdown of underlying basement membrane that triggers invasion (Sullivan and Graham, 2007).

Several genes that regulate motility of hypoxic cells and the processes of intravasation and extravastion that is driven by hypoxia are upregulated. These include vascular endothelial factor A and C (*VEGFA, VEGFC*), *MMP1* and *ANGPTL4*. Increased production of vascular endothelial growth factor is associated with increased tumor vascularity, increased interstitial pressure (Sullivan and Graham, 2007), metastasis and a high risk of biochemical failure in prostate cancer (Vergis *et al*., 2008). It also induces endothelial cell retraction on the basement membrane through disruption of adherens junctions, actin rearrangement, and induction of inter-endothelial cell gaps (Sullivan and Graham, 2007). MMP1 is a matrix metalloproteinase that is a synergistic mediator of vascular permeability and intravastion. It acts in cooperation with other factors that promotes vascular remodelling and metastatic progression to lungs in breast cancer. One of these partners include epidermal growth factor receptor (EGFR)/pan-HER ligand epiregulin (EREG), that is also upregulated upon knockdown (Gupta *et al*., 2007). These molecules play an equal role in extravasation along with *ANGPTL4*, a key adhesion that mediates vascular metastasis of hypoxic breast cancer cells and their extravastion in lung by inhibiting endothelial cell interaction. It must be noted that this molecule does not play a role in primary tumor growth and is purely required for vascular metastasis (Zhang *et al*., 2012).

Along with these, genes involved in homing and establishment of pre-metastatic niche are also upregulated. This includes the chemokine receptor

CXCR4 and lysyl oxidase *LOX*. Hypoxia increases the levels of *LOX* mRNA, which results in enhanced invasive migration that is required for metastatic spread. In addition, LOX remodels the extracellular matrix such as elastin and collagen that allows other cells to move freely thereby increasing migration and invasion. Its inhibition blocks *in vitro* migration and *in vivo* metastasis from subcutaneous xenografts or after tail vein injection (Erler *et al*., 2006). LOX has also been implicated in the recruitment of bone marrow-derived cells by crosslinking collagen IV and recruiting CD11b myeloid cells that create a pre-metastatic niche or an environment that allows for subsequent invasion and growth of tumor cells (Erler *et al*., 2009). CXCR4 is a chemokine receptor that binds the ligand CXCL12. This receptor has been studied widely in prostate cancer. It is a positive regulator of tumor growth and angiogenesis in prostate cancer cells (Darash-Yahana *et al*., 2004). Binding of CXCL12 to CXCR4 increases the expression of *ITGB3* that is upregulated upon knockdown of PHF19L in DU145 cells (Engl *et al*., 2006). Further, this interaction activates numerous signal transduction pathways that regulate proliferation, survival, chemotaxis, migration and adhesion in a wide variety of cancers (Pore and Maity, 2006). CXCR4 also plays a role in maintenance of tumor progenitor cells in prostate (Dubrovska *et al*., 2012) and its high levels are also associated with mitotically quiescent bone metastasis initiating cells in prostate cancer (Wang *et al*., 2015). Its expression is usually at the tumor front of prostate tumors promoting cell migration towards CXCL12 centrifugal gradient (Delongchamps *et* al., 2015) and in PC3 cells, hypoxia has been shown to upregulate VEGF and CXCR4 to regulate proliferation and migration (Huang *et al*., 2014).

We also observe upregulation of *SOX4* and *HMGA1*. SOX4 was initially identified as a transforming oncogene in prostate cancer cells with high expression in prostate tumor samples with increased Gleason grade. Its inhibition leads to apoptosis in prostate cancer cells (Liu *et al*., 2006). Genome-wide occupancy reveals many transcriptional targets in prostate cancer cells that regulate several developmental pathways, inhibits differentiation, promotes cell cycle progression and activate several growth factors that target the PI3K-AKT pathway. It also upregulates metastasis associated genes (Scharer *et al*., 2009).

Lastly, HMGA1 has been involved in development of androgen independence and required for growth of androgen independent prostate cancer cells (Takeuchi *et al*., 2012).

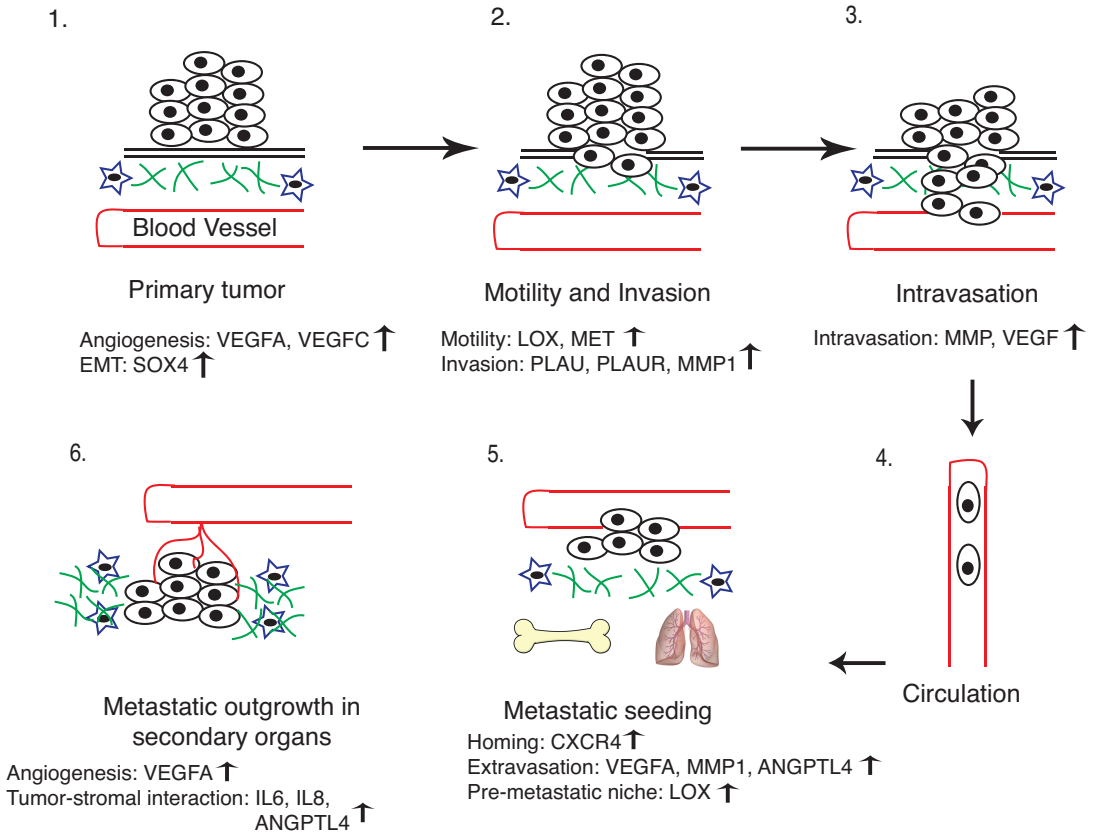

Figure 7: Transcriptional regulation of PHF19L in hypoxia induced metastasis in DU145 cells.

3.6 Attempts to ChIP PHF19

Although every antibody was specific in immunoprecipitation, we were unable to find any peaks with PHF19 long antibody and PHF19 Millipore antibody and unfortunately, in the third case, with the N-terminal antibody, the peaks were unspecific. In general, all the three antibodies although polyclonal had low affinity for PHF19 as substantial amount of protein had to be loaded in western blot and high concentration of the antibody had to be used for immunoprecipitation. With N-terminal antibody, the ChIP-seq was performed in cell line overexpressing PHF19L and therefore the ChIP-western looked promising. However, it is not clear why this antibody crossreacts with another chromatin bound protein in ChIP procedure. BLAST with the epitope for this antibody does not give any specific hits except PHF19 and the antibody does not detect at least the part of the protein that interacts with EZH2 and SUZ12

in the knockdown. We hypothesized that perhaps the short isoform could be recruited to chromatin in the absence of the long isoform or alternative splicing leads to production of another isoform. However, using siRNA approach that targets the N-terminal part of the protein, we still could see enrichment of ChIP signal in the complete knockdown. Therefore, the peaks come from another protein that is very similar to PHF19. Another limitation in recognition of the PHF19 epitope by the other two antibodies can be epitope masking due to cross-linking. It is true that we did not try an alternative method for cross-linking and therefor cannot conclude if this can be the reason.

In order to circumvent the problems with endogenous antibody, we generated PC3 and DU145 cell lines expressing commonly used tags 3XFLAG and 3XHA. The triple tags were used to increase the affinity of the antibody and both the tagged proteins were tested for their ability to co-immunoprecipitate PHF19 and EZH2 in nuclear extracts. In addition, as we have a good ChIP grade antibody for mouse Phf19, we also expressed the mouse Phf19 in both these cell lines. We ensured that this protein interacts with endogenous EZH2 and SUZ12. Although this system is artificial in the sense that this mouse Phf19 could complete with human Phf19 for the same locus and that mouse Phf19 may not mimic the binding profile of human Phf19, given the high conservation of two proteins and the demonstration that human PHF19 can rescue the mouse Phf19 effect in ES cells, we decided to use this approach. It is worth mentioning that initially it was difficult to perform FLAG ChIP in PC3 cells, as the cells are difficult to sonicate with lysis buffer less than 0.3% SDS and the FLAG M2 beads are extremely sensitive to SDS. We have now developed a variation of this protocol in order to be able to overcome this problem.

We are currently using the three approaches to perform ChIP-sequencing and therefore the results cannot be discussed at the present moment.

3.7 A PRC2 independent role of PHF19?

Briefly, the profiles of H3K27me3 in both the cell lines and associated peaks and genes were quite different. In DU145 cells, the peak distribution was more closely related to that observed in ES cells with small, focal and punctuated peak localised to the promoter of the gene. However, in PC3 cells, there was enrichment over broad regions, comprising genes and intergenic regions. Compared to DU145 cells, there were fewer peaks associated with promoters and more peaks associated with intergenic regions. On looking at the expression of these target genes, the genes associated with broad peaks in PC3 cells tend to be more repressed than genes associated with small and focal peaks at promoters in DU145 cells. There is a slight change on the expression upon knockdown; however, these changes are not very significant. The broad domains or broad local enrichments (BLOCs) formed by H3K27me3 have been previously reported in mouse embryonic fibroblasts where they associated more with gene body and intergenic regions compared to promoters. Secondly, in the same study, these BLOCs are associated with cluster of silent genes and are exclusive to genes that are expressed (Pauler *et al*., 2009). It has also been demonstrated that in cancer cells, DNA methylation and H3K2me3 can co-occur but is mutually exclusive on promoters with CpG rich regions. Loss of methylation in ES cells leads to the formation of BLOCs and well as regions that were marked by DNA methylation are replaced with megabase-sized regions of H3K27me3 (Brinkman *et al*., 2012). This shows an interesting link between DNA methylation and H3K27me3. It is known that global hypomethylation increases with prostate cancer aggressiveness, although not much is known on how this affects genes. It will be interesting to study if there are major changes in DNA methylation between DU145 cells and PC3 cells that can cause differences in enrichment pattern of H3K27me3. It will be also interesting to study if genes that contain DNA methylation in DU145 cells loose it in PC3 cells and this is replaced by BLOCs of H3K27me3 on those genes. It is clear that these genes are more silent than those containing focal peaks and therefore it will also be interesting to explore the additional layer of transcriptional repression that is conferred by these BLOCs on genes. Lastly,

the less enrichment of H3K27me3 peaks on promoters in PC3 cells could be explained by gain of DNA methylation on those promoters that are now exclusive to H3K27me3 deposition. Therefore, on one hand, one would expect a loss of DNA methylation from genic and intergenic regions in PC3 cells and on the other hand, one would expect gain of DNA methylation on promoter CpG islands.

As opposed to ES cells, we do not observe any global changes on the profile of H3K27me3 in these cells. In DU145 cells, although there is a 20% overlap between upregulated genes and H3K27me3 in initial state, no major differences were observed on the levels of this mark in the knockdown. The knockdown cells are in growth arrest and therefore one has to be critical to understand what happens to the mark during cell cycle and how growth arrest can affect the propagation of this mark. A recent article demonstrates that histone modifications H3K9me3 and H3K27me3 follow a different mode of propagation during cell cycle where old histones continue to be methylated during cell cycle and new histones slowly acquire the mark leading to self-propagation of the mark across cell generations. Further, they demonstrate that H3K27me3 is decreased on blocking cell cycle and accumulated in cells with G0 arrest compared to proliferating cells (Alabert *et al*., 2015). Thus, there could be accumulation of this mark in the knockdown cells that leads to failure to appreciate the differences in H3K27me3 between control and knockdown cells. However, in spite of this, it is clear that H3K27me3 is not dictating transcription of those genes, as those genes are upregulated even in the presence of the mark. In PC3 cells, there is a very poor overlap between the upregulated genes and H3K27me3 and therefore these genes are upregulated via different mechanisms. It is surprising that there are no appreciable changes on H3K27me3 at least on promoters, in PC3 cells in spite of decreased levels of both EZH2 and SUZ12 in the knockdown. However, we only looked at genes and cannot account for differences in other regions of the genome. It should also be taken into consideration that the role of phosphorylated EZH2 has not been explored in the context of PC3 cells and PHF19L can interact with this form of EZH2 and therefore these changes may not necessarily depend on H3K27me3.

Among the genes that change H3K27me3, majority of those genes do not change expression and therefore the transcriptional outcome accounting for this loss or gain cannot be explained. However, there are some interesting genes in DU145 cells, such as *PRKAB1*, that is usually activated upon stress and induce growth arrest and apoptosis (Li *et al*., 2003) or *EEF2* that is involved in translational elongation and protein synthesis and promotes growth of cancer cells (Nakamura *et al*., 2009). There is also a very minor decrease on *SNAI2*, gene that has been implicated in proliferation and invasion of prostate cancer cells (Emadi Baygi *et al*., 2010). Among the genes that gain H3K27me3 in DU145 cells, of note, include *CYP27B1*, low levels of which are usually associated with poorly differentiated cancer and its knockdown usually provides an intrinsic advantage to growth of cells as the hormone calcitriol that it metabolizes inhibits proliferation (Feldman *et al*., 2014). *ASCL2,* another example of a gene that gains H3K27me3 is a transcription factor that has been implicated in wide variety of cancers as well as maintenance of intestinal stem cells and cancer stem cells (Tian *et al*., 2014). *OAS1* is the only clear example where we see a gain of H3K27me3 and consequently downregulation of expression whereas on other genes such as *CCND1*, *IL6R*, and *DUSP6*, we only observe a very minor decrease of H3K27me3.

In PC3 cells, the loss on most of the genes that have been used for GO analysis is minor with clear losses only observed on few genes. The bioinformatics analysis did not include genes showing a moderate reduction of H3K27me3 such as *HIF1A* and *HEY1*. However, again, these genes do not change expression upon knockdown suggesting an additional event to be required for their derepression. NOTCH signalling via HEY1 has been studied more in the context of androgen receptor and its function as a co-repressor of AR and therefore it is not well known how its function is modulated in androgen negative prostate cancer cells (Carvalho *et al*., 2014). As for HIF1A, it is the central factor that triggers transcriptional responses to hypoxia and has been associated with prostate cancer progression as well a more aggressive phenotype in prostate cancer (Fraga *et al*., 2015)

POLR3A is the catalytic component of RNA polymerase III synthesizing small RNAs, however, there is not much known about its role in cancer. It must be

noted that gene is expressed but is associated with H3K27me3. *EEF1A2*, is also expressed and gains H3K27me3. This eukaryotic translation elongation factor has been shown to be overexpressed in prostate cancer tissues compared to benign samples (Scaggiante *et al*., 2012) and has also been shown to promote proliferation and inhibit apoptosis in DU145 and PC3 cells (Sun *et al*., 2014).

Thus, overall, PHF19L role with PRC2 does not depend on H3K27me3 in prostate cancer cells. However, as this is the only complex that it interacts with, it is difficult to postulate how PHF19 could exert its mechanistic function. In the light of these results, the most important experiment is to identify direct targets of PHF19 that change transcription upon knockdown to understand the interplay of histone modifications or other transcription factors that it could possibly co-operate with on chromatin.

CONCLUSIONS

Conclusions

1. *PHF19L* and *PHF19S* are overexpressed in castration resistant and metastatic prostate cancer clinical samples.
2. PHF19L and PHF19S are overexpressed in androgen negative and castration resistant prostate cancer cell lines DU145 and PC3.
3. PHF19L is expressed in normal prostate epithelial cells RWPE1.
4. PHF19L mainly interacts with PRC2 complex and PHF19S interacts with components of splicing and posttranscriptional mRNA processing complex.
5. PHF19L and PHF19S have a common interactor GNAI2.
6. PHF19L and PHF19S do not interact with each other.
7. PHF19L is chromatin bound and PHF19S is mainly expressed in cytoplasm.
8. PHF19L knockdown does not affect the expression of PHF19S and vice versa.
9. PHF19L knockdown leads to lower expression of PRC2 components EZH2 and SUZ12 in PC3 cells but does not affect the expression of these components in DU145 Cells.
10. EZH2 and SUZ12 can still interact with each other in the absence of PHF19L in PC3 cells.
11. RWPE1 cells resemble intermediate cells of the prostate.
12. PHF19L knockdown leads to differentiation and actin rearrangement in RWPE1 cells.
13. PHF19L knockdown leads to different gene expression changes in PC3 and DU145 cells.
14. PHF19L is required for cell growth and proliferation in both PC3 and DU145 cells.
15. PHF19L knockdown induces hypoxia-induced angiogenesis in DU145 cells and increased invasion in PC3 cells.
16. Genes associated with H3K27me3 in PC3 and DU145 cells show only a moderate overlap.

17. H3K27me3 forms broad domains in PC3 cells over gene body and intergenic regions whereas in DU145 cells, H3K27me3 maintains focal peaks and bimodal distribution over the TSS.
18. Broad domains are associated with more transcriptional repression.
19. PHF19L regulated transcriptional changes do not depend on H3K27me3.
20. PHF19L can interact with both phosphorylated and non-phosphorylated EZH2.

MATERIALS AND METHODS

4 Materials and methods

4.1 Cell lines and cell culture

RWPE1, LNCaP, PC3 and DU145 cells were obtained from laboratory of Dr. Bill Keyes at Centre for Genomic Regulation, Barcelona. LNCaP-abl cells were obtained from the laboratory of Dr. Miguel Beato at Centre for Genomic Regulation, Barcelona with the permission from Prof. Dr. Helmut Klocker, Innsbruck Medical University, Austria. Human Umbilical Vein Endothelial cells (HUVEC) were obtained from laboratory of Dr. Pia Cosma at Centre for Genomic Regulation, Barcelona. RWPE1 is a normal prostate epithelial cell line cultured in Keratinocyte Serum Free medium (K-SFM) supplemented with 0.05 mg/ml of bovine pituitary extract (BPE) and 5 ng/ml of human recombinant epidermal growth factor (EGF). PC3 and DU145 are prostate cancer cell lines derived from bone and brain metastasis of prostate adenocarcinoma respectively cultured in Dulbecco´s Modified Eagle Medium (DMEM) supplemented with 10% fetal bovine serum (FBS) (Gibco), 1X L-glutamine (Gibco) and 1X Pen/Strep (Gibco). LNCaP is a prostate cancer cell line derived from lymph node metastasis of prostate carcinoma cultured in RPMI-1640 supplemented with 10% FBS, L-glutamine and Pen/Strep. LNCaP-abl is an androgen independent derivative of LNCaP-abl cells cultured in RPMI-1640 supplemented with 5% charcoal stripped FBS. HUVEC cells were cultured in Medium200PRF (Life Technologies, Invitrogen) supplemented with Low Serum growth supplement (LSGS) (Life Technologies, Invitrogen). All the cell lines were cultured and maintained at 37^0C and 5% CO_2.

4.2 Cell growth curve

20,000 cells were seeded in 1ml medium in a 12-well plate for each condition. This day was considered as Day 0. Cells were counted on day 2, 4, 6 and 8 following seeding and the medium was changed every two days. The cells were split 1:6 on day 6 and the dilution factor was considered for calculating the total number of cells on day 8. The cells were counted under a light microscope using a counting chamber and trypan blue staining to exclude any

dead cells. Three biological replicates and two technical replicates were used for each condition.

4.3 BrdU Cell Proliferation assay

PC3 and DU145 cells were treated with 10 μM of BrdU solution for 30 minutes and 2 hours respectively and then analysed for BrdU incorporation using APC BrdU Flow Kit (BD Pharmingen) according to manufacturer´s protocol. The percentage of BrdU-positive cells were analysed by flow cytometer on Becton Dickinson FACSCanto.

4.4 Cell Apoptosis assay

The cell apoptosis assay was performed using Violet Annexin V/Dead Cell Apoptosis Kit with Pacific Blue Annexin V/Sytox AADvanced for Flow Cytometry kit (Invitrogen A35136) according to manufacturer´s protocol. The flow cytometry analysis was performed using LSRII.

4.5 Cell Invasion assay

BD Biocoat™ Tumor Invasion system was used to assess the invasion property *in vitro*. This consisted of a BD Falcon™ FluoroBlok™ 24-Mutliwell Insert Plate with an 8.0-micron pore size PET membrane that was uniformly coated with BD Matrigel™ Matrix. In addition, uncoated BD Falcon™ Fluoroblok™ 24-Multiwell Insert plate was used as a cell migration control. The cells were pre-labelled with 10 μg/ml $DilC_{12}(3)$ (BD Biosciences) fluorescent dye overnight at 37^0C. Cell suspensions were prepared by trypsinizing the cells and resuspending the cells in serum-free DMEM at 1 x 10^5 cells/ml. The remaining procedure was followed as per the manufacturer´s protocol. The system was incubated for 24 hours at 37^0C, 5% CO_2. Fluorescence of invaded and migrated cells was read at wavelength of 549/565 nm (Ex/Em) using Tecan Infinite 200 Pro microplate reader. The data was expressed as in the following equation:

$$\%\text{Invasion} = \frac{\text{Mean RFU of cells invaded through BD Matrigel}^{TM}\text{ Matrix coated membrane towards chemoattractant}}{\text{Mean RFU of cells migrated through uncoated BD Fluoroblok membrane towards chemoattractant}} \times 100$$

RFU = relative fluorescence units

4.6 Three dimensional (3D) matrigel cell culture and invasion assay

BD Matrigel^{TM} Basement membrane matrix was used for this assay. The assay was performed in Lab-Tek^{R} II Chamber slide (8-well glass slide). 80 µl of Matrigel was coated on each chamber and allowed to solidify at 37^0C for 30 minutes. Cell suspensions of 50,000 cells were prepared in 4ml media to generate 1250 cells/100 µl. Assay media was prepared containing media + 5% Matrigel. 200 µl of cell suspension was mixed with 200 µl of assay media and 400 µl of this mix was added to each coated well. The chamber slide was incubated at 37^0C, 5% CO_2. Medium was changed every 4 days with assay media containing 2.5% Matrigel + media. Phase images were recorded every 2-4 days. For immunostaining, prostapsheres were fixed with 4% formaldehyde in 1X PBS on day 7 inside the chamber. The spheres were then permeabilised using 0.1% Triton X-100 for 10 minutes at room temperature. This was followed by two washes with 1X PBS and blocking with 3% BSA for 1 hour. Anti-Laminin 5 (8LN5) antibody was diluted 1:1000 in 3% BSA and added to the chamber overnight in a humid environment at 4^0C. Next day, the wells were washed 3X with 1X PBS and Alexa Fluor 488 donkey anti-rabbit IgG (Invitrogen) secondary antibody was added at a dilution of 1:500 in 3% BSA for 2 hours at room temperature. After the last wash, the media chamber was removed and mounting medium (Vectorshield) containing DAPI was added to the slide. Coverslip was placed on top and images were taken using confocal microscope one day after the mounting.

4.7 *In vitro* HUVEC Tube-Formation assay

Conditioned medium was prepared by seeding DU145 shCTR and DU145 shPHF19L and grown to 30 – 40% confluence. The growth medium was then replaced with serum free DMEM for 24 hours and conditioned medium (CM) was harvested when cells reached 60-80% confluence.

70-80% confluent HUVEC cells were serum starved for 3 hours prior to performing the tube formation assay in Medium 200PRF. After serum starvation for 3 hours, cell were trypsinized and neutralised with DMEM with serum. The cells were pelleted at room temperature by centrifugation at 1200 rpm for 3 minutes. The pellet was resuspended in DMEM without serum and the cells were counted to obtain 4 x 10^5 cells/ml. 500 µl of this HUVEC cell suspension was aliquoted into a 1.5 ml tube. The cells were spun again at 4000 rpm for 3 minutes and resuspended in 500 µl of conditioned medium obtained from DU145 shCTR and DU145 shPHF19L supplemented with FBS to a final concentration of 1%. 100 µl of this suspension was then plated into a 96-well plate with growth factor-reduced Matrigel. This plate was then incubated at 37^0C, 5% CO_2 for 4-6 hours. The cells were visualized under the microscope and images taken 6 hours.

4.8 CD24/CD44 FACS staining

The cells were trypsinized and counted into aliquots of 300,000 cells/ml per 1.5 ml tube. The cells were then rinsed with 1ml PBS containing 0.5% BSA. The supernatant was discarded and the following antibodies were added:

PE Mouse Anti-human CD24 (BD Pharmingen): 6 µl

APC Mouse Anti-human CD44 (BD Pharmingen): 6 µl

(10 µl account for the volume of cells for a total of 100 µl)

This was incubated on ice for 30 minutes. The cells were rinsed with 1ml 0.5% BSA-PBS and spun at 1200 rom for 5 minutes. The wash was repeated one more time and the cells were resuspended in 400 µl of 1 µg/ml DAPI/0.5% BSA-PBS. The cells were then incubated for 10-15 minutes on ice. The cells were spun at the same speed and finally resuspended in 200 µl of 0.5% BSA-PBS for flow cytometer.

4.9 Immunofluorescence

Cells were grown on coverslips in 6-well plate for immunofluorescence. The cells were fixed with 4% paraformaldehyde for 20 minutes at room temperature. This was followed by two washes with 1X PBS. Permeabilization was carried out using 0.1% Triton X-100 in PBS containing 1% goat serum. This was followed by two washes with 1X PBS. Mouse IVL antibody was diluted 1:100 in PBS/1% goat serum and incubated for 60 minutes at room temperature. This was followed by two washes with 1X PBS and an additional blocking step with PBS/Goat serum 1% for 30 minutes at room temperature. Alexa Fluor 568 goat anti-mouse IgG (Invitrogen) secondary antibody was diluted 1:2000 in PBS/1% goat serum and incubated for 1 hour at room temperature protected from light. This was followed by two washes with 1X PBS. A final wash with water was carried out and the coverslips were mounted using vectorshield mounting medium containing DAPI. Images were taken the next day using Leica inverted microscope.

4.10 Generation of lentiviral vector for knock down of *PHF19L*

pLKO.1 replication-incompetent lentiviral vector was used for expression of shRNAs. The following oligos were ordered from SIGMA and used to clone shRNA specific for PHF19L into pLKO.1 vector:

shRNA	**Forward oligo**	**Reverse Oligo**
shPHF19L#1	CCGG*CCTGAAATGGA CAATCACTTT*CTCGAG *AAAGTGATTGTCCATT TCAGG*TTTTTG	AATTCAAAAA*CCTGAA ATGGACAATCACTTT*C TCGAG*AAAGTGATTG TCCATTTCAGG*
shPHF19L#4	CCGG*GCCACACATTT GAGAGCATCA*CTCGA G*TGATGCTCTCAAAT GTGTGGC*TTTTTG	AATTCAAAAA*GCCACA CATTTGAGAGCATCA* CTCGAG*TGATGCTCT CAAATGTGTGGC*

The specific 21-mer sense and antisense sequence is italicised and coloured for clarity.

The oligos were annealed by incubating the following reaction at 95^0C for 4 minutes followed by 70^0C for 10 minutes and then slowly cooling to room temperature over the period of 5 hours:

5 µl of 20µM Forward Oligo

5 µl of 20µM Reverse Oligo

5 µl 10x NEB Buffer 2

35 µl ddH_2O

The pLKO.1 vector was then digested with AgeI and EcoRI and purified by Qiagen Gel Extraction kit as per the manufacturer´s protocol. 20 ng of digested and purified pLKO.1 vector was ligated with 2 µl of annealed oligos using T4 DNA ligase from New England Biolabs (NEB) as per the manufacturer´s protocol. 2 µl of ligation mix was transformed into laboratory generated competent bacterial cells and plated on LB agar plates containing 100 µg/ml ampicillin. The colonies were grown overnight in 5ml of LB medium containing 100 µg/ml ampicillin. The plasmid DNA was purified from bacterial cells using GeneAll Exprep Plasmid purification kit as per the manufacturer´s protocol and 80 ng of purified plasmid DNA was sent for sequencing. The positive colonies were then grown in large bacterial cultures and plasmid DNA was purified using Invitrogen PureLink HiPure Plasmid Filter DNA purification kit for transfection and infection in mammalian cells.

4.11 Generation of retroviral vector for knockdown of *PHF19S*

pMSCV-mir30-PIG (LMP/MLP) retroviral vector was used for expression of shRNA. This vector was a kind gift from laboratory of Dr. Bill Keyes, Center for Genomic Regulation, Barcelona. The following shRNA sequences were designed using http://cancan.cshl.edu/RNAi_central/RNAi.cgi?type=shRNA and ordered as oligos from Invitrogen for cloning into MLP vector.

shRNA	**Oligo**
shPHF19S#55	TGCTGTTGACAGTGAGCG*CCCAGAGACTCCCATCACA GAG*TAGTGAAGCCACAGATGTA*CTCTGTGATGGGAGT CTCTGGT*TGCCTACTGCCTCGGA

shPHF19S#168	TGCTGTTGACAGTGAGCG*ACCTCAGTTTCCTCAACTG TAA*TAGTGAAGCCACAGATGTA*TTACAGTTGAGGAAAC TGAGGC*TGCCTACTGCCTCGGA

The specific 22-mer sense and antisense sequence is italicised and coloured for clarity.

The following PCR reaction was used to generate PCR product compatible for cloning into XhoI and EcoRI restriction sites of MLP vector:

22 µl ddH_2O
3 µl Thermo Buffer
1 µl dNTPs 10mM
1 µl Forward (XhoI) 10 µM
1 µl Reverse (EcoRI) 10 µM
1 µl Vent Polynuclease
1 µl shRNA (1 ng/µl)

Thermo cycler:
94^0C 2 minutes
94^0C 15s
54^0C 30s
68^0C 25s
for 33 cycles
68^0C 5 minutes
4^0C cooling

The following sequence of oligos were used for the PCR:

Oligo	**Sequence**
XhoI Forward	CAGAAGGCTCGAGAAGGTATATTGCTGTTGACAGTGAGCG
EcoRI Reverse	CTAAAGTAGCCCCTTGAATTCCGAGGCAGTAGGCA

The PCR product was purified using the GE Healthcare kit and diluted in 25 µl grey buffer. The purified PCR product was then digested with XhoI and EcoRI for 2 hours followed by Qiagen gel extraction and purification. 30 ng of digested and purified PCR product was ligated into pre-cut vector using NEB T4 DNA Ligase at a ratio of 1:4. 10 µl of ligation mix was transformed into laboratory generated competent bacterial cells and plated on LB agar plates containing 100 µg/ml ampicillin. The colonies were grown overnight in 5ml of LB medium containing 100 µg/ml ampicillin. The plasmid DNA was purified from bacterial cells using GeneAll Exprep Plasmid purification kit as per the manufacturer´s protocol and 80 ng of purified plasmid DNA was sent for sequencing. The positive colonies were then grown in large bacterial cultures and plasmid DNA was purified using Invitrogen PureLink HiPure Plasmid Filter DNA purification kit for transfection and infection in mammalian cells.

4.12 siRNA transfection

Commercial siRNAs were bought from SIGMA with the following sequence:
siPHF19#1: GGUCCUAUGGAAGGACAUA [dT][dT]
siPHF19#2: CCUCGUGACUUUCGAAGAU [dT][dT]
For the transfection, the cells were seeded so they reach 70% confluence on the day of transfection. For a 6-well, 7 µl of Lipofectamine RNAiMAX reagent (Invitrogen) was diluted in 120 µl of Opti-MEM medium (Gibco). 4 µl of siRNA (20 µM) was diluted in 120 µl of Opti-MEM medium. The diluted siRNA was added to diluted Lipofectamine RNAiMAX reagent in a 1:1 ratio. The RNA-Lipid complex was incubated for 10 minutes at room temperature after which it was added dropwise to the 6-well.
For transfection in 10 cm plate, everything was multiplied by a factor of 5.

4.13 Generation of retroviral vectors for FLAG tagged PHF19L and PHF19S

pMSCV-puro retroviral vector was used as a backbone for generating stable cell lines expressing FLAG-PHF19L and FLAG-PHF19S. A previous member in the lab generated pMSCV-puro-FLAG-PHF19L between *BglII* site of the plasmid and pMSCV-puro-FLAG-PHF19S was generated between *BglII* and

XhoI site of pMSCV-puro. FLAG-PHF19S was PCR purified from pCMVTag2-PCL3S (generated by former lab member) using the following primers to clone it into pMSCVpuro:

Primer	Sequence
BglII_FLAG_Forward	AGAGAGATCTATGGATTACAAGGATGACGACG
XhoI_Stop_PHF19S_Reverse	AGAGCTCGAGCTACAAATCCTGGCCAAGGA

This plasmid was digested with EcoRI to release PHF19S and generate pMSCVpuro-FLAG-empty.

For all the clonings, the plasmid was digested with the respective enzyme for 3 hours at 37^0C followed by purification using Qiagen Gel Extraction kit. The plasmid was then treated with Alkaline phosphatase (Roche) for 1 hour at 37^0C followed by another purification using Qiagen Gel Extraction kit.

The PCR products were purified using Qiagen PCR purification kit followed by restriction digestion for 2 hours at 37^0C and a final purification using Qiagen Gel Extraction kit. The plasmid and the PCR product were ligated overnight at 16^0C using NEB T4 DNA ligase and the ligated product was transformed and eventually purified for transfection and infection as mentioned in the above section.

4.14 Generation of Tagged constructs for Chromatin immunoprecipitation (ChIP) and EZH2 mutants

Empty_3X FLAG, PHF19L_3XFLAG, PHF19L_3XHA were cloned into pMSCV-puro backbone. In order to generate pMSCV-puro-PHF19L_3XFLAG, a previously generated plasmid in the lab (Ballare *et al*., 2012) was used to clone PHF19L_3XFLAG into *BglII* and *HpaI* site of pMSCVpuro. The 3X FLAG sequence has been described (SIGMA). Gibson cloning was used by the protein technology facility at CRG to generate Empty_3X FLAG from PHF19L_3XFLAG. Similarly, PHF19L_3XHA was cloned from pMSCV-puro-PHF19L_3XFLAG where the FLAG tag was replaced by HA tag using Gibson

cloning. All the plasmids generated via Gibson cloning were done with the protein technologies facility at CRG.

mPhf19_3XFLAG was excised from a previously generated vector in the lab (Ballare *et al*. 2012) using *BamHI* and *HpaI* and this was cloned into pMSCV-puro using *BglII* (compatible with *BamHI*) and *HpaI*. pMSCV-HA-EZH2 was generated by Gibson cloning using a previously generated plasmid pCMV-HA-EZH2 as a backbone for cloning HA-EZH2. pMSCV-HA-EZH2 S21D and S21A were generated by performing mutagenesis in pCMV-HA-EZH2 using QuikChange II XL Site-Directed Mutagenesis kit (Agilent Technologies) as per the manufacturer´s protocol using the following primers for introducing point mutation at Serine 21.

Name	Forward	Reverse
EZH2_S21A	GTCGCATGTACTCTGCTTTTACACGCTTCCGCCA	TGGCGGAAGCGTGTAAAAGCAGAGTACATGCGAC
EZH2_S21D	TTTGTTGGCGGAAGCGTGTAAAAGATGAGTACATGCGACTGAGACA	TGTCTCAGTCGCATGTACTCATCTTTTACACGCTTCCGCCAACAAA

4.15 Transfection and infection (Lentiviral vector)

For each plasmid to be transfected, 2.5 x 10^6 HEK293T cells in 10 ml media were plated in a 10 cm tissue culture plate 24 hours before transfection. The following cocktail was made for each transfection:

7 µg pLKO.1 plasmid

6 µg of pCMV-dR8.91

5 µg of pCMV-VSVG

62 µl of 2M $CaCl_2$

H_2O to 500 µl

This cocktail was then added dropwise to 500 µl of 2X HBS while bubbling the mix using a 1 ml pipette. The DNA: HBS mix was incubated for 10 minutes at room temperature before adding it dropwise to each 10 cm plate. The plates were gently swirled to disperse mixture evenly. The cells were incubated with

the transfection mix for 12-15 hours. Next morning, the medium was replaced by fresh medium and the cells were incubated for 24 hours.

Lentiviral particles were harvested by collecting the medium and passing it through a 0.45 µm filter into a 15 ml polypropylene tube. Fresh medium was added to the 10 cm plate and the lentivral particles were harvested again the following day. For infection in a 6-well plate, the virus was collected 36 hours after the replacement of medium and concentrated by spinning at 22000 rpm for 2 hours at 4^0C. The pellet was resuspended in fresh medium and aliquoted for storage at -80^0C.

For infection, one day before infection, target cells were seeded at a density to achieve 70% confluency on the day of infection. Filtered virus was added to the target cells for 6 hours before replacing with fresh medium. The following day, second round of infection was carried out by adding the filtered virus collected on second day and incubating for 24 hours. Following two rounds of infection, the cells were split and plated in fresh medium for selection. The infected cells (PC3) were selected using 2 µg/ml Puromycin for 3 days for mRNA analysis and 5 days for protein analysis. For RWPE1, LNCaP and DU145 cells, 1 µg/ml of Puromycin was used for selection.

4.16 Transfection and infection (Retroviral vector)

For each plasmid to be transfected, 2.5 x 10^6 Phoenix-AMPHO cells in 10 ml media were plated in a 10 cm tissue culture dish 24 hours before transfection. The following cocktail was used for each transfection:

For pMSCV-mir30-PIG (LMP/MLP),
10 µg pMLP plasmid
6.6 µg Helper plasmid (envelope plasmid)
62 µl of 2M $CaCl_2$
H_2O to 500 µl.

For pMSCV-puro
8 µg of pMSCV-puro
4 µg of pVSVG

91 µl of 2M $CaCl_2$
H_2O to 500 µl

In both cases, the DNA mix was added dropwise to 500 µl of 2X HBS while bubbling with a 1 ml pipette. The DNA: HBS mix was incubated for 10 minutes before adding it dropwise to Phoenix-AMPHO cells. The plates were gently swirled to disperse mixture evenly. The cells were incubated with the transfection mix for 12-15 hours. Next morning, the medium was replaced by fresh medium and the cells were incubated for 24 hours.

Two days following transfection, supernatant of transfected cells was harvested by passing it through a 0.45 µm filter into a 15 ml polypropylene tube. Polybrene was added at a concentration of 10 µg/ml to the filtered virus.

For infection with pMLP vector, target cells were plated in a 6-well plate one day before infection to achieve 70% confluency on the day of infection. 2 ml of virus was added to each well and incubated for 2 hours at 37^0C. This was repeated twice and following three rounds of infection, the medium was replaced by fresh medium. Two days after infection, infection efficiency was checked using GFP and infected cells were selected with 2 µg/ml puromycin.

For infection with pMSCVpuro, spin infection was used. 2 ml of filtered virus was added to each well in a 6-well plate and the plates were spun at 1000g, 32^0C for 90 minutes. The infected cells were then incubated for 3 hours at 37^0C and the medium was replaced with fresh medium. This was repeated the following day. Following second round of infection, the cells were selected with 2 µg/ml puromycin (PC3) and 1 µg/ml (RWPE1, DU145) 24 hours after infection.

4.17 Gene expression analysis

RNA was extracted using RNeasy mini kit (Qiagen). 1 µg of RNA was converted to cDNA using qScript cDNA synthesis kit (Quanta Biosciences). The cDNA was diluted 6-fold and 2 µl of cDNA was used for each reaction. Real-time PCR analysis was performed using SYBR Green I PCR Master Mix (Roche) and the Roche Lightcycler 480. Expression values were normalized to the housekeeping gene *RPO*.

Paired end RNA-sequencing was performed using 1 µg RNA and using two samples per lane to achieve maximum sequencing depth. The Genomics unit performed quality control and library preparation. The libraries were sequenced using Illumina HiSeq2000 sequencer. Genes with a fold change of two were considered to be differentially expressed.

4.18 Preparation of protein extracts and Western blot

Whole cell extracts were prepared using IP300 buffer (50 mM Tris-HCl at pH 7.5, 300 mM NaCl, 10% glycerol, 0.2% NP40, protease inhibitors). The cells were lysed in IP300 buffer and sonicated with Brandson sonicator for 10 seconds at 10% amplitude. This was followed by centrifugation at 13,000 rpm for 30 minutes at 4^0C and the supernatant was transferred into a new tube. The protein was quantified using Bradford assay (Bio-Rad), diluted with 4X Laemmli buffer, heated for 10 minutes and analysed by SDS-PAGE using acrylamide gels in Running buffer (25 mM Tris-base, 200 mM Glycine, 0.1% w/v SDS). Proteins were then transferred to nitrocellulose membrane at 310 mA for 90 minutes on ice in Transfer Buffer (25mM Tris-HCl pH 8.3, 200 mM glycine, 20% v/v methanol). Protein transfer was checked by staining with Ponceau S (Sigma). Transferred membranes were blocked 1 hour at room temperature in an orbital shaker with 5% w/v skimmed milk in TBS-T (10 mM Tris-HCl, pH 7.5, 100 mM NaCl and 0.1% Tween-20). Membranes were incubated overnight at 4^0C with the corresponding primary antibody diluted in 5% skimmed milk in TBS-T. After two brief washes, one 15 minutes wash, and three 5 minutes washes with TBS-T, membranes were incubated for 1 hour at room temperature with the corresponding secondary antibody conjugated to horseradish peroxidase diluted in TBS-T. Following the same number of washes as after the primary antibody, protein detection was performed by chemiluminiscence with Pierce ECL Western blotting substrate (Thermo Scientific).

4.19 Co-immunoprecipitation

Cells were lysed in 50 mM Tris-HCl, pH 7.5, 150 mM NaCl, 1 mM EDTA, 1 mM EGTA, 0.5% Triton X-100 supplemented with protease inhibitors. The

cells were incubated in lysis buffer for 30 minutes on a rotating wheel at 4^0C followed by sonication set at medium for 3 cycles' 10´´on and 30´´off. The lysate was spun at full speed for 30 minutes at 4^0C and the supernatant was collected. 1-2 mg of cell lysate was used for immunoprecipitation with the respective antibody overnight. The next day, depending on the source of antibody, 60 µl protein A or G sepharose beads (GE healthcare) were blocked by 5% BSA followed by incubation with the antibody-lysate complex for 3 hours at 4^0C. The beads were then washed three times 5 minutes each at 4^0C with the lysis buffer and the complex was eluted with boiling the beads with 2X SDS Laemmli buffer for 5 minutes. All the centrifugation steps with the beads were carried out at 3000 rpm for 3 minutes at 4^0C.

4.20 Preparation of Nuclear extracts and immunoprecipitation

The cell pellets were resuspended in 1ml of hypotonic buffer and incubated 10 minutes on ice. This was followed by centrifugation at 700 g for 5 minutes at 4^0C. The supernatant (cytoplasm) was discarded and nuclei were reuspended in 500 µl of nuclear lysis buffer supplemented with 50 units of Benzonase Nuclease (Novagen) for 1 hour on ice. This was followed by centrifugation at full speed for 30 minutes at 4^0C. The supernatant was collected and protein concentration was measured using Bradford. 1mg of nuclear lysate was used for immunoprecipitation. The lysate was diluted with dilution buffer if required and the antibodies were added and incubated overnight in a rotating wheel at 4^0C. The next day, beads were prepared as described previously followed by incubation of beads:antibody complex for 2 hours at 4^0C in a rotating wheel. The beads were washed three times 5 minutes each at 4^0C with the dilution buffer and the complex was eluted by boiling the beads with 2X SDS Laemmli buffer for 5 minutes. All the centrifugation steps with the beads were carried out at 3000 rpm for 3 minutes at 4^0C.

Hypotonic buffer

10 mM Tris HCl pH 7.4

10 mM KCl

15 mM $MgCl_2$

Nuclear lysis buffer

300 mM NaCl

50 mM Hepes pH 7.5

0.5% NP40

2.5 mM $MgCl_2$

Dilution buffer

300 mM NaCl

50 mM Hepes pH 7.5

0.5% NP40

5 mM EDTA

4.21 FLAG affinity purification and mass spectrometry

PC3 cells expressing FLAG tagged constructs were lysed in 50 mM Tris-HCl, pH 7.5, 150 mM NaCl, 1 mM EDTA, 1 mM EGTA, 0.5% Triton X-100 supplemented with protease inhibitors. The cells were incubated in lysis buffer for 30 minutes on a rotating wheel at 4^0C followed by sonication for 3 cycles' 10´´on and 30´´off. The lysate was spun at full speed for 30 minutes at 4^0C and the supernatant was collected. 5 mg of cell lysate was incubated with 100 µl of prewashed (with TBS) FLAG M2 affinity gel (SIGMA) for 3 hours at 4^0C. The beads were then washed three times with the lysis buffer followed by two washes with TBS only. This was followed by two rounds of elution (30 minutes each) with 6M urea and 200 mM $NaHCO_3$ using the same volume of elution buffer as beads. The elution was performed at room temperature in a thermo shaker at 1000 rpm. The eluted complex was then sent to UPF/CRG proteomics unit for further analysis using mass spectrometry. 10% of the eluate was loaded for western blot to validate the FLAG immunoprecipitation.
Mass spectrometry data was analysed by the Proteomics unit at CRG/UPF and proteins were considered as interactors only when 2 or more peptides were assigned to the protein and no peptide was found in FLAG-empty.

4.22 Cell fractionation

Chromatin isolation was carried out using the following buffers:

Buffer A

10 mM HEPES, pH 7.9

10 mM KCl

1.5 mM $MgCl_2$

0.34M Sucrose

10% Glycerol

1mM DTT

Protease inhibitor cocktail

Buffer B

3 mM EDTA

0.2 mM EGTA

1mM DTT

Protease inhibitor cocktail

10^7 cells were resupended in 200 µl of Buffer A. Triton X-100 was added to a final concentration of 0.1% and the cells were incubated on ice for 8 minutes. Centrifugation was then carried out at 1,300 g, 4^0C, for 5 minutes. The supernatant = fraction S1 was separated from pellet (nuclei) = fraction P1. S1 was clarified by high-speed centrifugation at 20,000 g, 4^0C, for 15 minutes and the supernatant was collected as the cytoplasmic fraction. Pellet was discarded. P1 was washed once with 1X PBS and lysed for 30 minutes in 100 µl Buffer B on ice. Centrifugation was carried out at 1,700 g, 4^0C, for 5 minutes to separate the solubilized nuclear proteins (supernatant) from insoluble chromatin fraction (pellet). The insoluble chromatin fraction was washed once with Buffer B and resuspended in 1X Laemmli buffer followed by sonication with Brandson sonicator for 15s at 10% amplitude. Proportional volumes of each fraction were loaded for western blot.

4.23 Chromatin immunoprecipitation (ChIP)

2 or 3 x 150 cm^2 plates (3 - 5 x 10^7 cells) were fixed with 1% formaldehyde for 10 minutes at 37^0C followed by quenching with 680 µl of 2M Glycine (final concentration 125 mM) for 5 minutes at room temperature. The plates were then washed twice with ice cold PBS followed by scarping with 3 ml PBS containing protease inhibitors. The scraped cells were collected in 15 ml polystyrene tube and centrifuged at 4000 rpm 4^0C for 5 minutes to obtain cell pellet. The pellet was resuspended in ChIP lysis buffer (500 µl per 15 million cells). The cells were lysed for 10 minutes on ice followed by two rounds of sonication for 6 cycles each 30´´on 30´´off. This was then transferred to an eppendorf tube to precipitate SDS for one hour. This was followed by centrifugation at 13000 rpm for 10 minutes at 4^0C to pellet cell debris and obtain supernatant containing sheared and soluble chromatin.

DNA was purified from chromatin by performing reverse crosslinking overnight using 25 µl chromatin + 175 µl lysis buffer + 2.5 µl Proteinase K (20 mg/ml) followed by DNA extraction using Qiagen PCR purification kit. DNA was quantified using Nano drop and 500 ng of extracted DNA was run on 1.2% Agarose gel to check the chromatin fragment size (200-400 bp)

50 µg of DNA was used per immunoprecipitation and diluted 1:10 with IP Dilution buffer. 1-10 µg of each antibody was used per 50 µg of DNA and incubated overnight in a rotating wheel at 4^0C.

Next day, Protein A (Dynabeads) or Protein G (GE healthcare) were blocked with 5% BSA and added to the chromatin:antibody mix for 2 hours at 4^0C.

The beads were washed twice with IP buffer, once with IP Buffer with 400 mM NaCl and twice with TE. The chromatin was eluted from the beads using 200 µl of Elution buffer and rotating in a wheel at room temperature for 20 minutes. The supernatant containing chipped chromatin was collected after centrifugation and reverse crosslinked by adding 8 µl of 5M NaCl overnight.

This was then treated with Proteinase K using the following mix for 1 hour at 45^0C. DNA was extracted using Qiagen PCR purification kit and the DNA was eluted in 50 µl of elution buffer.

4.24 FLAG ChIP

The protocol was the same as above with the following changes:

1. The SDS concentration in the Lysis buffer was reduced to 0.3% and the sonication was performed for 24 cycles 30´ on 30´´off.
2. The samples were diluted in the IP buffer 1/10 so the final concentration of SDS in the lysate was 0.03%.
3. FLAG M2 affinity gel was used to ChIP FLAG tagged protein.
4. The ChIP IP was incubated for 4 hours at 4^0C.

4.25 ChIP-sequencing (ChIP-seq)

ChIP-seq for all samples were performed using either 1ng or 10 ng of immunoprecipitated ChIP DNA prepared using the protocol above followed by sequencing library preparation, quality control and quantification. The libraries were then run on Illumina HiSeq2000 sequencer. Genomics Facility at CRG carried out the library preparation and quality control before sequencing.

4.26 Bioinformatics analysis

For the gene expression scatterplots, internally normalized expression values were extracted from GEO using the following accession numbers: GSE35988 (Grasso *et al,* 2012) and GDS1439 (Varambally *et al*, 2005) and analysed using galaxy. Prism6 Graphpad was used to create a scatter plot and one-way ANOVA test for multiple comparisons was used to carry out statistical analysis between the clinical samples.

The ChIPseq samples were mapped against the hg19 human genome assembly using bowtie with the option -m 1 to discard those reads that could not be uniquely mapped in just one region. MACS was run with the default parameters but adjusting the shiftsize to 75 bp to perform the peak calling and each set of target genes was retrieved by matching those ChIPseq peaks in the region from 2.5 Kb upstream of the TSS until the end of the transcripts as annotated in RefSeq.

The RNAseq samples were mapped against the hg19 human genome assembly using TopHat with the option -g 1 to discard those reads that could not be uniquely mapped in just one region. Cufflinks was run to quantify the

expression in FPKMs of each annotated transcript in RefSeq. Genes showing one or more FPKMs are considered to be expressed. Up and down-regulated gene lists in control against knockdown samples were generated applying a fold-change threshold of two.

For the TSS-TES plot, graphical distribution of normalized count of reads between the TSS and TES of target genes for each ChIP-seq was generated by calculating the weighted number of reads on each position from 5kb upstream of the TSS to 5kb downstream of the TES of these genes according to Refseq, normalizing these values within each gene by its length to build the plot of uniform size representing an idealized gene.

4.27 Statistical analysis

All the statistical analysis was performed using Student t-test using Graphpad Prism6 software.

4.28 Antibodies

Antibody	Company	Application
PHF19 long (Rabbit)	Homemade	ChIP, IP: 5 µg
PHF19 N-terminal (Rabbit)	Homemade	WB 1:500 ChIP, IP: 5 µg
PHF19 (Rabbit)	Millipore	WB 1:1000
EZH2 (Mouse)	Cell signalling	WB 1:2000 IP: 5 µg
GAPDH (Mouse)	Santa Cruz	WB 1:5000
FLAG M2 (Mouse)	SIGMA	WB: 1:1000 ChIP, IP: 5 µg
H3 (Rabbit)	Abcam	WB: 1:10,000
SUZ12 (Rabbit)	Abcam	WB: 1:2000 IP: 5 µg
TUBULIN (Mouse)	Abcam	WB: 1:10,000
CD24 (Mouse)	BD Pharmigen	FACS: 6 µl/300,000 cells
CD44 (Mouse)	BD Pharmingen	FACS: 6 µl/300,000 cells
LAMA5 (Rabbit)	Dr. Salvador´s lab	IF: 1:1000
IVL (Mouse)	Dr. Salvador´s lab	IF: 1:100
HA (Rabbit)	Covance	IP: 5 µg
H3K27me3 (Rabbit)	Active Motif	ChIP: 5 µg

4.29 Primers (Gene expression)

Gene	Forward	Reverse
AARS	GCCAATACCCAGAAGTGCAT	CCCCGCCAAAGTAAGTAACA
AATF	CTTGGACACGGACAAAAGGT	CACACTCCTGTTCCTCAGCA
ACTB	CCACCATGTACCCTGGCATT	CGGACTCGTCATACTCCTGC
ACTG1	CTGTGGCTTGGTGAGTCTGT	AAACTGGGTCCTACGGCTTG
ACVR2B	GATCTTCCCACTCCAGGACA	CTCGGCAGCAATGAACTGTA
ANGPTL4	GCCTATAGCCTGCAGCTCAC	AGTACTGGCCGTTGAGGTTG
BEX2	GAGAATCGGGAGGAGGAGAC	AGGGCTCCCCTTTATTAGCA
CBX4	GGTCGCCCAAATATAACACG	GGTCAGGACATTGGAACGAC
CCNA2	TTATTGCTGGAGCTGCCTTT	GGTCTGGTGAAGGTCCATGA
CCNB1	GAACAACTGCAGGCCAAAAT	CACTGGCACCAGCATAGGTA
CCND1	CCTAAGTTCGGTTCCGATGA	ACGTCAGCCTCCACACTCTT
CD24	GCCAGTCTCTTCGTGGTCTC	TTCCTTGCCACATTGGACTT
CDK4	GAAACTCTGAAGCCGACCAG	AGGCAGAGATTCGCTTGTGT
CDKN1A	GCAGACCAGCATGACAGATT	AAGATGTAGAGCGGGCCTTT
CXCR4	CCGTGGCAAACTGGTACTTT	GACGCCAACATAGACCACCT
DUSP10	GCGGCAGTACTTTGAAGAGG	ATTGGTCGTTTGCCTTTGAC
DUSP4	CCTCTACTCGGCGGTCATC	TCTGGGTACTCGGAGGAAAA
DUSP5	ATCAGCCAGTGTGGAAAACC	GAGACATTCAGCAGGGCTGT
DUSP6	ATGGTAGTCCGCTGTCCAAC	ATTCCTCCAACACGTCCAAG
E2F1	CACAGATCCCAGCCAGTCTC	GAGAAGTCCTCCCGCACAT
EIF4B	CAAACCTGATCAGCCCCTAA	AGTTCCCAGTTTGGCCTTTT
EIF5A2	CTTTGCCAGCTGAAAGTTCC	ACCATGCTTTCCAGTTTTGG
EZH2	TTCATGCAACACCCAACACT	CTCCCTCCAAATGCTGGTAA
FST	GCTCTGCCAGTTCATGGAG	TCCTTGCTCAGTTCGGTCTT
HMGA1	TCACTCTTCCACCTGCTCCT	TTGTTTTTGCTTCCCTTTGG
ID1	GGAATCCGAAGTTGGAACC	CGCTTCAGCGACACAAGAT
ID3	ACTCAGCTTAGCCAGGTGGA	AAGCTCCTTTTGTCGTTGGA
IFI27	CCAAGCTTAAGACGGTGAGG	ACTTCAGCCAGACCCAAAGA
IFI6	CTCGGAGAGCTCGGACAG	CGACTGCGAGTCCTCCTC
IFITM1	CCGTGAAGTCTAGGGACAGG	GTCATGAGGATGCCCAGAAT
IL6	GAAAGCAGCAAAGAGGCACT	TTTCACCAGGCAAGTCTCCT
IL6R	CTCCTGCCAGTTAGCAGTCC	TCTTGCCAGGTGACACTGAG
IL8	CAGGAATTGAATGGGTTTGC	AAACCAAGGCACAGTGGAAC
IRF9	AGGTCCAGCTGTCTGGAAGA	ACTGTGCTGTCGCTTTGATG
ITGA1	ACAGCGAAGAACCTCCTGAA	GACTGTCTCATTGGCAGCAA
ITGB6	AAGAACTGCGGTCTGAGGTG	TGTGCCTGCTTCTTCTCTCG
IVL	GACTGCTGTAAAGGGACTGCC	CATTCCCAGTTGCTCATCTCTC
JAK3	CAAACACCACTCCCTGTCCT	TGGGGGTGTTCCTGAAGTAG
KLF4	TTCCCATCTCAAGGCACACC	CATGTGTAAGGCGAGGTGGT
LOR	AGCGGCTGCATCATCAGT	TGGAAAACACCTCCAACTCC
LOX	CCCCAAAGAGTGAAAAACCA	CCTTCAGCCACTCTCCTCTG
LTBP1	GTGCTGTCATGGCTGGAGTA	GTGTCCTGGGCAGCTATTGT

MET	CAGGCAGTGCAGCATGTAGT	CTCGGTCAGAAATTGGGAAA
MMP1	GGTCTCTGAGGGTCAAGCAG	AGTTCATGAGCTGCAACACG
MRPL44	CATCGTTTTCTCTCGTGCAA	CCAGTTCGGCTTCTCTGAAC
MYC	CATCAGCACAACTACGCAGC	CGTTGTGTGTTCGCCTCTTG
NOTCH3	CAACCCGGTGTACGAGAAGT	GAACGCAGTAGCTCCTCTGG
OAS1	ACAGGCAGAAGAGGACTGGA	TAGAAGGCCAGGAGTCAGGA
PHF19 (exon 3-4)	AAAGCTGCCTCGTGACTTTC	TAGGCAGATGTTGCACTTGG
PHF19L (exon 11-13)	GGCCAGACCTTCTTCTCAGAT	CCACTGTCCATCTGGAGTCAT
PHF19L (exon 6-7)	CGTGAAGATGGTGCTGTCCT	TGGAACCACTGCCTGCAC
PHF19S	GCAGACCAGAGACTCCCATCAC	GAGGCGCTATCTGTCTCCAAAG
PLAU	TGTGAGATCACTGGCTTTGG	GTCAGCAGCACACAGCATTT
PLAUR	GCCTTACCGAGGTTGTGTGT	CATCCAGGCACTGTTCTTCA
RNMT	CTTGGGGGAGAGAAGAATCC	CCCTGACACCAACAACAGTG
SOX4	CCAGCAAGAAGGCGAGTTAG	CGGAGCCTTCTGTCTTCATC
TGFBR1	TGTTGGTACCCAAGGAAAGC	CACTCTGTGGTTTGGAGCAA
TWIST1	AAGGCATCACTATGGACTTTCTCT	GCCAGTTTGATCCCAGTATTTT
UPF2	CGACTGGGGAATTTGAAAGA	GCTCAGCTGGCATTATGTGA
VEGFA	CCCACTGAGGAGTCCAACAT	TTTCTTGCGCTTTCGTTTTT
VEGFC	AGAGAACAGGCCAACCTCAA	TGGCATGCATTGAGTCTTTC

Primers (ChIP)

Gene	Forward	Reverse
CDK4	GAGGAGGGCGAAGAGTGTAA	GTAGCCACACCTCTGCTCCT
AATF	AGCGAATCTCGCACAAATCT	GCAGAAGGTTGAAGGGATTG
RNMT	GACCGTCTCCACGTGACTCT	CCGAGGGACAAACACAAAGA
EIF5A2	GGCTACCATTGGCTACCAGA	TAAGAGTTGGAAGGCGCAAG
ATG3	GTCTGTCCTCGCTTTGCTTC	CAGGCACGTTCAGTGTTACG
SGOL1	CTCGCTCCTCCATTGGTTG	GGATGTGGACTTGAGCGAAT
OGDHL	GTGCCAATTACCTGGGTCAC	GTTCTGCGGTCTCAGAGAGG
BEX2	ACGCCACAACGAGGTAAGAC	CCTCTGGCGATGACAACAG
CDK20	AGCAAGCTTAATCCCGCATA	GGTCGAAGCCTGAACCTCTA
RPS6KA2	ACACCTTCTGCAGGAACCAG	GGGCACTGGACAGATGAACT
CYP27B1	CTCTGGAGGCGTACTTGAGG	ACCACTCAGGAGGAGGGATT
Intergenic	AGTGGAAGACTGGTGGGATG	AGCGAAAAGATGGCAGATGT

BIBLIOGRAPHY

BIBLIOGRAPHY

Abate-Shen, C. and M. M. Shen (2000). "Molecular genetics of prostate cancer." Genes Dev **14**(19): 2410-2434.

Adamson, B., A. Smogorzewska, et al. (2012). "A genome-wide homologous recombination screen identifies the RNA-binding protein RBMX as a component of the DNA-damage response." Nat Cell Biol **14**(3): 318-328.

Aksoy, I., et al. (2014). "Klf4 and Klf5 differentially inhibit mesoderm and endoderm differentiation in embryonic stem cells." Nat Commun **5**: 3719.

Alabert, C., T. K. Barth, et al. (2015). "Two distinct modes for propagation of histone PTMs across the cell cycle." Genes Dev **29**(6): 585-590.

Alimirah, F., et al. (2006). "DU-145 and PC-3 human prostate cancer cell lines express androgen receptor: implications for the androgen receptor functions and regulation." FEBS Lett **580**(9): 2294-2300.

Araki, S., Y. Omori, et al. (2007). "Interleukin-8 is a molecular determinant of androgen independence and progression in prostate cancer." Cancer Res **67**(14): 6854-6862.

Arnold, P., A. Scholer, et al. (2013). "Modeling of epigenome dynamics identifies transcription factors that mediate Polycomb targeting." Genome Res **23**(1): 60-73.

Arnoldussen, Y. J. and F. Saatcioglu (2009). "Dual specificity phosphatases in prostate cancer." Mol Cell Endocrinol **309**(1-2): 1-7.

Asangani, I. A., et al. (2013). "Characterization of the EZH2-MMSET histone methyltransferase regulatory axis in cancer." Mol Cell **49**(1): 80-93.

Azare, J., K. Leslie, et al. (2007). "Constitutively activated Stat3 induces tumorigenesis and enhances cell motility of prostate epithelial cells through integrin beta 6." Mol Cell Biol **27**(12): 4444-4453.

Ballare, C., M. Lange, et al. (2012). "Phf19 links methylated Lys36 of histone H3 to regulation of Polycomb activity." Nat Struct Mol Biol **19**(12): 1257-1265.

Barbieri, C. E., C. H. Bangma, et al. (2013). "The mutational landscape of prostate cancer." Eur Urol **64**(4): 567-576.

Beckedorff, F. C., A. C. Ayupe, et al. (2013). "The intronic long noncoding RNA ANRASSF1 recruits PRC2 to the RASSF1A promoter, reducing the expression of RASSF1A and increasing cell proliferation." PLoS Genet **9**(8): e1003705.

Beke, L., et al. (2007). "The gene encoding the prostatic tumor suppressor PSP94 is a target for repression by the Polycomb group protein EZH2." Oncogene **26**(31): 4590-4595.

Berquin, I. M., Y. Min, et al. (2005). "Expression signature of the mouse prostate." J Biol Chem **280**(43): 36442-36451.

Bisteau, X., S. Paternot, et al. (2013). "CDK4 T172 phosphorylation is central in a CDK7-dependent bidirectional CDK4/CDK2 interplay mediated by p21 phosphorylation at the restriction point." PLoS Genet **9**(5): e1003546.

Blackledge, N. P., A. M. Farcas, et al. (2014). "Variant PRC1 complex-dependent H2A ubiquitylation drives PRC2 recruitment and polycomb domain formation." Cell **157**(6): 1445-1459.

Bohrer, L. R., et al. (2010). "Androgens suppress EZH2 expression via retinoblastoma (RB) and p130-dependent pathways: a potential mechanism of androgen-refractory progression of prostate cancer." Endocrinology **151**(11): 5136-5145.

Boulay, G., C. Rosnoblet, et al. (2011). "Functional characterization of human Polycomb-like 3 isoforms identifies them as components of distinct EZH2 protein complexes." Biochem J **434**(2): 333-342.

Boulay, G., M. Dubuissez, et al. (2012). "Hypermethylated in cancer 1 (HIC1) recruits polycomb repressive complex 2 (PRC2) to a subset of its target genes through interaction with human polycomb-like (hPCL) proteins." J Biol Chem **287**(13): 10509-10524.

Bracken, A. P., et al. (2003). "EZH2 is downstream of the pRB-E2F pathway, essential for proliferation and amplified in cancer." EMBO J **22**(20): 5323-5335.

Brase, J. C., M. Johannes, et al. (2011). "Circulating miRNAs are correlated with tumor progression in prostate cancer." Int J Cancer **128**(3): 608-616.

Brien, G. L., G. Gambero, et al. (2012). "Polycomb PHF19 binds H3K36me3 and recruits PRC2 and demethylase NO66 to embryonic stem cell genes during differentiation." Nat Struct Mol Biol **19**(12): 1273-1281.

Brinkman, A. B., H. Gu, et al. (2012). "Sequential ChIP-bisulfite sequencing enables direct genome-scale investigation of chromatin and DNA methylation cross-talk." Genome Res **22**(6): 1128-1138.

Bruno, T., R. De Angelis, et al. (2002). "Che-1 affects cell growth by interfering with the recruitment of HDAC1 by Rb." Cancer Cell **2**(5): 387-399.

Buchanan, G., N. M. Greenberg, et al. (2001). "Collocation of androgen receptor gene mutations in prostate cancer." Clin Cancer Res **7**(5): 1273-1281.

Bunnell, T. M. and J. M. Ervasti (2010). "Delayed embryonic development and impaired cell growth and survival in Actg1 null mice." Cytoskeleton (Hoboken) **67**(9): 564-572.

Bunnell, T. M., et al. (2011). "beta-Actin specifically controls cell growth, migration, and the G-actin pool." Mol Biol Cell **22**(21): 4047-4058.

Cagnol, S. and N. Rivard (2013). "Oncogenic KRAS and BRAF activation of the MEK/ERK signaling pathway promotes expression of dual-specificity phosphatase 4 (DUSP4/MKP2) resulting in nuclear ERK1/2 inhibition." Oncogene **32**(5): 564-576.

Cai, C., H. H. He, et al. (2011). "Androgen receptor gene expression in prostate cancer is directly suppressed by the androgen receptor through recruitment of lysine-specific demethylase 1." Cancer Cell **20**(4): 457-471.

Cai, H., et al. (2012). "Collaboration of Kras and androgen receptor signaling stimulates EZH2 expression and tumor-propagating cells in prostate cancer." Cancer Res **72**(18): 4672-4681.

Cai, L., S. B. Rothbart, et al. (2013). "An H3K36 methylation-engaging Tudor motif of polycomb-like proteins mediates PRC2 complex targeting." Mol Cell **49**(3): 571-582.

Cao, P., et al. (2010). "MicroRNA-101 negatively regulates Ezh2 and its expression is modulated by androgen receptor and HIF-1alpha/HIF-1beta." Mol Cancer **9**: 108.

Cao, Q., et al. (2008). "Repression of E-cadherin by the polycomb group protein EZH2 in cancer." Oncogene **27**(58): 7274-7284.

Cao, Q., et al. (2011). "Coordinated regulation of polycomb group complexes through microRNAs in cancer." Cancer Cell **20**(2): 187-199.

Cao, R. and Y. Zhang (2004). "SUZ12 is required for both the histone methyltransferase activity and the silencing function of the EED-EZH2 complex." Mol Cell **15**(1): 57-67.

Cao, R., H. Wang, et al. (2008). "Role of hPHF1 in H3K27 methylation and Hox gene silencing." Mol Cell Biol **28**(5): 1862-1872.

Carvalho, F. L., B. W. Simons, et al. (2014). "Notch signaling in prostate cancer: a moving target." Prostate **74**(9): 933-945.

Casanova, M., T. Preissner, et al. (2011). "Polycomblike 2 facilitates the recruitment of PRC2 Polycomb group complexes to the inactive X chromosome and to target loci in embryonic stem cells." Development **138**(8): 1471-1482.

Caunt, C. J. and S. M. Keyse (2013). "Dual-specificity MAP kinase phosphatases (MKPs): shaping the outcome of MAP kinase signalling." FEBS J **280**(2): 489-504.

Cerase, A., D. Smeets, et al. (2014). "Spatial separation of Xist RNA and polycomb proteins revealed by superresolution microscopy." Proc Natl Acad Sci U S A **111**(6): 2235-2240.

Cha, T. L., B. P. Zhou, et al. (2005). "Akt-mediated phosphorylation of EZH2 suppresses methylation of lysine 27 in histone H3." Science **310**(5746): 306-310.

Chang, Y. M., L. Bai, et al. (2008). "Src family kinase oncogenic potential and pathways in prostate cancer as revealed by AZD0530." Oncogene **27**(49): 6365-6375.

Chen, H., et al. (2005). "Down-regulation of human DAB2IP gene expression mediated by polycomb Ezh2 complex and histone deacetylase in prostate cancer." J Biol Chem **280**(23): 22437-22444.

Chiam, K., C. Ricciardelli, et al. (2014). "Epigenetic biomarkers in prostate cancer: Current and future uses." Cancer Lett **342**(2): 248-256.

Chin, Y. E., M. Kitagawa, et al. (1996). "Cell growth arrest and induction of cyclin-dependent kinase inhibitor p21 WAF1/CIP1 mediated by STAT1." Science **272**(5262): 719-722.

Chinaranagari, S., et al. (2014). "EZH2 dependent H3K27me3 is involved in epigenetic silencing of ID4 in prostate cancer." Oncotarget **5**(16): 7172-7182.

Chipuk, J. E., S. C. Cornelius, et al. (2002). "The androgen receptor represses transforming growth factor-beta signaling through interaction with Smad3." J Biol Chem **277**(2): 1240-1248.

Chng, K. R., et al. (2012). "A transcriptional repressor co-regulatory network governing androgen response in prostate cancers." EMBO J **31**(12): 2810-2823.

Cho, N. Y., B. H. Kim, et al. (2007). "Hypermethylation of CpG island loci and hypomethylation of LINE-1 and Alu repeats in prostate adenocarcinoma and their relationship to clinicopathological features." J Pathol **211**(3): 269-277.

Christophersen, N. S. and K. Helin (2010). "Epigenetic control of embryonic stem cell fate." J Exp Med **207**(11): 2287-2295.

Ciferri, C., G. C. Lander, et al. (2012). "Molecular architecture of human polycomb repressive complex 2." Elife **1**: e00005.

Cifuentes-Rojas, C., A. J. Hernandez, et al. (2014). "Regulatory interactions between RNA and polycomb repressive complex 2." Mol Cell **55**(2): 171-185.

Clerici, M., A. Deniaud, et al. (2014). "Structural and functional analysis of the three MIF4G domains of nonsense-mediated decay factor UPF2." Nucleic Acids Res **42**(4): 2673-2686.

Clermont, P. L., et al. (2015). "Polycomb-mediated silencing in neuroendocrine prostate cancer." Clin Epigenetics **7**(1): 40.

Cole, M. D. and V. H. Cowling (2008). "Transcription-independent functions of MYC: regulation of translation and DNA replication." Nat Rev Mol Cell Biol **9**(10): 810-815.

Cole, M. D. and V. H. Cowling (2009). "Specific regulation of mRNA cap methylation by the c-Myc and E2F1 transcription factors." Oncogene **28**(9): 1169-1175.

Cooper, S., M. Dienstbier, et al. (2014). "Targeting polycomb to pericentric heterochromatin in embryonic stem cells reveals a role for H2AK119u1 in PRC2 recruitment." Cell Rep **7**(5): 1456-1470.

Coppe, J. P., Y. Itahana, et al. (2004). "Id-1 and Id-2 proteins as molecular markers for human prostate cancer progression." Clin Cancer Res **10**(6): 2044-2051.

Coulson, M., S. Robert, et al. (1998). "The identification and localization of a human gene with sequence similarity to Polycomblike of Drosophila melanogaster." Genomics **48**(3): 381-383.

Craft, N., Y. Shostak, et al. (1999). "A mechanism for hormone-independent prostate cancer through modulation of androgen receptor signaling by the HER-2/neu tyrosine kinase." Nat Med **5**(3): 280-285.

Culig, Z. (2014). "Proinflammatory cytokine interleukin-6 in prostate carcinogenesis." Am J Clin Exp Urol **2**(3): 231-238.

Culig, Z., A. Hobisch, et al. (1995). "Androgen receptor activation in prostatic tumor cell lines by insulin-like growth factor-I, keratinocyte growth factor and epidermal growth factor." Eur Urol **27 Suppl 2**: 45-47.

Culig, Z., et al. (1999). "Switch from antagonist to agonist of the androgen receptor bicalutamide is associated with prostate tumour progression in a new model system." Br J Cancer **81**(2): 242-251.

Da Rocha, S. T., V. Boeva, et al. (2014). "Jarid2 Is Implicated in the Initial Xist-Induced Targeting of PRC2 to the Inactive X Chromosome." Mol Cell **53**(2): 301-316.

Darash-Yahana, M., E. Pikarsky, et al. (2004). "Role of high expression levels of CXCR4 in tumor growth, vascularization, and metastasis." FASEB J **18**(11): 1240-1242.

Davidovich, C., X. Wang, et al. (2015). "Toward a consensus on the binding specificity and promiscuity of PRC2 for RNA." Mol Cell **57**(3): 552-558.

De Cegli, R., S. Iacobacci, et al. (2013). "Reverse engineering a mouse embryonic stem cell-specific transcriptional network reveals a new modulator of neuronal differentiation." Nucleic Acids Res **41**(2): 711-726.

Delongchamps, N. B., F. Beuvon, et al. (2015). "CXCR4 is highly expressed at the tumor front but not in the center of prostate cancers." World J Urol **33**(2): 281-287.

Dhanasekaran, N., et al. (1998). "Regulation of cell proliferation by G proteins." Oncogene **17**(11 Reviews): 1383-1394.

Di Bona, D., M. Cippitelli, et al. (2006). "Oxidative stress inhibits IFN-alpha-induced antiviral gene expression by blocking the JAK-STAT pathway." J Hepatol **45**(2): 271-279.

Di Croce, L. and K. Helin (2013). "Transcriptional regulation by Polycomb group proteins." Nat Struct Mol Biol **20**(10): 1147-1155.

Dietrich, N., M. Lerdrup, et al. (2012). "REST-mediated recruitment of polycomb repressor complexes in mammalian cells." PLoS Genet **8**(3): e1002494.

Ding, L., et al. (2014). "CBP loss cooperates with PTEN haploinsufficiency to drive prostate cancer: implications for epigenetic therapy." Cancer Res **74**(7): 2050-2061.

Dubrovska, A., J. Elliott, et al. (2012). "CXCR4 expression in prostate cancer progenitor cells." PLoS One **7**(2): e31226.

Duncan, I. M. (1982). "Polycomblike: a gene that appears to be required for the normal expression of the bithorax and antennapedia gene complexes of Drosophila melanogaster." Genetics **102**(1): 49-70.

Ellinger, J., et al. (2010). "Global levels of histone modifications predict prostate cancer recurrence." Prostate **70**(1): 61-69.

Ellinger, J., et al. (2012). "Global histone H3K27 methylation levels are different in localized and metastatic prostate cancer." Cancer Invest **30**(2): 92-97.

Emadi Baygi, M., Z. S. Soheili, et al. (2010). "Slug/SNAI2 regulates cell proliferation and invasiveness of metastatic prostate cancer cell lines." Tumour Biol **31**(4): 297-307.

Engl, T., B. Relja, et al. (2006). "CXCR4 chemokine receptor mediates prostate tumor cell adhesion through alpha5 and beta3 integrins." Neoplasia **8**(4): 290-301.

Erler, J. T., K. L. Bennewith, et al. (2006). "Lysyl oxidase is essential for hypoxia-induced metastasis." Nature **440**(7088): 1222-1226.

Erler, J. T., K. L. Bennewith, et al. (2009). "Hypoxia-induced lysyl oxidase is a critical mediator of bone marrow cell recruitment to form the premetastatic niche." Cancer Cell **15**(1): 35-44.

Ezhkova, E., et al. (2009). "Ezh2 orchestrates gene expression for the stepwise differentiation of tissue-specific stem cells." Cell **136**(6): 1122-1135.

Feldman, B. J. and D. Feldman (2001). "The development of androgen-independent prostate cancer." Nat Rev Cancer **1**(1): 34-45.

Feldman, D., A. V. Krishnan, et al. (2014). "The role of vitamin D in reducing cancer risk and progression." Nat Rev Cancer **14**(5): 342-357.

Forbes, K., K. Gillette, et al. (2004). "Increased levels of urokinase plasminogen activator receptor in prostate cancer cells derived from repeated metastasis." World J Urol **22**(1): 67-71.

Fraga, M. F., et al. (2005). "Loss of acetylation at Lys16 and trimethylation at Lys20 of histone H4 is a common hallmark of human cancer." Nat Genet **37**(4): 391-400.

Frank, S. B. and C. K. Miranti (2013). "Disruption of prostate epithelial differentiation pathways and prostate cancer development." Front Oncol **3**: 273.

Gao, J., J. T. Arnold, et al. (2001). "Conversion from a paracrine to an autocrine mechanism of androgen-stimulated growth during malignant transformation of prostatic epithelial cells." Cancer Res **61**(13): 5038-5044.

Gao, S., P. Lee, et al. (2005). "The androgen receptor directly targets the cellular Fas/FasL-associated death domain protein-like inhibitory protein gene to promote the androgen-independent growth of prostate cancer cells." Mol Endocrinol **19**(7): 1792-1802.

Ghislin, S., F. Deshayes, et al. (2012). "PHF19 and Akt control the switch between proliferative and invasive states in melanoma." Cell Cycle **11**(8): 1634-1645.

Gilloteaux, J., J. M. Jamison, et al. (2013). "Human prostate DU145 carcinoma cells implanted in nude mice remove the peritoneal mesothelium to invade and grow as carcinomas." Anat Rec (Hoboken) **296**(1): 40-55.

Graff, J. R., B. W. Konicek, et al. (2000). "Increased AKT activity contributes to prostate cancer progression by dramatically accelerating prostate tumor growth and diminishing p27Kip1 expression." J Biol Chem **275**(32): 24500-24505.

Grasso, C. S., Y. M. Wu, et al. (2012). "The mutational landscape of lethal castration-resistant prostate cancer." Nature **487**(7406): 239-243.

Gregory (a), C. W., B. He, et al. (2001). "A mechanism for androgen receptor-mediated prostate cancer recurrence after androgen deprivation therapy." Cancer Res **61**(11): 4315-4319.

Gregory, C. W., K. G. Hamil, et al. (1998). "Androgen receptor expression in androgen-independent prostate cancer is associated with increased expression of androgen-regulated genes." Cancer Res **58**(24): 5718-5724.

Gregory, C. W., R. T. Johnson, Jr., et al. (2001). "Androgen receptor stabilization in recurrent prostate cancer is associated with hypersensitivity to low androgen." Cancer Res **61**(7): 2892-2898.

Grote, P., L. Wittler, et al. (2013). "The tissue-specific lncRNA Fendrr is an essential regulator of heart and body wall development in the mouse." Dev Cell **24**(2): 206-214.

Gu, L., et al. (2015). "BAZ2A (TIP5) is involved in epigenetic alterations in prostate cancer and its overexpression predicts disease recurrence." Nat Genet **47**(1): 22-30.

Guo, Z., X. Yang, et al. (2009). "A novel androgen receptor splice variant is up-regulated during prostate cancer progression and promotes androgen depletion-resistant growth." Cancer Res **69**(6): 2305-2313.

Gupta, G. P., D. X. Nguyen, et al. (2007). "Mediators of vascular remodelling co-opted for sequential steps in lung metastasis." Nature **446**(7137): 765-770.

Haffner, M. C., A. Chaux, et al. (2011). "Global 5-hydroxymethylcytosine content is significantly reduced in tissue stem/progenitor cell compartments and in human cancers." Oncotarget **2**(8): 627-637.

Hagman, Z., O. Larne, et al. (2010). "miR-34c is downregulated in prostate cancer and exerts tumor suppressive functions." Int J Cancer **127**(12): 2768-2776.

Harris, W. P., E. A. Mostaghel, et al. (2009). "Androgen deprivation therapy: progress in understanding mechanisms of resistance and optimizing androgen depletion." Nat Clin Pract Urol **6**(2): 76-85.

He, A., X. Shen, et al. (2012). "PRC2 directly methylates GATA4 and represses its transcriptional activity." Genes Dev **26**(1): 37-42.

He, G. P., S. Kim, et al. (1999). "Cloning and characterization of a novel zinc finger transcriptional repressor. A direct role of the zinc finger motif in repression." J Biol Chem **274**(21): 14678-14684.

Herranz, N., D. Pasini, et al. (2008). "Polycomb complex 2 is required for E-cadherin repression by the Snail1 transcription factor." Mol Cell Biol **28**(15): 4772-4781.

Herz, H. M., M. Mohan, et al. (2012). "Polycomb repressive complex 2-dependent and -independent functions of Jarid2 in transcriptional regulation in Drosophila." Mol Cell Biol **32**(9): 1683-1693.

Hong, Z., J. Jiang, et al. (2008). "A polycomb group protein, PHF1, is involved in the response to DNA double-strand breaks in human cell." Nucleic Acids Res **36**(9): 2939-2947.

Horoszewicz, J. S., et al. (1983). "LNCaP model of human prostatic carcinoma." Cancer Res **43**(4): 1809-1818.

Huang, X., J. Zhou, et al. (2014). "Biological characteristics of prostate cancer cells are regulated by hypoxia-inducible factor 1alpha." Oncol Lett **8**(3): 1217-1221.

Hulf, T., T. Sibbritt, et al. (2013). "Epigenetic-induced repression of microRNA-205 is associated with MED1 activation and a poorer prognosis in localized prostate cancer." Oncogene **32**(23): 2891-2899.

Hunkapiller, J., Y. Shen, et al. (2012). "Polycomb-like 3 promotes polycomb repressive complex 2 binding to CpG islands and embryonic stem cell self-renewal." PLoS Genet **8**(3): e1002576.

Inoue, K., J. W. Slaton, et al. (2000). "Interleukin 8 expression regulates tumorigenicity and metastases in androgen-independent prostate cancer." Clin Cancer Res **6**(5): 2104-2119.

Jarrard, D. F., et al. (1998). "Methylation of the androgen receptor promoter CpG island is associated with loss of androgen receptor expression in prostate cancer cells." Cancer Res **58**(23): 5310-5314.

Jermann, P., L. Hoerner, et al. (2014). "Short sequences can efficiently recruit histone H3 lysine 27 trimethylation in the absence of enhancer activity and DNA methylation." Proc Natl Acad Sci U S A **111**(33): E3415-3421.

Kalb, R., S. Latwiel, et al. (2014). "Histone H2A monoubiquitination promotes histone H3 methylation in Polycomb repression." Nat Struct Mol Biol **21**(6): 569-571.

Kaneko, S., R. Bonasio, et al. (2014). "Interactions between JARID2 and noncoding RNAs regulate PRC2 recruitment to chromatin." Mol Cell **53**(2): 290-300.

Kanhoush, R., B. Beenders, et al. (2010). "Novel domains in the hnRNP G/RBMX protein with distinct roles in RNA binding and targeting nascent transcripts." Nucleus **1**(1): 109-122.

Karanikolas, B. D., et al. (2009). "Polycomb group protein enhancer of zeste 2 is an oncogene that promotes the neoplastic transformation of a benign prostatic epithelial cell line." Mol Cancer Res **7**(9): 1456-1465.

Kim, E., M. Kim, et al. (2013). "Phosphorylation of EZH2 activates STAT3 signaling via STAT3 methylation and promotes tumorigenicity of glioblastoma stem-like cells." Cancer Cell **23**(6): 839-852.

Kim, H., K. Kang, et al. (2009). "AEBP2 as a potential targeting protein for Polycomb Repression Complex PRC2." Nucleic Acids Res **37**(9): 2940-2950.

Kitaguchi, T., K. Nakata, et al. (2001). "Xenopus Polycomblike 2 (XPcl2) controls anterior to posterior patterning of the neural tissue." Dev Genes Evol **211**(6): 309-314.

Klattenhoff, C. A., J. C. Scheuermann, et al. (2013). "Braveheart, a long noncoding RNA required for cardiovascular lineage commitment." Cell **152**(3): 570-583.

Koh, C. M., et al. (2011). "Myc enforces overexpression of EZH2 in early prostatic neoplasia via transcriptional and post-transcriptional mechanisms." Oncotarget **2**(9): 669-683.

Kohlmaier, A., F. Savarese, et al. (2004). "A chromosomal memory triggered by Xist regulates histone methylation in X inactivation." PLoS Biol **2**(7): E171.

Kondo, Y., et al. (2008). "Gene silencing in cancer by histone H3 lysine 27 trimethylation independent of promoter DNA methylation." Nat Genet **40**(6): 741-750.

Kong, D., et al. (2012). "Loss of let-7 up-regulates EZH2 in prostate cancer consistent with the acquisition of cancer stem cell signatures that are attenuated by BR-DIM." PLoS One **7**(3): e33729.

Kotake, Y., T. Nakagawa, et al. (2011). "Long non-coding RNA ANRIL is required for the PRC2 recruitment to and silencing of p15(INK4B) tumor suppressor gene." Oncogene **30**(16): 1956-1962.

Kristiansen, G., C. Pilarsky, et al. (2004). "CD24 expression is a significant predictor of PSA relapse and poor prognosis in low grade or organ confined prostate cancer." Prostate **58**(2): 183-192.

Ku, M., R. P. Koche, et al. (2008). "Genomewide analysis of PRC1 and PRC2 occupancy identifies two classes of bivalent domains." PLoS Genet **4**(10): e1000242.

Kwok, W. K., et al. (2005). "Up-regulation of TWIST in prostate cancer and its implication as a therapeutic target." Cancer Res **65**(12): 5153-5162.

Kypriotou, M., et al. (2012). "The human epidermal differentiation complex: cornified envelope precursors, S100 proteins and the 'fused genes' family." Exp Dermatol **21**(9): 643-649.

Landeira, D., S. Sauer, et al. (2010). "Jarid2 is a PRC2 component in embryonic stem cells required for multi-lineage differentiation and recruitment of PRC1 and RNA Polymerase II to developmental regulators." Nat Cell Biol **12**(6): 618-624.

Li, G., R. Margueron, et al. (2010). "Jarid2 and PRC2, partners in regulating gene expression." Genes Dev **24**(4): 368-380.

Li, J., P. Jiang, et al. (2003). "AMPK-beta1 subunit is a p53-independent stress responsive protein that inhibits tumor cell growth upon forced expression." Carcinogenesis **24**(5): 827-834.

Li, J., Y. H. Xu, et al. (2013). "Identifying differentially expressed genes and small molecule drugs for prostate cancer by a bioinformatics strategy." Asian Pac J Cancer Prev **14**(9): 5281-5286.

Li, X., K. Isono, et al. (2011). "Mammalian polycomb-like Pcl2/Mtf2 is a novel regulatory component of PRC2 that can differentially modulate polycomb activity both at the Hox gene cluster and at Cdkn2a genes." Mol Cell Biol **31**(2): 351-364.

Li, Y., D. Kong, et al. (2012). "Epigenetic deregulation of miR-29a and miR-1256 by isoflavone contributes to the inhibition of prostate cancer cell growth and invasion." Epigenetics **7**(8): 940-949.

Li, Y., L. Fu, et al. (2014). "Increased expression of EIF5A2, via hypoxia or gene amplification, contributes to metastasis and angiogenesis of esophageal squamous cell carcinoma." Gastroenterology **146**(7): 1701-1713 e1709.

Lin, J., et al. (2008). "Genetics of melanoma predisposition." Br J Dermatol **159**(2): 286-291.

Liu, P., S. Ramachandran, et al. (2006). "Sex-determining region Y box 4 is a transforming oncogene in human prostate cancer cells." Cancer Res **66**(8): 4011-4019.

Liu, Y., R. Zhang, et al. (2011). "Identification of S100A16 as a novel adipogenesis promoting factor in 3T3-L1 cells." Endocrinology **152**(3): 903-911.

Locke, J. A., E. S. Guns, et al. (2008). "Androgen levels increase by intratumoral de novo steroidogenesis during progression of castration-resistant prostate cancer." Cancer Res **68**(15): 6407-6415.

Locke, J. A., E. S. Guns, et al. (2010). "Arachidonic acid activation of intratumoral steroid synthesis during prostate cancer progression to castration resistance." Prostate **70**(3): 239-251.

Lonie, A., R. D'Andrea, et al. (1994). "Molecular characterisation of the Polycomblike gene of Drosophila melanogaster, a trans-acting negative regulator of homeotic gene expression." Development **120**(9): 2629-2636.

Lu, X. and Y. Kang (2010). "Hypoxia and hypoxia-inducible factors: master regulators of metastasis." Clin Cancer Res **16**(24): 5928-5935.

Luis, N. M., et al. (2011). "Regulation of human epidermal stem cell proliferation and senescence requires polycomb- dependent and -independent functions of Cbx4." Cell Stem Cell **9**(3): 233-246.

Lupien, M., J. Eeckhoute, et al. (2008). "FoxA1 translates epigenetic signatures into enhancer-driven lineage-specific transcription." Cell **132**(6): 958-970.

Lynch, M. D., A. J. Smith, et al. (2012). "An interspecies analysis reveals a key role for unmethylated CpG dinucleotides in vertebrate Polycomb complex recruitment." EMBO J **31**(2): 317-329.

Maenner, S., M. Blaud, et al. (2010). "2-D structure of the A region of Xist RNA and its implication for PRC2 association." PLoS Biol **8**(1): e1000276.

Mak, W., J. Baxter, et al. (2002). "Mitotically stable association of polycomb group proteins eed and enx1 with the inactive x chromosome in trophoblast stem cells." Curr Biol **12**(12): 1016-1020.

Mandal, M., D. Bandyopadhyay, et al. (1998). "Interferon-induces expression of cyclin-dependent kinase-inhibitors p21WAF1 and p27Kip1 that prevent activation of cyclin-dependent kinase by CDK-activating kinase (CAK)." Oncogene **16**(2): 217-225.

Mani, S. A., et al. (2008). "The epithelial-mesenchymal transition generates cells with properties of stem cells." Cell **133**(4): 704-715.

Matsunaga, S., H. Takata, et al. (2012). "RBMX: a regulator for maintenance and centromeric protection of sister chromatid cohesion." Cell Rep **1**(4): 299-308.

Maxwell, P. J., J. Coulter, et al. (2013). "Potentiation of inflammatory CXCL8 signalling sustains cell survival in PTEN-deficient prostate carcinoma." Eur Urol **64**(2): 177-188.

Mazaris, E. and A. Tsiotras (2013). "Molecular pathways in prostate cancer." Nephrourol Mon **5**(3): 792-800.

McGann, J. C., J. A. Oyer, et al. (2014). "Polycomb- and REST-associated histone deacetylases are independent pathways toward a mature neuronal phenotype." Elife **3**: e04235.

McHugh, C. A., C. K. Chen, et al. (2015). "The Xist lncRNA interacts directly with SHARP to silence transcription through HDAC3." Nature.

Mejetta, S., L. Morey, et al. (2011). "Jarid2 regulates mouse epidermal stem cell activation and differentiation." EMBO J **30**(17): 3635-3646.

Metzger, E., A. Imhof, et al. (2010). "Phosphorylation of histone H3T6 by PKCbeta(I) controls demethylation at histone H3K4." Nature **464**(7289): 792-796.

Metzger, E., et al. (2005). "LSD1 demethylates repressive histone marks to promote androgen-receptor-dependent transcription." Nature **437**(7057): 436-439.

Metzger, E., N. Yin, et al. (2008). "Phosphorylation of histone H3 at threonine 11 establishes a novel chromatin mark for transcriptional regulation." Nat Cell Biol **10**(1): 53-60.

Min, J., et al. (2010). "An oncogene-tumor suppressor cascade drives metastatic prostate cancer by coordinately activating Ras and nuclear factor-kappaB." Nat Med **16**(3): 286-294.

Mironchik, Y., et al. (2005). "Twist overexpression induces in vivo angiogenesis and correlates with chromosomal instability in breast cancer." Cancer Res **65**(23): 10801-10809.

Moison, C., et al. (2013). "DNA methylation associated with polycomb repression in retinoic acid receptor beta silencing." FASEB J **27**(4): 1468-1478.

Moison, C., et al. (2014). "Synergistic chromatin repression of the tumor suppressor gene RARB in human prostate cancers." Epigenetics **9**(4): 477-482.

Montgomery, R. B., E. A. Mostaghel, et al. (2008). "Maintenance of intratumoral androgens in metastatic prostate cancer: a mechanism for castration-resistant tumor growth." Cancer Res **68**(11): 4447-4454.

Moore, K. M., G. J. Thomas, et al. (2014). "Therapeutic targeting of integrin alphavbeta6 in breast cancer." J Natl Cancer Inst **106**(8).

Mori, R., et al. (2008). "Both beta-actin and GAPDH are useful reference genes for normalization of quantitative RT-PCR in human FFPE tissue samples of prostate cancer." Prostate **68**(14): 1555-1560.

Mukhopadhyay, N. K., et al. (2014). "Scaffold attachment factor B1 regulates the androgen receptor in concert with the growth inhibitory kinase MST1 and the methyltransferase EZH2." Oncogene **33**(25): 3235-3245.

Munger, J. S., X. Huang, et al. (1999). "The integrin alpha v beta 6 binds and activates latent TGF beta 1: a mechanism for regulating pulmonary inflammation and fibrosis." Cell **96**(3): 319-328.

Naderi, A., J. Liu, et al. (2010). "BEX2 regulates mitochondrial apoptosis and G1 cell cycle in breast cancer." Int J Cancer **126**(7): 1596-1610.

Nakamura, J., S. Aoyagi, et al. (2009). "Overexpression of eukaryotic elongation factor eEF2 in gastrointestinal cancers and its involvement in G2/M progression in the cell cycle." Int J Oncol **34**(5): 1181-1189.

Nekrasov, M., T. Klymenko, et al. (2007). "Pcl-PRC2 is needed to generate high levels of H3-K27 trimethylation at Polycomb target genes." EMBO J **26**(18): 4078-4088.

Ng, S. Y., R. Johnson, et al. (2012). "Human long non-coding RNAs promote pluripotency and neuronal differentiation by association with chromatin modifiers and transcription factors." EMBO J **31**(3): 522-533.

Nozawa, R. S., K. Nagao, et al. (2013). "Human inactive X chromosome is compacted through a PRC2-independent SMCHD1-HBiX1 pathway." Nat Struct Mol Biol **20**(5): 566-573.

O'Connell, S., L. Wang, et al. (2001). "Polycomblike PHD fingers mediate conserved interaction with enhancer of zeste protein." J Biol Chem **276**(46): 43065-43073.

Pandey, R. R., T. Mondal, et al. (2008). "Kcnq1ot1 antisense noncoding RNA mediates lineage-specific transcriptional silencing through chromatin-level regulation." Mol Cell **32**(2): 232-246.

Pasini, D., P. A. Cloos, et al. (2010). "JARID2 regulates binding of the Polycomb repressive complex 2 to target genes in ES cells." Nature **464**(7286): 306-310.

Passananti, C., A. Floridi, et al. (2007). "Che-1/AATF, a multivalent adaptor connecting transcriptional regulation, checkpoint control, and apoptosis." Biochem Cell Biol **85**(4): 477-483.

Pauler, F. M., M. A. Sloane, et al. (2009). "H3K27me3 forms BLOCs over silent genes and intergenic regions and specifies a histone banding pattern on a mouse autosomal chromosome." Genome Res **19**(2): 221-233.

Peehl, D. M. (2005). "Primary cell cultures as models of prostate cancer development." Endocr Relat Cancer **12**(1): 19-47.

Pellakuru, L. G., et al. (2012). "Global levels of H3K27me3 track with differentiation in vivo and are deregulated by MYC in prostate cancer." Am J Pathol **181**(2): 560-569.

Peng, J. C., A. Valouev, et al. (2009). "Jarid2/Jumonji coordinates control of PRC2 enzymatic activity and target gene occupancy in pluripotent cells." Cell **139**(7): 1290-1302.

Platanias, L. C. (2005). "Mechanisms of type-I- and type-II-interferon-mediated signalling." Nat Rev Immunol **5**(5): 375-386.

Plath, K., J. Fang, et al. (2003). "Role of histone H3 lysine 27 methylation in X inactivation." Science **300**(5616): 131-135.

Pore, N. and A. Maity (2006). "The chemokine receptor CXCR4: a homing device for hypoxic cancer cells?" Cancer Biol Ther **5**(11): 1563-1565.

Prensner, J. R., et al. (2011). "Transcriptome sequencing across a prostate cancer cohort identifies PCAT-1, an unannotated lincRNA implicated in disease progression." Nat Biotechnol **29**(8): 742-749.

Qin, S., Y. Guo, et al. (2013). "Tudor domains of the PRC2 components PHF1 and PHF19 selectively bind to histone H3K36me3." Biochem Biophys Res Commun **430**(2): 547-553.

Ren, G., et al. (2012). "Polycomb protein EZH2 regulates tumor invasion via the transcriptional repression of the metastasis suppressor RKIP in breast and prostate cancer." Cancer Res **72**(12): 3091-3104.

Ren, X. and T. K. Kerppola (2011). "REST interacts with Cbx proteins and regulates polycomb repressive complex 1 occupancy at RE1 elements." Mol Cell Biol **31**(10): 2100-2110.

Rentala, S., P. D. Yalavarthy, et al. (2010). "Alpha1 and beta1 integrins enhance the homing and differentiation of cultured prostate cancer stem cells." Asian J Androl **12**(4): 548-555.

Riising, E. M., I. Comet, et al. (2014). "Gene silencing triggers polycomb repressive complex 2 recruitment to CpG islands genome wide." Mol Cell **55**(3): 347-360.

Rokhlin, O. W., A. F. Taghiyev, et al. (2005). "Androgen regulates apoptosis induced by TNFR family ligands via multiple signaling pathways in LNCaP." Oncogene **24**(45): 6773-6784.

Ross, A. E., L. Marchionni, et al. (2011). "Gene expression pathways of high grade localized prostate cancer." Prostate **71**(14): 1568-1577.

Sanulli, S., N. Justin, et al. (2015). "Jarid2 Methylation via the PRC2 Complex Regulates H3K27me3 Deposition during Cell Differentiation." Mol Cell **57**(5): 769-783.

Saramaki, O. R., et al. (2006). "The gene for polycomb group protein enhancer of zeste homolog 2 (EZH2) is amplified in late-stage prostate cancer." Genes Chromosomes Cancer **45**(7): 639-645.

Sarma, K., C. Cifuentes-Rojas, et al. (2014). "ATRX directs binding of PRC2 to Xist RNA and Polycomb targets." Cell **159**(4): 869-883.

Sarma, K., R. Margueron, et al. (2008). "Ezh2 requires PHF1 to efficiently catalyze H3 lysine 27 trimethylation in vivo." Mol Cell Biol **28**(8): 2718-2731.

Scaggiante, B., B. Dapas, et al. (2012). "Dissecting the expression of EEF1A1/2 genes in human prostate cancer cells: the potential of EEF1A2 as a hallmark for prostate transformation and progression." Br J Cancer **106**(1): 166-173.

Schaefer, A., M. Jung, et al. (2010). "Diagnostic and prognostic implications of microRNA profiling in prostate carcinoma." Int J Cancer **126**(5): 1166-1176.

Scharer, C. D., C. D. McCabe, et al. (2009). "Genome-wide promoter analysis of the SOX4 transcriptional network in prostate cancer cells." Cancer Res **69**(2): 709-717.

Schoeftner, S., A. K. Sengupta, et al. (2006). "Recruitment of PRC1 function at the initiation of X inactivation independent of PRC2 and silencing." EMBO J **25**(13): 3110-3122.

Schulz, W. A., J. P. Elo, et al. (2002). "Genomewide DNA hypomethylation is associated with alterations on chromosome 8 in prostate carcinoma." Genes Chromosomes Cancer **35**(1): 58-65.

Segre, J. A., et al. (1999). "Klf4 is a transcription factor required for establishing the barrier function of the skin." Nat Genet **22**(4): 356-360.

Seligson, D. B., et al. (2005). "Global histone modification patterns predict risk of prostate cancer recurrence." Nature **435**(7046): 1262-1266.

Sepporta, M. V., F. M. Tumminello, et al. (2013). "Follistatin as potential therapeutic target in prostate cancer." Target Oncol **8**(4): 215-223.

Shahbazian, D., A. Parsyan, et al. (2010). "Control of cell survival and proliferation by mammalian eukaryotic initiation factor 4B." Mol Cell Biol **30**(6): 1478-1485.

Shang, Y., M. Myers, et al. (2002). "Formation of the androgen receptor transcription complex." Mol Cell **9**(3): 601-610.

Sharma, A., W. S. Yeow, et al. (2010). "The retinoblastoma tumor suppressor controls androgen signaling and human prostate cancer progression." J Clin Invest **120**(12): 4478-4492.

Shen, M. M. and C. Abate-Shen (2010). "Molecular genetics of prostate cancer: new prospects for old challenges." Genes Dev **24**(18): 1967-2000.

Shen, X., W. Kim, et al. (2009). "Jumonji modulates polycomb activity and self-renewal versus differentiation of stem cells." Cell **139**(7): 1303-1314.

Shin, Y. J. and J. H. Kim (2012). "The role of EZH2 in the regulation of the activity of matrix metalloproteinases in prostate cancer cells." PLoS One **7**(1): e30393.

Simon, M. D., S. F. Pinter, et al. (2013). "High-resolution Xist binding maps reveal two-step spreading during X-chromosome inactivation." Nature **504**(7480): 465-469.

Son, J., S. S. Shen, et al. (2013). "Nucleosome-binding activities within JARID2 and EZH1 regulate the function of PRC2 on chromatin." Genes Dev **27**(24): 2663-2677.

Son, J., S. S. Shen, et al. (2013). "Nucleosome-binding activities within JARID2 and EZH1 regulate the function of PRC2 on chromatin." Genes Dev **27**(24): 2663-2677.

Strong, N., A. C. Millena, et al. (2013). "Inhibitor of differentiation 1 (Id1) and Id3 proteins play different roles in TGFbeta effects on cell proliferation and migration in prostate cancer cells." Prostate **73**(6): 624-633.

Sturchler, E., J. A. Cox, et al. (2006). "S100A16, a novel calcium-binding protein of the EF-hand superfamily." J Biol Chem **281**(50): 38905-38917.

Sullivan, R. and C. H. Graham (2007). "Hypoxia-driven selection of the metastatic phenotype." Cancer Metastasis Rev **26**(2): 319-331.

Sun, S., C. C. Sprenger, et al. (2010). "Castration resistance in human prostate cancer is conferred by a frequently occurring androgen receptor splice variant." J Clin Invest **120**(8): 2715-2730.

Sun, Y., C. Du, et al. (2014). "Up-regulation of eEF1A2 promotes proliferation and inhibits apoptosis in prostate cancer." Biochem Biophys Res Commun **450**(1): 1-6.

Takayama, K., et al. (2015). "RUNX1, an androgen- and EZH2-regulated gene, has differential roles in AR-dependent and -independent prostate cancer." Oncotarget **6**(4): 2263-2276.

Takeuchi, I., N. Takaha, et al. (2012). "High mobility group protein AT-hook 1 (HMGA1) is associated with the development of androgen independence in prostate cancer cells." Prostate **72**(10): 1124-1132.

Tan, M. H., et al. (2015). "Androgen receptor: structure, role in prostate cancer and drug discovery." Acta Pharmacol Sin **36**(1): 3-23.

Taniguchi, H., et al. (2012). "Silencing of Kruppel-like factor 2 by the histone methyltransferase EZH2 in human cancer." Oncogene **31**(15): 1988-1994.

Tie, F., J. Prasad-Sinha, et al. (2003). "A 1-megadalton ESC/E(Z) complex from Drosophila that contains polycomblike and RPD3." Mol Cell Biol **23**(9): 3352-3362.

Tilki, D. and C. P. Evans (2014). "The changing landscape of advanced and castration resistant prostate cancer: latest science and revised definitions." Can J Urol **21**(2 Supp 1): 7-13.

Tomlins, S. A., et al. (2007). "Integrative molecular concept modeling of prostate cancer progression." Nat Genet **39**(1): 41-51.

Tong, A. W., P. Fulgham, et al. (2009). "MicroRNA profile analysis of human prostate cancers." Cancer Gene Ther **16**(3): 206-216.

Tonini, T., et al. (2004). "Ezh2 reduces the ability of HDAC1-dependent pRb2/p130 transcriptional repression of cyclin A." Oncogene **23**(28): 4930-4937.

Tsai, M. C., O. Manor, et al. (2010). "Long noncoding RNA as modular scaffold of histone modification complexes." Science **329**(5992): 689-693.

Tsuno, T., J. Mejido, et al. (2009). "IRF9 is a key factor for eliciting the antiproliferative activity of IFN-alpha." J Immunother **32**(8): 803-816.

Varambally, S., et al. (2002). "The polycomb group protein EZH2 is involved in progression of prostate cancer." Nature **419**(6907): 624-629

Varambally, S., et al. (2008). "Genomic loss of microRNA-101 leads to overexpression of histone methyltransferase EZH2 in cancer." Science **322**(5908): 1695-1699.

Varambally, S., J. Yu, et al. (2005). "Integrative genomic and proteomic analysis of prostate cancer reveals signatures of metastatic progression." Cancer Cell **8**(5): 393-406.

Vergis, R., C. M. Corbishley, et al. (2008). "Intrinsic markers of tumour hypoxia and angiogenesis in localised prostate cancer and outcome of radical treatment: a retrospective analysis of two randomised radiotherapy trials and one surgical cohort study." Lancet Oncol **9**(4): 342-351.

Verras, M., J. Lee, et al. (2007). "The androgen receptor negatively regulates the expression of c-Met: implications for a novel mechanism of prostate cancer progression." Cancer Res **67**(3): 967-975.

Visakorpi, T., E. Hyytinen, et al. (1995). "In vivo amplification of the androgen receptor gene and progression of human prostate cancer." Nat Genet **9**(4): 401-406.

Walker, E., W. Y. Chang, et al. (2010). "Polycomb-like 2 associates with PRC2 and regulates transcriptional networks during mouse embryonic stem cell self-renewal and differentiation." Cell Stem Cell **6**(2): 153-166.

Wang, N., F. Docherty, et al. (2015). "Mitotic quiescence, but not unique "stemness," marks the phenotype of bone metastasis-initiating cells in prostate cancer." FASEB J.

Wang, Q., J. S. Carroll, et al. (2005). "Spatial and temporal recruitment of androgen receptor and its coactivators involves chromosomal looping and polymerase tracking." Mol Cell **19**(5): 631-642.

Wang, Q., W. Li, et al. (2009). "Androgen receptor regulates a distinct transcription program in androgen-independent prostate cancer." Cell **138**(2): 245-256.

Wang, S (a)., F. He, et al. (2007). "Polycomblike-2-deficient mice exhibit normal left-right asymmetry." Dev Dyn **236**(3): 853-861.

Wang, S (b)., G. P. Robertson, et al. (2004). "A novel human homologue of Drosophila polycomblike gene is up-regulated in multiple cancers." Gene **343**(1): 69-78.

Wang, S., G. P. Robertson, et al. (2004). "A novel human homologue of Drosophila polycomblike gene is up-regulated in multiple cancers." Gene **343**(1): 69-78.

Wang, S., X. Yu, et al. (2004). "Chick Pcl2 regulates the left-right asymmetry by repressing Shh expression in Hensen's node." Development **131**(17): 4381-4391.

Warfel, N. A. and W. S. El-Deiry (2013). "p21WAF1 and tumourigenesis: 20 years after." Curr Opin Oncol **25**(1): 52-58.

Watson, J. A., C. J. Watson, et al. (2009). "Generation of an epigenetic signature by chronic hypoxia in prostate cells." Hum Mol Genet **18**(19): 3594-3604.

Waugh, D. J. and C. Wilson (2008). "The interleukin-8 pathway in cancer." Clin Cancer Res **14**(21): 6735-6741.

Wee, Z. N., et al. (2014). "EZH2-mediated inactivation of IFN-gamma-JAK-STAT1 signaling is an effective therapeutic target in MYC-driven prostate cancer." Cell Rep **8**(1): 204-216.

Wei, J. H., J. Z. Cao, et al. (2014). "EIF5A2 predicts outcome in localised invasive bladder cancer and promotes bladder cancer cell aggressiveness in vitro and in vivo." Br J Cancer **110**(7): 1767-1777.

Wissmann, M., et al. (2007). "Cooperative demethylation by JMJD2C and LSD1 promotes androgen receptor-dependent gene expression." Nat Cell Biol **9**(3): 347-353.

Wittmann, J., E. M. Hol, et al. (2006). "hUPF2 silencing identifies physiologic substrates of mammalian nonsense-mediated mRNA decay." Mol Cell Biol **26**(4): 1272-1287.

Wright, J. L., E. M. Kwon, et al. (2011). "Expression of SLCO transport genes in castration-resistant prostate cancer and impact of genetic variation in SLCO1B3 and SLCO2B1 on prostate cancer outcomes." Cancer Epidemiol Biomarkers Prev **20**(4): 619-627.

Wu, L., et al. (2014). "CCN3/NOV gene expression in human prostate cancer is directly suppressed by the androgen receptor." Oncogene **33**(4): 504-513.

Wu, L., P. Murat, et al. (2013). "Binding interactions between long noncoding RNA HOTAIR and PRC2 proteins." Biochemistry **52**(52): 9519-9527.

Xu, K., Z. J. Wu, et al. (2012). "EZH2 oncogenic activity in castration-resistant prostate cancer cells is Polycomb-independent." Science **338**(6113): 1465-1469.

Xu, Y., S. Y. Chen, et al. (2006). "Androgens induce prostate cancer cell proliferation through mammalian target of rapamycin activation and post-transcriptional increases in cyclin D proteins." Cancer Res **66**(15): 7783-7792.

Xue, B., W. Wu, et al. (2013). "Stromal cell-derived factor-1 (SDF-1) enhances cells invasion by alphavbeta6 integrin-mediated signaling in ovarian cancer." Mol Cell Biochem **380**(1-2): 177-184.

Yang, G., Y. Xu, et al. (2007). "IFITM1 plays an essential role in the antiproliferative action of interferon-gamma." Oncogene **26**(4): 594-603.

Yang, H., Y. Liu, et al. (2013). "Tumor development is associated with decrease of TET gene expression and 5-methylcytosine hydroxylation." Oncogene **32**(5): 663-669.

Yang, L., C. Lin, et al. (2013). "lncRNA-dependent mechanisms of androgen-receptor-regulated gene activation programs." Nature **500**(7464): 598-602.

Yang, Y., C. Wang, et al. (2013). "Polycomb group protein PHF1 regulates p53-dependent cell growth arrest and apoptosis." J Biol Chem **288**(1): 529-539.

Yeh, S., H. K. Lin, et al. (1999). "From HER2/Neu signal cascade to androgen receptor and its coactivators: a novel pathway by induction of androgen target genes through MAP kinase in prostate cancer cells." Proc Natl Acad Sci U S A **96**(10): 5458-5463.

Yu (a), J., et al. (2007). "A polycomb repression signature in metastatic prostate cancer predicts cancer outcome." Cancer Res **67**(22): 10657-10663.

Yu (a), J., et al. (2010). "An integrated network of androgen receptor, polycomb, and TMPRSS2-ERG gene fusions in prostate cancer progression." Cancer Cell **17**(5): 443-454.

Yu, J., et al. (2007). "Integrative genomics analysis reveals silencing of beta-adrenergic signaling by polycomb in prostate cancer." Cancer Cell **12**(5): 419-431.

Yu, J., et al. (2010). "The neuronal repellent SLIT2 is a target for repression by EZH2 in prostate cancer." Oncogene **29**(39): 5370-5380.

Zhai, X., Q. Han, et al. (2014). "Dual specificity phosphatase 6 suppresses the growth and metastasis of prostate cancer cells." Mol Med Rep **10**(6): 3052-3058.

Zhang, H., C. C. Wong, et al. (2012). "HIF-1-dependent expression of angiopoietin-like 4 and L1CAM mediates vascular metastasis of hypoxic breast cancer cells to the lungs." Oncogene **31**(14): 1757-1770.

Zhang, Q., et al. (2014). "Polycomb protein EZH2 suppresses apoptosis by silencing the proapoptotic miR-31." Cell Death Dis **5**: e1486.

Zhang, Z., et al. (2003). "Antisense therapy targeting MDM2 oncogene in prostate cancer: Effects on proliferation, apoptosis, multiple gene expression, and chemotherapy." Proc Natl Acad Sci U S A **100**(20): 11636-11641.

Zhao, J. C., et al. (2012). "Cooperation between Polycomb and androgen receptor during oncogenic transformation." Genome Res **22**(2): 322-331.

Zhao, J., B. K. Sun, et al. (2008). "Polycomb proteins targeted by a short repeat RNA to the mouse X chromosome." Science **322**(5902): 750-756.

Zhao, J., T. K. Ohsumi, et al. (2010). "Genome-wide identification of polycomb-associated RNAs by RIP-seq." Mol Cell **40**(6): 939-953.

Zhong, M., et al. (2012). "The essential role of Gialpha2 in prostate cancer cell migration." Mol Cancer Res **10**(10): 1380-1388.

Zhou, L. X., T. Li, et al. (2010). "Application of histone modification in the risk prediction of the biochemical recurrence after radical prostatectomy." Asian J Androl **12**(2): 171-179.

Zhou, X., X. Xu, et al. (2013). "Bex2 is critical for migration and invasion in malignant glioma cells." J Mol Neurosci **50**(1): 78-87.